Winter 2014

Advances in Understanding the Molecular Composition of Dissolved Organic Matter and Its Reactivity in the Environment

Rajaa Mesfioui
Old Dominion University

ADVANCES IN UNDERSTANDING THE MOLECULAR COMPOSITION OF DISSOLVED ORGANIC MATTER AND ITS REACTIVITY IN THE ENVIRONMENT

by

Rajaa Mesfioui
M.S. May 2008, Old Dominion University

A Dissertation Submitted to the Faculty of
Old Dominion University in Partial Fulfillment of the
Requirements for the Degree of

DOCTOR OF PHILOSOPHY

CHEMISTRY

OLD DOMINION UNIVERSITY
December 2014

Approved by:

_____
Patrick G Hatcher (Director)

_____
Kenneth Mopper (Member)

_____
Margaret R. Mulholland (Member)

_____
James Lee (Member)

ABSTRACT

ADVANCES IN UNDERSTANDING THE MOLECULAR COMPOSITION OF DISSOLVED ORGANIC MATTER AND ITS REACTIVITY IN THE ENVIRONMENT

Rajaa Mesfioui
Old Dominion University, 2014
Director: Dr. Patrick G. Hatcher

Dissolved organic matter (DOM) is the ultimate product of Earth's systems dynamics. DOM chemical signature is strongly shaped by the interaction among Earth's spheres, such as the atmosphere, the geosphere, the biosphere, and the hydrosphere, but also life and human activity. DOM source, composition, photochemical alteration and availability affect freshwater ecosystems, their carbon and nitrogen fluxes and, thus, the global carbon and nitrogen cycles. The aim of this thesis was to gain an understanding of the molecular composition of DOM and its photochemical and biological reactivity in an environment impacted by anthropogenic disturbance. The York and James River systems within the Cheasapeake Bay watershed provided an excellent study site for such studies. The experiments included monitoring the alteration of DOM and its subcomponents dissolved organic nitrogen (DON) and carbon (DOC) from both natural and anthropogenic sources during photochemical and biological processes. My combined analytical and statistical approach identified the molecular signature of the photolabile and the photoproduced DOM and the biolabile and the bioproduced DOM during these processes.

My approach depicted differences in DON assimilation by the York River biota depending on the DOM source, where anthropogenic DON showed more bioavailability than naturally derived DON. Furthermore, anthropogenically-derived DON showed an

intense bioavailability in the freshwater end member of the James River, VA. These findings suggest that anthropogenic DON is highly reactive in the natural environment and that simple assays examining net consumption or production of bulk DON pools are inadequate for assessing its bioavailability.

The studied photochemical alterations of natural and anthropogenic DOM induced production of newly dissolved organic nitrogen (DON) even from natural sources that are relatively N-poor. My experimental results demonstrated that photochemistry transforms DON from complex structural entities to ammonia, aliphatic molecules, and low carbon number molecules that might enhance microbial metabolism, and eventually increases CO_2 emissions and reduces DOM concentrations in stream ecosystems.

This dissertation is dedicated to my amazing husband
Aziz Matar for his encouragement and endless support.

ACKNOWLEDGMENTS

I would like to acknowledge colleagues, family and friends for their unconditional support throughout my graduate career. My deepest gratitude is to my advisor Dr. Patrick G. Hatcher for his optimism, enthusiasm, and faith in my ability to complete the program. I have been amazingly fortunate to have such an advisor who gave me the freedom to explore at large my capabilities, and to guide me to the right path whenever it is needed. His patience and support helped me overcome many hurdles and finish this dissertation. His mentoring, support, and understanding of the different background and personalities among our research group is the driving force for our groups' harmony and friendship that will last beyond this program.

I also appreciate the support of my other committee members, Dr. Margaret R. Mulholland's insightful comments and constructive criticisms at different stages of my research were very appreciated and they helped me focus my ideas, I am indebted to her and to Dr. Kenneth Mopper for giving me full access to their Lab and for their continuous encouragement and guidance. I would like to thank to Dr. James Lee for his constructive criticisms and insightful discussions.

I must thank the current and former members of the Hatcher research group for their friendship and support. I extend my special thanks to Dr. Hussain A. Abdulla for his advise and wisdom in sciences and life matters.

I am also grateful to the following former or current staff at Old Dominion University, for their various forms of support during my graduate study—Dr. Rachel Sleighter, Dr. Aron Stubbins, and Dr. Zhanfei Liu.

I also thank Susan Hatcher and Jarod Collard at the COSMIC (College of Sciences Major Instrumentation Cluster) facility for their assistance with the FTICR-MS analyses.

My friends have helped me stay focus through these difficult years. Their friendship and support have helped me overcome setbacks and stay focused throughout my graduate career. I greatly value their friendship and their belief in me. I am also grateful to all my Moroccan friends that helped me adjust to a new country.

Most importantly, I would like to thank my family for their love, concern, support and patience throughout this endeavor. I would like to express my heart-felt gratitude to my husband Aziz Matar, none of this would have been possible without his love and patience.

Finally, I appreciate the financial support from NSF (Grant No.0756475) and NOAA (award No.NA12NOS4200081) that funded parts of the research discussed in this dissertation.

TABLE OF CONTENTS

LIST OF TABLES

LIST OF FIGURES

CHAPTER I

INTRODUCTION

Over the past century, human activity has dramatically changed the global nutrient cycles, resulting in detrimental effects on human health and the Earth's dynamics (Rockstrom and Karlberg, 2010). In particular, the Carbon (C), Nitrogen (N), and Phosphorus (P) biogeochemical cycles have been altered significantly due to nutrient overload in a variety of marine, freshwater, terrestrial, and atmospheric ecosystems (Canfield et al., 2010; Dolman et al., 2010; Howarth et al., 2011; Lerman et al., 2004; Vitousek et al., 1997). The sources of this nutrient over-enrichment include, but are not limited to, fossil fuel emissions, exhaustive land use, excessive use of chemical fertilizers, and the increasing discharge of municipal sewage associated with widespread urbanization (Canadell et al., 2007).

While land use practices and fossil fuel emissions constitute the main perturbations to the C cycle (Morel et al., 2009), poor management of agricultural activities, in particular, and land use, in general, represent the main perturbations to both N and P cycles (Han et al., 2011; Howarth et al., 1995; Schlesinger, 2009). Moreover, improper practices of land use are increasingly facilitating organic C, N, and P discharge from soil and sediments to aquatic systems (Van Kessel et al., 2009; Zhang et al., 2011), especially to the oceanic coastal zone where most of the oceanic biological primary production (PP) takes place (Chavez et al., 2011). As the interface between land and ocean, the oceanic coastal zone plays a key role in mediating C, N, and P dynamics. However, by being the downstream recipient of improper land use, this role has been greatly jeopardized, resulting in a shift from a balanced, productive ecosystem into an

impaired and degraded ecosystem (Burak, 2004; Howarth, 2008). In fact, 60% of US estuaries have been reported degraded or impaired due to nutrient overload, which leads to hypoxia, anoxia, harmful algae blooms, and resulting losses of ecological biodiversity (Dodds et al., 2008; Howarth, 2008).

Given the pressing need for mitigating and predicting human impact on Earth dynamics, it is of critical importance to intensify research on the coupling between C, N, and P cycles in the different environmental reservoirs, and especially, in the oceanic coastal zone that represents the fringe between these different ecosystems and constitutes the primary sink of the global organic C production (Chen and Borges, 2009; Mackenzie et al., 1998). Dissolved organic matter (DOM) and its measured surrogates, dissolved organic carbon (DOC), and dissolved organic nitrogen (DON), form the main links between the C and N cycles. DOM plays a critical role in supplying labile organic carbon (Hedges et al., 1997; Wetzel, 1992) and nitrogen (Wiegner et al., 2006) to microbial communities in coastal areas. Recent evidence suggests that terrigenous DOM is utilized within streams and rivers, as well as within estuaries and coastal waters, on timescales comparable to water transport and mixing (Benner et al., 1995). This evidence is supported by budgets showing that the amount of carbon delivered to the oceans from rivers is actually only a small portion of the amount of carbon entering rivers from the terrestrial environment (Aufdenkampe et al., 2011). Indeed, rivers and estuaries are the highest emitters of CO_2 per unit area (Cole et al., 2001), indicative of the high rates of respiration and processing of terrigenous DOM within them. Once exported from watersheds, DOM components may be recycled by bacteria and respired or incorporated into microbial and higher organism food webs (Dagg et al., 2008; Del Giorgio and Pace,

2008; Nakagawa et al., 2007) serving as C, N, and P sources. Alternatively, DOM may either be altered by abiotic processes such as photochemical transformation (Amon and Benner, 1996; Asmala et al., 2013; Bertilsson et al., 1999), flocculation (Chen et al., 2014), and sorption (Shank et al., 2005) before its residual and most refractory portion is discharged into the oceans (Hedges et al., 1997). Moreover, the lability of DOC and DON has been shown recently to vary largely according to the biochemical composition and source of their constituent DOM (Benner, 2003; Lu et al., 2013; Wiegner et al., 2006).

Land use practices are starting to influence the quantity, and the quality, of the DOM discharged into rivers and streams, and ultimately its fate and dynamics in aquatic systems (Aufdenkampe et al., 2011; Kaushal et al., 2014). These changes are predicted to lead to alterations in DOM processing and metabolism in aquatic systems, of which photochemical and microbial transformations are two essential components. In fact, an increase in microbial activity is being observed in human impacted watersheds relative to those with less anthropogenic input (Hosen et al., 2014; Rabalais et al., 2002; Williams et al., 2010; Wilson and Xenopoulos, 2013). Therefore, understanding the transformation and utilization of DOC and DON in aquatic ecosystems by natural biota and abiotic phenomena is a crucial step in deciphering the interrelationships between C and N cycles and source materials, and ultimately gaining a better understanding for processes associated with downstream eutrophication.

While the lability of dissolved inorganic N (DIN, e.g., NH_4 and NO_x) and its role as a pollution indicator are well established (Galloway et al., 2008; Howarth and Marino, 2006), the role of anthropogenic DON has regularly been overlooked by the scientific

community (Bronk et al., 2007). The view that DON in marine environments forms a persistently stable pool of N, compared to the constantly depleted DIN pool, is responsible for the traditional belief that DON is mostly bio-refractory, cannot be taken up by phytoplankton, and hence does not contribute to eutrophication. While anthropogenic DIN (e.g., NO_3^-) export from disturbed watersheds to the oceans has been the focus of widespread international research, DON pollution has received less attention. Lately, however, Pellerin et al. (2006) compiled N data for 348 disturbed watersheds, reporting that DON represents, on average, 49% of TDN concentrations in mixed watersheds and that DON concentrations are, on average, 2.5–4 times higher in surface waters from disturbed watersheds than in forested watersheds, suggesting that DON concentrations are highly influenced by N loads in human impacted catchments. Therefore, the dominant form of N in human-impacted watersheds has been overlooked as a potential source of bioavailable N and its reactivity has been neglected for almost a century.

Recently, the preconceived view that DON is bio-refractory has been challenged in the literature with emerging evidence for its bioavailability and its role in fueling primary production(Bronk et al., 2007; Mulholland and Lomas, 2008a; Seitzinger et al., 2002). While these studies have shed some light on the importance of DON in both C and N cycles, they lacked the ability to investigate its structural complexity in order to draw a conclusive picture on the dynamics of natural and anthropogenic DON from landscapes to receiving waters. Most studies of DON dynamics are limited to examining the net changes in concentrations of particular nitrogen species over time and/or quantifying the net change of DON using bulk analysis (Bronk et al., 2010; Filippino et

al., 2011; Seitzinger et al., 2002). Unfortunately, this approach has only addressed bulk measurements of DON, and we know little about how the molecular composition of DON changes in response to biodegradation or photodegradation processes. To date, there is no standard method to accurately assess DON reactivity at the molecular level in natural systems. Further, the high polarity and complexity of this material, along with the analytical challenges encountered by the presence of inorganic salts, some of which are N-containing salts, make it difficult to obtain molecular level information using standard techniques (McCarthy and Bronk, 2008). In fact, bulk spectroscopic techniques, such as ultraviolet/visible absorbance, infrared, and nuclear magnetic resonance, have provided functional group information on complex mixtures such as wastewater effluents (Dignac et al., 2001) but lacked the ability to provide molecular level information. Furthermore, by being a Lewis base, N in DON can be easily protonated making its isolation difficult when using conventional extraction methods. Up till now, approximately 50% of the DON pool is still uncharacterized. This is especially true for anthropogenic DON, considering that it is typically, and likely incorrectly, considered to be recalcitrant without direct evidence, and that there are limitations to methods for its characterization (Vähätalo and Zepp, 2005).

DOM and its subcomponents delivered from the surrounding watershed to the estuary may fuel eutrophication and hypoxia in several ways, including: (1) remineralization to inorganic forms, which subsequently stimulate primary production and lead to excess organic matter accumulation in the estuary, and (2) respiration or decomposition of DOM, which consumes dissolved oxygen. Thus, understanding the factors that control DOM dynamics and composition, including the effect of

photochemistry, changes in salinity, and differences in source material is necessary for developing sound management practices. However, despite the recognized importance of DOM to the estuarine ecosystem it is often difficult to predict how DOM dynamics will impact downstream waters, since its composition is highly variable thereby influencing its chemical properties and biological availability (Fellman et al., 2010; Yamashita et al., 2010)

This thesis is a compilation of work that addresses these gaps in knowledge by examining the reactivity of DOM from different sources under biological, photochemical, and salinity change stressors. I demonstrate in this thesis that true reactivity can be readily masked by examination of bulk changes in DOM, mainly because degradative losses can be offset by new production in a metabolically and photochemically active system. We show that molecular-level geochemistry capable of distinguishing between new production and degradative loss is essential to evaluate the extent of DOM transformations. Such specificity is afforded by use of electrospray ionization coupled to Fourier transform ion cyclotron resonance mass spectrometry (ESI-FTICR-MS), a technique that provides the ability to obtain unique elemental formulas for components of DOM in aquatic environments including marine waters (Reemtsma et al., 2006; Sleighter and Hatcher, 2008b) and freshwaters (Kim et al., 2006). Moreover, this technique has been shown to be an excellent tool for the study of DOM biodegradation (Kim et al., 2006). In this thesis, I advance this concept and further demonstrate that both biodegradation and photodegradation can be examined at the molecular level by this approach.

The overall objectives of this research are to probe the dynamics of DOC and

DON from a variety of sources (natural and anthropogenic) using new analytical techniques in order to assess its potential reactivity in the York and James Rivers of the Chesapeake Bay watershed. The specific objectives and hypotheses are:

Chapter II: In biologically productive systems, such as the James River, the uptake and production of the DON and DOC component molecules can occur at similar rates with no net change in bulk measurements. This can mask the true reactivity of DOM if only bulk chemical analysis are examined. I hypothesized that I could resolve this problem by investigating molecular level biotransformation of wastewater treatment plant (WWTP) effluents spiked into waters of the James River, Virginia using ESI-FTICR-MS. This chapter, published in *Water Research*, is the first to demonstrate the power of FTICR-MS to discern molecular level changes that discount the claim of biorecalcitrance for DON. My advanced chemical analysis demonstrated that DON in both examined effluents from two very different treatment processes were more reactive than was predicted from the net changes in bulk DON concentrations in the incubation bottles. My findings have important implications for management and suggest that it may not be appropriate to discount DON from WWTP nutrient loading estimates; rather, it should be counted towards the nutrient allocations for wastewater plant discharges to aquatic systems

Chapter III: Photochemistry is considered one of the main processes that governs the abiotic fate and turnover of DOM along the land-to-river-to-ocean continuum (Opsahl and Benner, 1998; Smith and Benner, 2005; Stubbins et al., 2010; Wiegner and Seitzinger, 2001). In contrast to the numerous studies published on DOC photochemistry (Amon and Benner, 1996; Mopper et al., 1991; Stubbins et al., 2010), little is known

about the response of DON and inorganic N to photochemical transformation. With access to water samples with different ranges of DOM sources, I hypothesize that I could use ESI-FTICR-MS to investigate the structural transformation of both DOM and its component DON from natural and anthropogenic sources under the influence of long-term photoirradiation, to better understand the ecological significance of DOM in disturbed watersheds and to elucidate the impact of land-use changes on the reactivity and the transfer of DOM from sources to receiving waters of the York River System in southeastern Virginia. To the best of my knowledge, this is the first study to molecularly investigate long-term photoirradiation of anthropogenic DOM and DON while, at the same time, comparing them with natural sources of DOM and DON using ESI-FTICR-MS, and while still employing conventional bulk analysis approaches. My approach depicted an intense photoproduction of new DON even from the natural source that is relatively N-poor. I was able to demonstrate that photochemistry transforms DON from complex structural entities to ammonia, aliphatic molecules, and low carbon number molecules that might be easily digested by biota. Furthermore, we validate that photochemistry is one of the main processes that shapes the DON quality in aquatic systems regardless of its original source.

Chapter IV: Once exported from watersheds, DOM components may be recycled by bacteria and respired or incorporated into microbial and higher organism food webs (Dagg et al., 2008; Del Giorgio and Pace, 2008; Nakagawa et al., 2007) serving as C, N, and P sources. Moreover, the lability of DOC and DON has been shown recently to vary largely according to the biochemical composition and source of their constituent DOM (Benner, 2003; Lu et al., 2013; Wiegner et al., 2006). I hypothesize that anthropogenic

DOM is functionally different than naturally derived DOM, and that this difference is predicted to affect DOM processing and metabolism as it is transported downstream the mesohaline section of the York River. I substantiated my hypothesis by using inoculum from two different stations on the York River to perform bioassays on samples from both natural and anthropogenic sources. I used a combination of multi-analytical and statistical approaches to detect intrinsic changes in the DOM pertinent to each source while being subjected to different salinities. My results demonstrate that DOM from these different sources exhibited differences in the degree of biodegradation and type of bioproduced compounds, which can be related to the dramatic differences of their DOM source and structural signature. These findings suggest that anthropogenic DON is highly reactive in the natural environment in comparison to the naturally derived DON and that change in salinity enhances DOM biodegradation. I was able to ascertain that simple assays examining net consumption or production of bulk dissolved organic N pools are inadequate for assessing the bioavailability of DON from these different sources.

Findings from this research will enhance scientific understanding of non-point source pollution effects and/or nutrient dynamics on coastal ecosystems. This research will i) characterize the variability, at the molecular level, of the DOC and the DON from natural and anthropogenic sources, one that has a critical effect on the functioning of coastal ecosystems such as variation in energy sources to higher food webs, and ii) assess factors affecting the reactivity of natural versus anthropogenic DOC, and DON as it is transported from source areas downstream to the mouth of the York River. The latter information is essential for coastal planning, as changes in the materials supporting food

webs is critical for sustenance of estuarine ecosystems and prevention of eutrophication. Finally, the proposed work is of global interest, as it will provide a critical understanding of how changes in DON and DOC composition impact the reactivity of DOM delivered to riverine and estuarine systems. Furthermore, the results of these studies allows us to further demonstrate that ESI-FTICR-MS shows a unique potential for elucidating the dynamics of DOM in aquatic systems.

CHAPTER II

REACTIVITY AND CHEMICAL CHARACTERIZATION OF EFFLUENT ORGANIC NITROGEN FROM WASTEWATER TREATMENT PLANTS DETERMINED BY FOURIER TRANSFORM ION CYCLOTRON RESONANCE MASS SPECTROMETRY

PREFACE

The content of this CHAPTER was published in 2012 in the Water Research Journal, and below is the full citation. See Appendix A for the copyright permission.

Mesfioui, R.; Love, N. G.; Bronk, D. A.; Mulholland, M. R.; Hatcher, P. G., Reactivity and chemical characterization of effluent organic nitrogen from wastewater treatment plants determined by Fourier transform ion cyclotron resonance mass spectrometry. *Water Research.* 2012, 46, (3), 622-634.

1. INTRODUCTION

Over the past century, human activity has dramatically changed global nutrient cycles, resulting in detrimental effects on human health and Earth system dynamics (Gruber and Galloway, 2008; Schlesinger, 2009). In particular, eutrophication has resulted from the high nitrogen (N) flux to coastal marine systems from both natural (Inglett et al., 2011; Perakis and Hedin, 2002) and anthropogenic sources (Howarth et al., 2011; Howarth, 2008). The impact of nutrient over-enrichment is seen most dramatically in estuarine regions, such as Chesapeake Bay where the estimated cost of rehabilitation is estimated at nearly $18 billion (The Chesapeake Bay commission, 2010).

Wastewater treatment plants (WWTPs) are an important point source for N loading in many aquatic environments, including Chesapeake Bay. Wastewater-derived

N currently contributes approximately 19% of the total N load to the Bay (The Chesapeake Bay resource library, 2009). In N-sensitive estuaries such as Chesapeake Bay, WWTPs are required to implement more advanced treatment methods in order to meet increasingly stringent effluent guidelines for total N (TN); in some cases this will require effluent TN concentrations to be below 3 mg N/L. In advanced N removal treatment systems, the percentage of N that is organic in the final effluent can be as much as one-third of the TN (Urgun-Demirtas et al., 2008).

While we now know that many phytoplankton take up organic N (Mulholland and Lomas, 2008), there are relatively few data on the bioavailability of EON. Some studies have investigated EON in defined cultures or seed cultures (Pehlivanoglu and Sedlak, 2004; Sattayatewa et al., 2009). Other studies examined the bioavailability of EON by monitoring changes in concentrations of particular nutrient elements over time in incubations with microbial communities in natural waters (Bronk et al., 2010; Filippino et al., 2011) or by treatment plant microbes (Parkin and McCarty, 1981). While bioassays can quantify the net changes in the organic N pool, they cannot rigorously characterize true bioavailability of specific compounds in the environment because organic compounds are both taken up and released during bottle incubations and because the diversity of microbes in natural systems is great such that what is bioavailable to one community might not be to another.

Currently, we know little about the molecular composition of EON and dissolved organic nitrogen (DON) in general. The high polarity and complexity of this material, along with the analytical challenges encountered due to the presence of inorganic salts, some of which are N salts (McCarthy and Bronk, 2008), make it difficult to obtain

molecular level information using standard techniques. In fact, bulk spectroscopy techniques, such as ultraviolet/visible, infrared, and nuclear magnetic resonance, which have provided functional group information on complex mixtures such as wastewater effluents (Dignac et al., 2001; Pehlivanoglu-Mantas and Sedlak, 2006) lack the ability to provide molecular level information.

Electrospray ionization (ESI) coupled to Fourier transform ion cyclotron resonance mass spectrometry (FT-ICR-MS) at high magnetic field (>9 Tesla) has provided a major breakthrough for molecular studies of environmental samples (Marshall et al., 1998; Sleighter and Hatcher, 2008b). Because of its ultrahigh resolving power (>200,000) and high mass accuracy (<1ppm), ESI-FT-ICR-MS is capable of determining the exact mass for the thousands of molecules in a single complex sample of DOM (Kim et al., 2003; Kujawinski et al., 2002). The mass accuracy is sufficiently high to allow for the assignment of a unique molecular formula to each constituent (Stenson et al., 2003). Recently, ESI-FTICR-MS has been used to characterize DOM in aquatic environments including marine waters (Reemtsma et al., 2006; Sleighter et al., 2008b) and freshwaters (Kim et al., 2006). Moreover, this technique has been shown to be an excellent tool for the study of DOM biodegradation (Kim et al., 2006). Currently, ESI-FTICR-MS is the most powerful analytical tool for elucidating the detailed molecular characterization of DOM, which can be accomplished by assigning unambiguously single formula to each peak in the mass spectrum.

As part of a comprehensive study to evaluate the utility of bioassays to assess the reactivity of EON from wastewater treatment plant effluents (Bronk et al., 2010; Filippino et al., 2011), ESI-FTICR-MS was used to determine the molecular (i.e.,

formula) composition of DOM isolated from two biological reactor effluents obtained from WWTPs employing different treatment processes. The results, coupled with bioassay data published elsewhere (Bronk et al., 2010), allowed us to better understand the biological lability of the EON samples tested.

The results of this study demonstrate that bioassay data is best interpreted in conjunction with advanced chemical analysis to assess the true bioavailability of EON. The outcomes of this study will offer new insight into our understanding of the fate of EON in receiving waters and may influence management decisions regarding how we determine allowable N loads from WWTPs to aquatic systems.

2. EXPERIMENTAL PLAN

2.1. Source of effluents

The biological reactor effluents used in this study were from two WWTPs that employ enhanced nutrient removal technologies (ENR facilities). These plants were selected because their final effluents were expected to contain high concentrations of DON relative to DIN (Pagilla et al., 2006); high concentrations of DIN are known to stimulate growth in natural microbial communities (Mulholland and Lomas, 2008) and can also reduce the sensitivity of the bioassay to the organic N component (Bronk et al., 2010). The effluents are designated EON4 and EON5 (Bronk et al., 2010). EON4 was collected from a small WWTP equipped with a membrane bioreactor system (<0.05 million gallons per day) and has a solids residence time of 20-30 days prior to discharges within the Chesapeake Bay watershed. The plant receives a variable influent containing both sewage and septage discharges, and uses a biological TN removal process with influent equalization prior to a four stages Bardenpho process followed by UV

disinfection process. EON5 was isolated from a large domestic WWTP (40 million gallons per day) located in the arid Western US. This facility uses a sophisticated multistage system that has a solid retention time of 3 days. The system includes an anaerobic/oxic (A/O) biological phosphorus removal process, a nitrification/denitrification process, and a final chlorination disinfection process. EON4 samples were collected, placed in a cooler with ice, and transported to Old Dominion University (ODU, Norfolk, VA) the same day. Effluents were collected prior to the disinfection step, because treatment plants are increasingly turning to UV disinfection and we wanted the results to be representative for non-chlorinated effluents. Because the EON5 sampling point still contained large amounts of microbial biomass from the treatment system itself, the samples were filtered with a 1 μm pleated sediment cartridge (Safe Water Technologies, Inc., Elgin, IL) prior to packaging and shipping overnight on ice to ODU. Upon arrival to ODU, both effluents were filtered through a 0.2 μm polysulfone cartridge filter (conditioned for 5 min with the effluent) then concentrated from 13 L to 270 mL for EON4 and from 19L to 450 mL for EON5 using a rotary evaporator system that was maintained at low temperatures (< 35 °C) in order to minimize DOM degradation. Furthermore, most volatile substances generally have m/z values less than 200, and are below the mass range that the FTICR-MS can analyze. Effluents were concentrated to allow addition of a small volume of EONs concentrates to JR water, thus avoid "diluting" the natural population of microorganisms and to allow detection of the added DON. This process makes the total N of both EON additions about equal.

2.2. Sampling sites and bioassay experiments

Water containing microbiota for the bioassays was collected from the James River (southeastern VA, USA) at a salinity of 0.9 (considered freshwater), as described previously in Bronk et al. (2010). Briefly, the field samples were collected in Niskin bottles, and transferred to 0.5 L acid washed polyethylene terephthalate glycol bottles once in the lab. The bottles were divided into three sets. The first set did not receive any effluent (Ctrl). The second set was amended with 369 μg N L^{-1} (final concentration) of concentrated EON5 (where DON represents 97.5% of the TDN), and the third set received 427 μg N L^{-1} (final concentration) of concentrated EON4 (where DON represents 56% of the TDN). All samples were incubated in an environmental chamber at the Virginia Institute of Marine Sciences (VIMS, Gloucester Point, VA) supplied with a 13.5/10.5 hour light/dark cycle and maintained at a constant temperature of 25°C. At time initial (T_0) and after a 48-hr incubation period (T_f), aliquots of 20 mL from experimental treatments were filtered through pre-combusted glass fiber filters (nominal pore size 0.7 µm, GF/F), then dispensed into precombusted borosilicate glass bottles and were frozen for MS analysis.

Dissolved organic carbon (DOC) and TDN concentrations were measured in triplicate on the filtered samples at VIMS using the high temperature catalytic combustion method (Shimadzu TOC-5000) and the persulfate oxidation method, respectively. DON concentrations were calculated by subtracting the concentrations of ammonium ion (NH_4^+), nitrate ion (NO_3^-), and nitrite ion (NO_2^-), from the TDN (Table 1).

2.3. Desalting protocol

Salts can interfere with MS analysis by either clogging the ESI-FICR-MS skimmer, which mitigates ionization, or by forming unwanted peaks that compete for the charge, thereby suppressing signals from organic constituents in the sample. Therefore, sample desalting is mandatory before MS analysis. As mainly a Lewis base, N in DON can be easily protonated, making its isolation nearly impossible when using conventional extraction methods, which rely upon acidification to render acidic DOM molecules neutral. Up until now, approximately 50% of the DON pool is still uncharacterized. Recently, efforts are being earnestly employed to find the most effective method in isolating DON. Solid phase extraction (C_{18}, PPL), XAD resins, and ultrafiltration have been successfully used for isolating DOM but yielded either low or no recovery for DON (Mopper et al., 2007; Simjouw et al., 2005). So far, the most effective technique seems to be electrodialysis (ED); which has been successfully employed in isola FWHM ting DOM with the highest percent recovery (>85%) from both fresh and marine waters and without any contamination or fractionation (Koprivnjak et al., 2006; Koprivnjak et al., 2009; Vetter et al., 2007). After defrosting, samples were concentrated 5-fold using rotary evaporator and then desalted using a small-scale electrodialysis (ED) system (Harvard apparatus, hereafter referred to as a mini-ED. Each sample was charged into a Teflon sample compartment (1.5 mL) between two cellulose acetate membranes (molecular weight cut-off of 500 Da). This sample compartment was inserted into the mini-ED chamber where it was subsequently completely surrounded by fresh ultrapure water in order to maintain a salt gradient between the sample and chamber. Salt removal occurs by transfer of salts through the membrane driven by the electric field and requires

several days to two weeks. This technique promotes the removal of the vast majority of salts while the sample compartment retains ~55% of the DOC within the sample compartment. The measurement of DON recovery efficiency is not practical at this point because reliable methods are not readily available to measure the amounts of organic N in our sample volume (~1.5 mL). We make the assumption that DON recovery is similar to DOC recovery. In a study in our laboratory (Chen et al., 2011) we were able to demonstrate that this mini-ED performs reasonably well and does not selectively fractionate the DOM but recoveries are lower than observed for larger-scale ED systems where values of above 75% have been reported (Koprivnjak et al., 2009). Our use of 500 Da membranes probably contributed to lower recoveries. The reproducibility of this technique was assessed using replicates of EON5 where the two replicates were desalted then analyzed under the same conditions using the same MS parameters as the remainder of bioassays samples. This technique showed a high level of reproducibility. The MS spectra of both replicates were virtually identical when salt derived peaks were removed from consideration. Approximately 83% of all the DOM peaks were observed in both replicates and their relative magnitude accounted for 97% of total summed peak magnitude in both replicates. Most of the mismatch between replicates was due to the integration and non-integration of small peaks, which was dictated by signal-to-noise settings. This excellent reproducibility gives us great confidence that single MS measurements are sufficient to describe the distribution of peaks.

2.4. Instrumentation

All MS analyses were performed at the College of Sciences Major Instrumentation Cluster (COSMIC) at Old Dominion University using an Apollo II ESI

ion source coupled to a Bruker Daltonics 12 Tesla Apex Qe FTICR-MS. Prior to analysis, the instrument was externally calibrated using polyethylene glycol. Samples were first diluted with LC-MS grade methanol to 50:50 (v/v) methanol:water, then spiked with 0.1% ammonium hydroxide (increasing pH to 8) right before introduction to the ESI to increase the ionization efficiency. Sample flow rate was maintained using a syringe pump set at 120 μL/hr and the ESI voltages for each sample were maintained at 3.4 kV on the spray shield and 4.1 kV on the capillary under 200 °C in order to maintain a consistent ion current entering the capillary to the MS.

All samples were analyzed in negative ion mode to minimize complications due to sodium adduct formation. By using the negative ion mode, the multi-functional part of the EON analyte that is attached to N can be effectively ionized without giving complicated adduct signals. Furthermore, cyanide and nitrate/nitrite functionalities can best be ionized in negative ion mode (Sleighter and Hatcher, 2011). Electrospray voltages and mass spectrometer parameters were held constant throughout all experiments. Ions were accumulated in a hexapole for a period of 3 s before transfer to the ICR cell. This accumulation time was found to be optimal; because shorter ion accumulation times resulted in fewer peaks with lower S/N, while longer times led to poor resolution. For each sample, 300 time-domain transients were acquired (at 4M Word), zero-filled once, sine-bell apodized, and then Fourier transformed in the Bruker data analysis software, resulting in an overall analysis time of approximately 40 min.

2.5. Mass calibration and molecular formula assignments

The general mass distribution of compounds that were ionized in all samples was in the range of 200-700 m/z, which is consistent to previous DOM studies using ESI-

FTICR-MS (Koch et al., 2005; Sleighter and Hatcher, 2008b). Because low m/z peaks (<200) have very high excitation frequencies, the excitation required to increase the ion radius to sufficient amplitude be detected by the detection plates is more difficult to generate. Furthermore ions below 200 are discriminated against in the quadrupole, where ions of a broad specified m/z range are allowed to pass through before being accumulated in the hexapole, and then transferred to the ICR cell (see Appendix C for more detailed information on the principle of FTICR-MS). Our samples were analyzed in broadband mode, meaning we used a very wide m/z range (m/z 100-2000) however peaks were only detected and observed in the range of 200-700 m/z. The eventual loss of peaks above 700 m/z can be attributed to space charge effects within the ICR cell that can result in a decrease of high molecular weight signals (Kujawinski et al., 2002).

All acquired spectra were internally calibrated with indigenous fatty acids (Sleighter et al., 2008a), providing a mass accuracy of 1 ppm or less throughout the mass range of interest. Molecular formulae were assigned to peaks with a signal to noise (S/N) ratio > 3 in the mass range of 200-700 m/z by means of a Formula Calculator Program (v.1.0 © 1998 NHMFL) that was developed at the National High Magnetic Field Laboratory in Tallahassee, FL. In our study, the vast majority of formulas were unambiguously assigned below m/z 500, because we only allow up to 0.5 ppm error in assigning correct molecular formulas. When multiple assignments existed for a single m/z value, then the correct formula was assigned based on elemental rules, functional group relationships, and patterns and homologous series, as described in detail previously in the literature (Koch et al., 2007; Koch et al., 2005).

3. RESULTS AND DISCUSSION

3.1. Chemical characterization of EON5 and EON4

Consistent with the pattern observed from other DOM studies using FTICR-MS (Sleighter and Hatcher, 2008b), the spectra obtained for each desalted sample set contained the routinely-observed complex pattern of multiple peaks at each nominal mass over the studied range (m/z 200-700). Included in this set of peaks are extraneous peaks related to residual salts, many of which are rather intense and have a distinct mass defect that separates them from the DOM peaks. Electrodialysis is not 100% effective at salt removal, so we do not show a comparison of the raw spectral data over the mass range where salt-derived peaks may predominate. Instead we focus here on the spectral data that are reconstructed histograms for the DOM peaks that have been assigned molecular formulae after data processing. Essentially this is a reconstituted mass spectrum from which extraneous salt-derived peaks have been removed. Reconstructed mass spectra of natural James River (JR) water, concentrated EON5, and concentrated EON4 are shown in Figure 1. Both JR and EON5 reconstructed mass spectra show a pattern consistent with previous DOM studies (Sleighter and Hatcher, 2008b), where peaks are generally distributed over the mass range of 200-700 m/z with a maximum in the range of 420-450 m/z; excluding the intense peaks that are predominantly fatty acids. However, the EON4 spectrum shows a distinct pattern where peak intensities are equally distributed over the range of 200-700 m/z. Differences between effluents are likely due to a combination of factors, including: the different treatment processes used at the two WWTPs; the unique mixed liquor ecologies of each plant; and different influent wastewater characteristics.

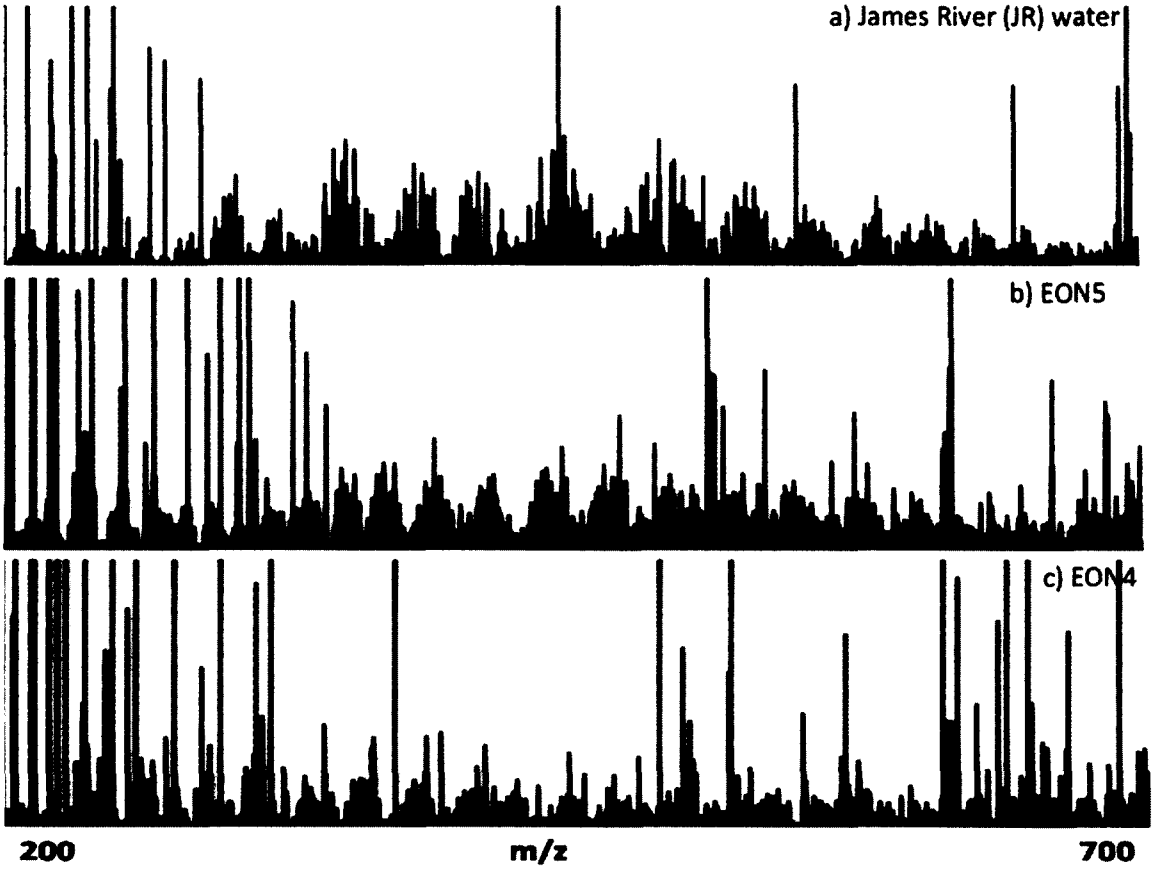

Figure 1. Comparison of (a) James River natural water, (b) EON5, and (c) EON4 reconstructed FTICR broadband mass spectra.

Most peaks are assigned a unique molecular formula (84%-92% of the peaks in each spectrum, data shown in Table 1). These formulae will help examine the elemental relationships among peaks within the same sample and between different samples. These formulae can be sub-categorized according to their elemental make up. Thus, all formulae can be grouped into CHO-containing molecules, CHNO-containing molecules, and CHSO-containing molecules (Figure 2). Formulae containing only C, H, and O dominated the three spectra, yet EON5 and EON4 samples include more CHNO

compounds (19% and 9%, respectively) than JR water (2%), which is consistent with the fact that effluents are rich in N-bearing organic compounds.

Table 1

Total dissolved nitrogen (TDN), dissolved organic carbon (DOC), and dissolved organic nitrogen (DON) data for the analyzed samples (salinity 0‰) by FTICR-MS. Percentage of assigned formulae are determined in the studied range of 200-700 m/z.

Sample	[DOC](μM C)	[TDN](μM N)	[DON](μM N)	Percentage of assigned formulas
JR[a] water T_0	362.6 ± 1.6	28.8 ± 0.1	21.3 ± 0.1	86%
JR water T_f	372.2 ± 2.5	22.6 ± 0.4	22.4 ± 0.4	89%
(EON5[b]+JR) T_0	604.3 ± 3.4	55.5± 0.7	47.6 ± 0.7	92%
(EON5 + JR) T_f	600.0 ± 3.7	43.1 ± 0.6	42.7 ± 0.6	92%
(EON4[c]+ JR) T_0	528.9 ± 2.9	59.6 ± 0.6	38.5 ± 0.6	84%
(EON4+ JR) T_f	547.5 ± 2.4	38.6± 0.6	38.1 ± 0.6	92%

[a] James River water, [b] concentrated effluent from EON5 plant, [c] concentrated effluent from EON4 plant, T_0: time zero, T_f: after 48-hr incubation.

Van Krevelen (VK) plots (Kim et al., 2003), which display the molar H/C and O/C ratios for individual peaks, cluster elemental formulae according to their functional group compositions into major biochemical compounds classes that have characteristic H/C and O/C ratios (Figure 2; compound classes indicated with black circles). It is well known that the location of a point on the VK diagram relates to specific compound classes in DOM, and interested readers are referred to the literature for more details (Hockaday et al., 2009; Ohno et al., 2010; Reemtsma, 2009; Sleighter and Hatcher, 2011; Van Krevelen, 1950). These compound classes include aliphatic structures (region I), carboxyl-rich alicyclic molecule-like structures [CRAM (Hertkorn et al., 2006)] or lignin-like structures (region II), condensed aromatic structures [(Koch and Dittmar, 2006)

(region III)], tannin (region IV), carbohydrate-like structures (region V), and lipids (region VI). EON5 appears more diverse in composition than both EON4 and JR natural water, For example, EON5 encompasses more formulas in all regions of the VK diagram especially more nitrogenous species in the aliphatic and the CRAM- or Lignin-like regions compared to EON4 and JR natural water (Figure 2).

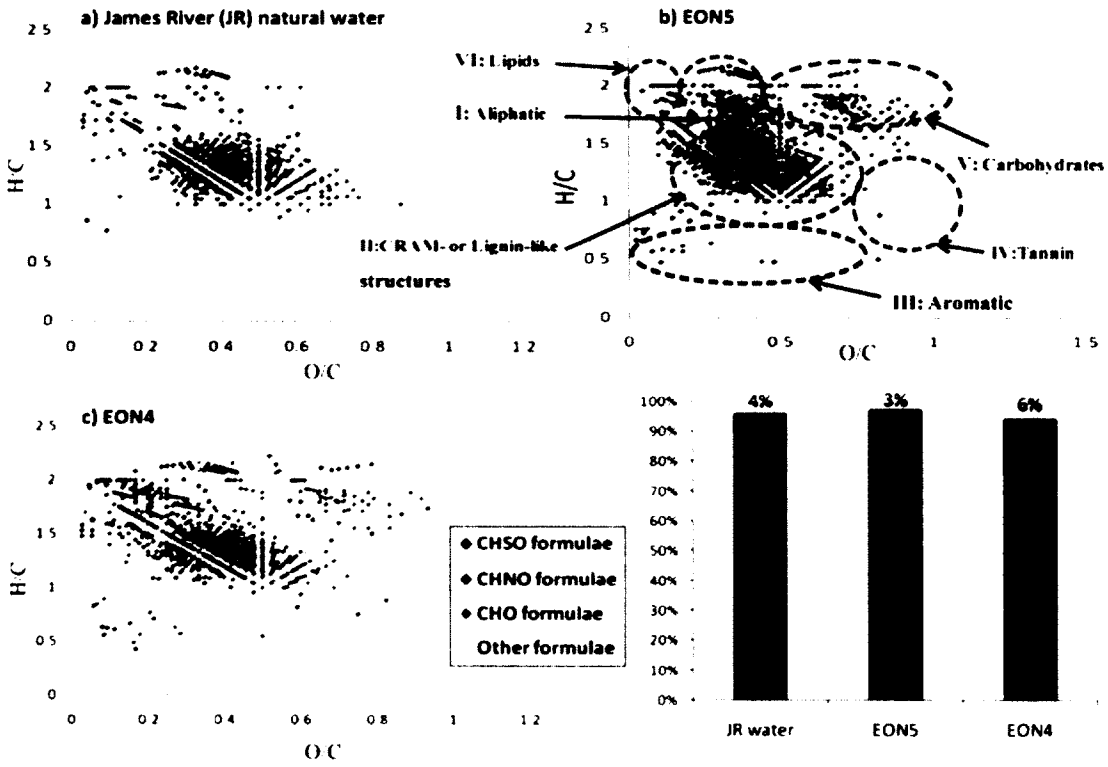

Figure 2. Comparison of James River natural water, EON5, and EON4 compositions. van Krevelen diagram of (a) James River natural water (b) EON5, and (c) EON4 color coded to emphasize the type of compounds existing in each sample: green for CHO, blue for CHSO, dark red for CHNO, and yellow for other formulae. The overlain black circles correspond to major biochemical classes of compounds that can be expected in dissolved organic matter (DOM). Bar diagrams show the contribution of the major subcategories (CHNO, CHO, and CHSO) in the three samples.

3.2. Biodegradation of effluent-amended James River water

3.2.1. EON5 effluent amendment

3.2.1.1. Reactivity of EON5

After a 48-hr incubation period, the peaks observed to be added to JR water with the EON5 amendments (denoted by solid triangles ▲) either disappeared completely or their relative intensities changed compared to the peaks that originated mainly from the JR water (denoted by solid stars ✱), presumably as the result of biotic and abiotic alterations that occurred during the 48-hr incubation (Figure 3c,d). This disappearance or diminution in relative intensity indicates a decrease in relative concentration of these compounds, suggesting they were labile.

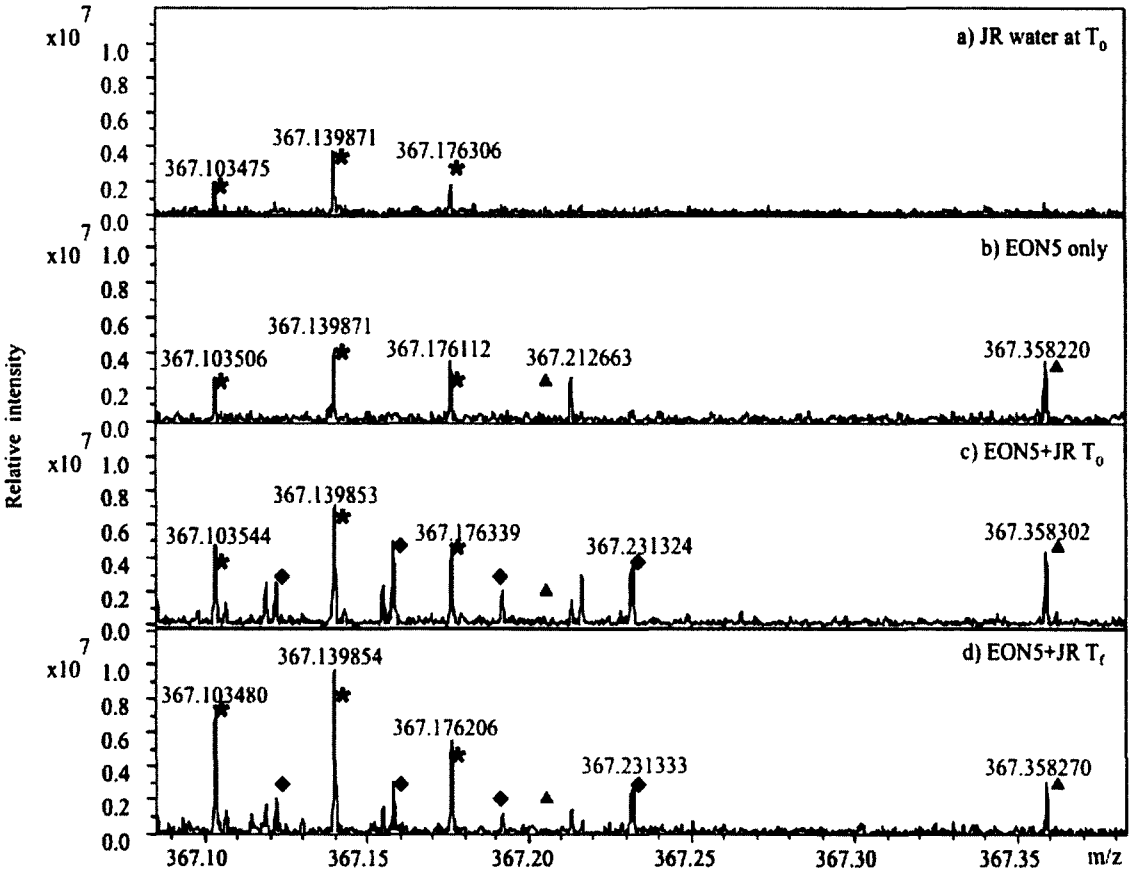

Figure 3. Reactivity of the incubated EON5. Negative ion mass spectra expanded at nominal mass 339 of (a) James River (JR) water at T_0, (b) EON5, (c) EON5+JR at T_0, and (d) EON5+JR at T_f. Peaks added by the James River water are shown with solid stars, peaks added by the effluent are shown with solid triangles, and peaks produced upon incubation are shown with solid circles.

As an example of what was observed throughout the mass range examined, we show an expanded mass region of the spectra obtained for JR water (Ctrl), EON5, and EON5+JR samples before (T_0) and after the 48-hr incubation (T_f) in Figure 3. In this narrow spectra window, the major peak added by the effluent (m/z~339.127) disappears after incubation while a new peak (m/z~ 339.093) emerges (denoted by a solid circle).

To identify changes throughout the mass range (200 to 700 m/z), the assigned formulae for peaks in the EON5+JR sample before and after incubation were parsed into 3 groups according to their heteroatom contents, and then each was plotted in a three dimensional VK diagram (Figure 4a,b). These 3D VK plots highlight changes occurring to N- and S-containing molecules separately from those molecules containing only C, H, and O. The relative contributions (based simply on total number of formulae) of each elemental class to the general composition are also calculated and listed in a bar diagram (Figure 4). There was a major removal of CHNO and CHSO compounds over the 48-hr incubation. The removal of these effluent-derived compounds suggests that they were bioavailable or degradable (but not necessarily mineralized) when introduced to natural water samples. There was also removal of CHO compounds but this information was not readily discernable from this type of diagram because we also observed production of new CHO compounds that offset the molecules lost during degradation.

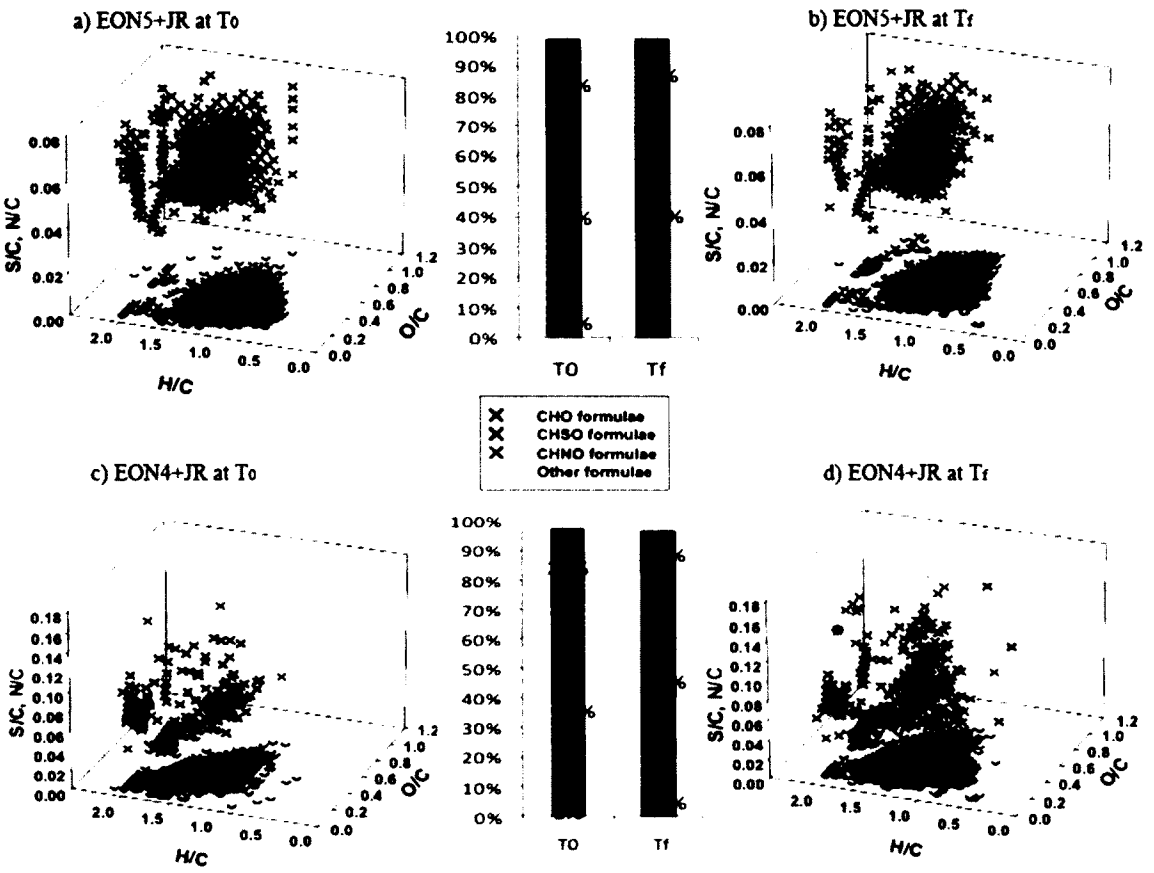

Figure 4. Three-dimensional van Krevelen diagrams of the incubated EON4 and EON5. Three dimensional van Krevelen diagrams of the amended James River water with EON5 and EON4 at T_0 (a and c) and after 48-hr incubation T_f (b and d), color coded to emphasize the type of compounds existing in each sample: green for CHO, blue for CHSO, red for CHNO, and yellow for other formulae.

In order to elucidate clearly the changes occurring within each subcategory, the consumed (peak lost), produced (new peak gained either as a new compound or a byproduct of small changes to consumed compounds), and conserved (peak retained) formulae were plotted after the 48-hr incubations (T_f) in VK diagrams relative to samples collected at T_0 (Figure 5). Peaks attributed to JR DOM were not plotted in order to

highlight the effects due to changes in effluent DOM only during the 48-hr incubation. Approximately 79%, 36%, and 39% of CHNO, CHO, and CHSO formulae of EON5, respectively, were consumed (Figure 5, bar diagrams). However, about 54%, 42%, and 33% of CHNO, CHO, and CHSO formulae, respectively, were produced during the 48-hr incubations. These results confirm that, while some components of EON5 were labile, production of new chemical compounds during the bioassay can confound assessments of bioavailability based on net changes in DON concentrations (Bronk et al., 2010). Production of new compounds may be due to partial digestion of the consumed DOM or to production of new compounds as a result of microbial or abiotic transformations. It is important to note that the above estimates of alterations are conservative estimates because they do not include peaks with diminished intensities or peaks that increased during the bioassay. Only peaks that disappeared completely and new ones that emerged after the 48-hr incubation period were considered in this analysis.

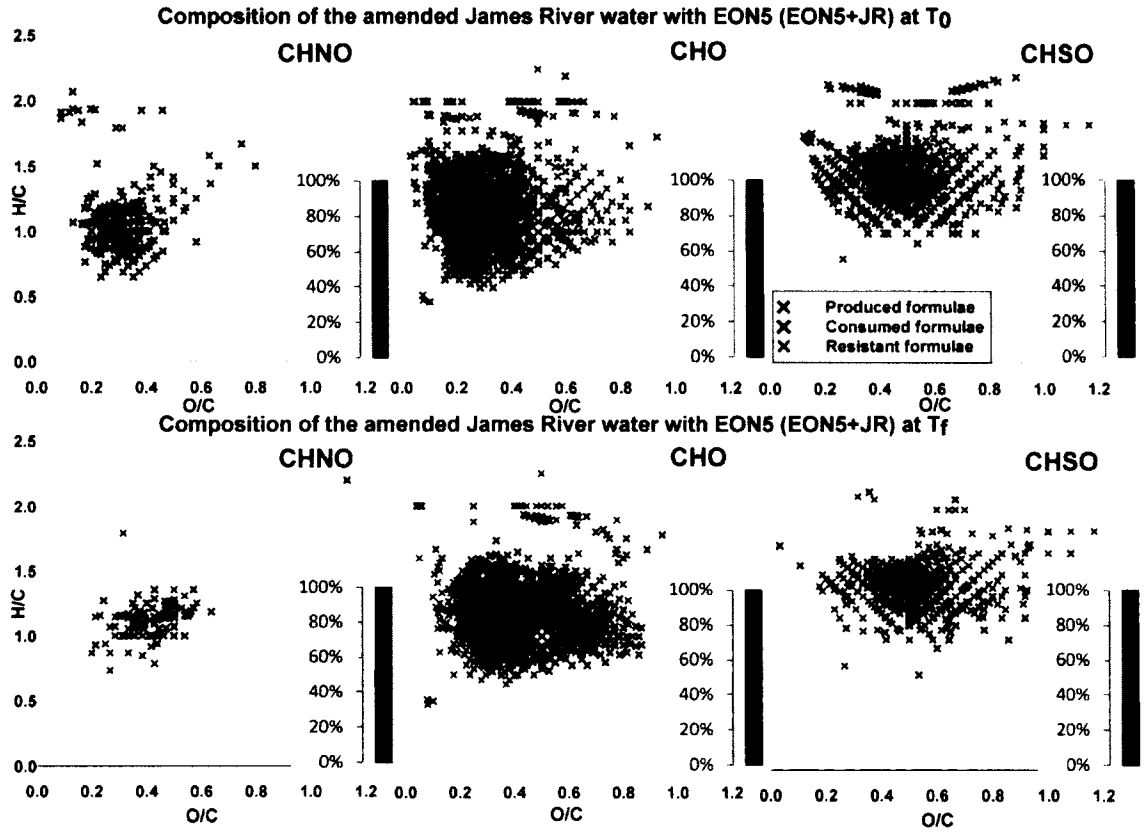

Figure 5. van Krevelen diagrams of the incubated EON5. VK diagrams showing the consumed, resistant, and produced formulae of the initial and final (CHNO, CHO, and CHSO) formulae in EON5+JR sample. Points in dark green represent EON5 peaks that disappeared upon incubation (consumed), points in red represent EON5 peaks that were unchanged (resistant), and points in blue denote new peaks that appeared during incubation (produced). Bar diagrams show the percent contribution of the consumed, resistant, and produced formulae in EON5 at time zero (T_0) and after incubation (T_f).

3.2.1.2. Chemical characterization of incubated EON5

3.2.1.2.1. Consumed DOM compared to the produced DOM

Consumed, newly produced, and resistant molecules were segregated according to the major groups of biochemical compounds present in the DOM (Figure 6). These

groups include: I) aliphatics, II) CRAM or lignin-like molecules, III) aromatics, and IV) molecules from other regions of the VK diagram. EON5-CHO formulae were sorted into these different groups using previously established rules (Hertkorn et al., 2006; Koch and Dittmar, 2006; Perdue, 1984). We extended these rules to apply to CHNO and CHSO formulae. Finding CHNO or CHSO peaks in these four regions means that the compounds defined by these regions were N-substituted or sulfurized. In general, EON5 showed a high level of reactivity (compounds were consumed) for both CHO and CHSO molecules, mainly from region I (31%; 54%), and region II (16%; 29%), respectively (Figure 6). In contrast, the consumption of CHNO molecules was mainly from region II (23%) and region III (52 %). The newly produced compounds were mainly attributed to region II, where 92%, 57%, and 25% of the produced CHNO, CHO, and CHSO molecules are CRAM or lignin-like molecules.

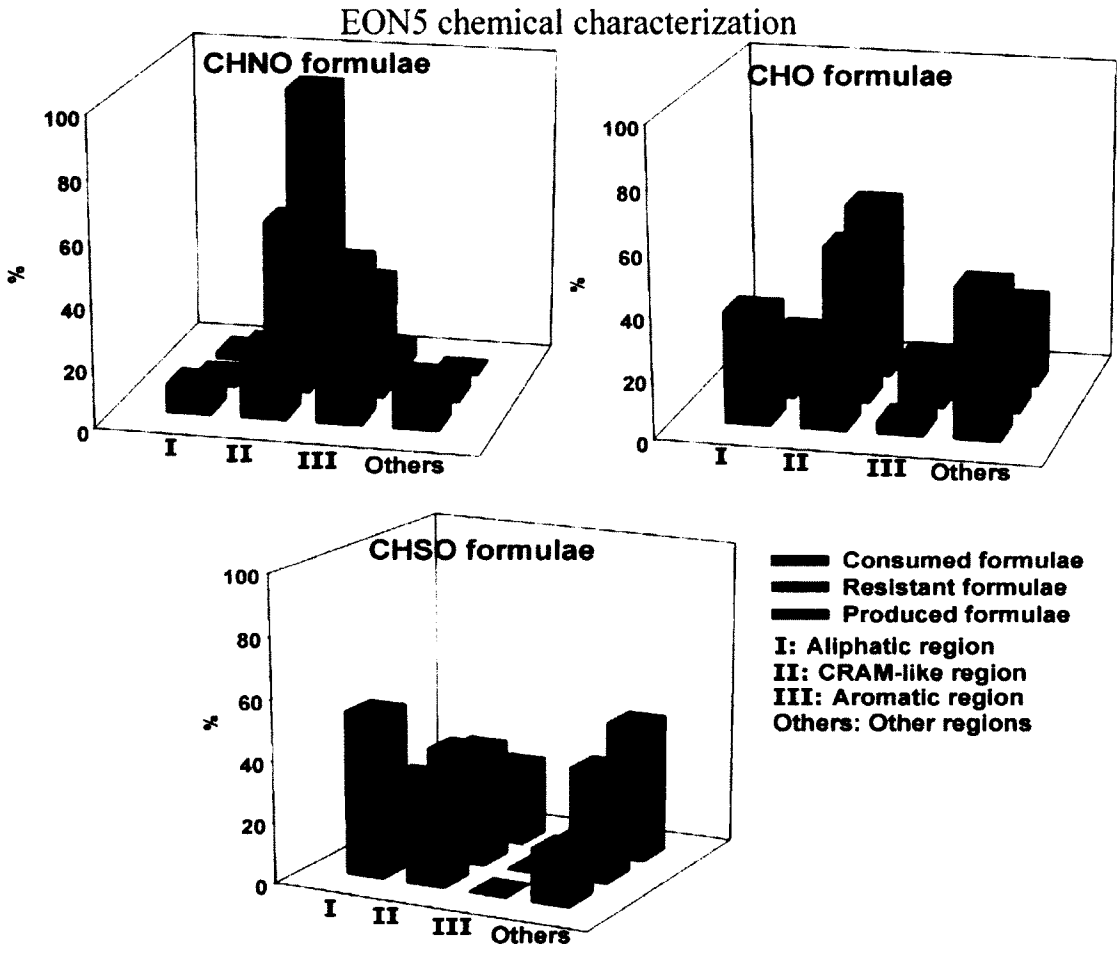

Figure 6. Chemical characterization of the incubated EON5. EON5+JR bar diagrams showing the chemical characterization of the consumed, resistant, and produced molecules in the three major subgroups (CHNO, CHO, and CHSO) upon incubation.

3.2.1.2.2. Refractory DOM

A fraction of EON5, about 21%, 64%, and 61% of CHNO, CHO, and CHSO formulae, respectively, was not degraded over the course of our incubation experiment (Figure 5, bar diagrams). The refractory portion of EON5 plotted mainly in the CRAM or lignin-like structural region, where about 56%, 51%, and 38% of the resistant CHNO, CHO, and CHSO molecules, respectively, were attributed to region II (Figure 6). These

results are consistent with the proposed refractory nature of CRAM and lignin molecules (Hertkorn et al., 2006; Opsahl and Benner, 1997).

3.2.2. EON4 effluent

3.2.2.1. Reactivity of EON4

Incubations amended with EON4 showed a remarkable production of new compounds compared to EON5 incubation bottles over the 48-hr bioassay experiment. When similar nominal mass regions of the JR water, EON4 and EON4+JR samples are compared before (T_0) and after incubation (T_f), a significant production of new peaks (denoted by solid circles •) was observed at nearly every nominal mass (Figure 7). Additionally, EON4 was significantly degraded; the peaks from the mass spectrum attributed to the EON4 addition (▲) either disappeared completely or significantly decreased in relative intensity compared to JR indigenous DOM (✱).

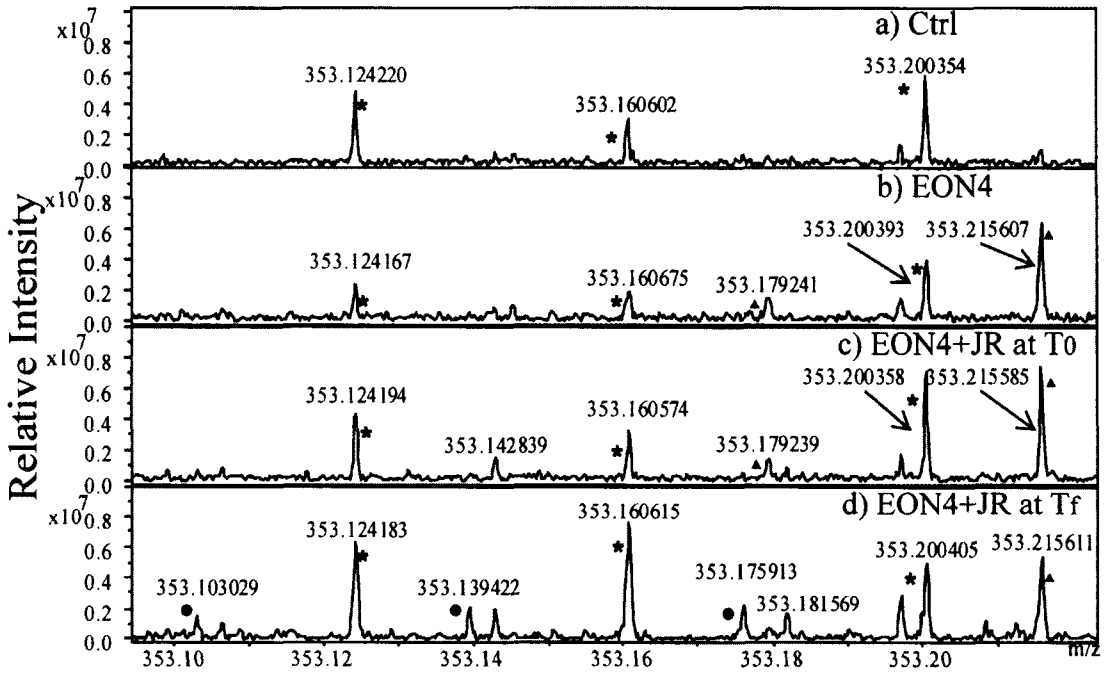

Figure 7. Reactivity of the incubated EON4. Negative ion mass spectra expanded at nominal mass 353 of (a) Control at T_0, (b) EON4, (c) EON4+JR at T_0, and (d) EON4+JR at T_f. Peaks added by the James River water are shown with solid stars, peaks added by the effluent are shown with solid triangles, and peaks produced upon incubation are shown with solid circles.

A 3-dimensional VK plot for the EON4+JR before and after the 48-hr incubation shows a significant production of compounds in all the subcategories (CHO, CHNO, and CHSO molecules) (Figure 4c,d). Approximately 100%, 86%, and 66% of CHNO, CHO, and CHSO formulae, respectively, were compounds produced during the incubations (Figure 8). About 100%, 77%, and 58% of the initial CHNO, CHO, and CHSO molecules, respectively, disappeared completely after the 48-h incubation (Figure 8). Overall, EON4 and EON5 mass spectra were dissimilar and incubations of natural water

amended with EON4 versus EON5 produced distinct results with net production of new compounds in the EON4-amended incubations.

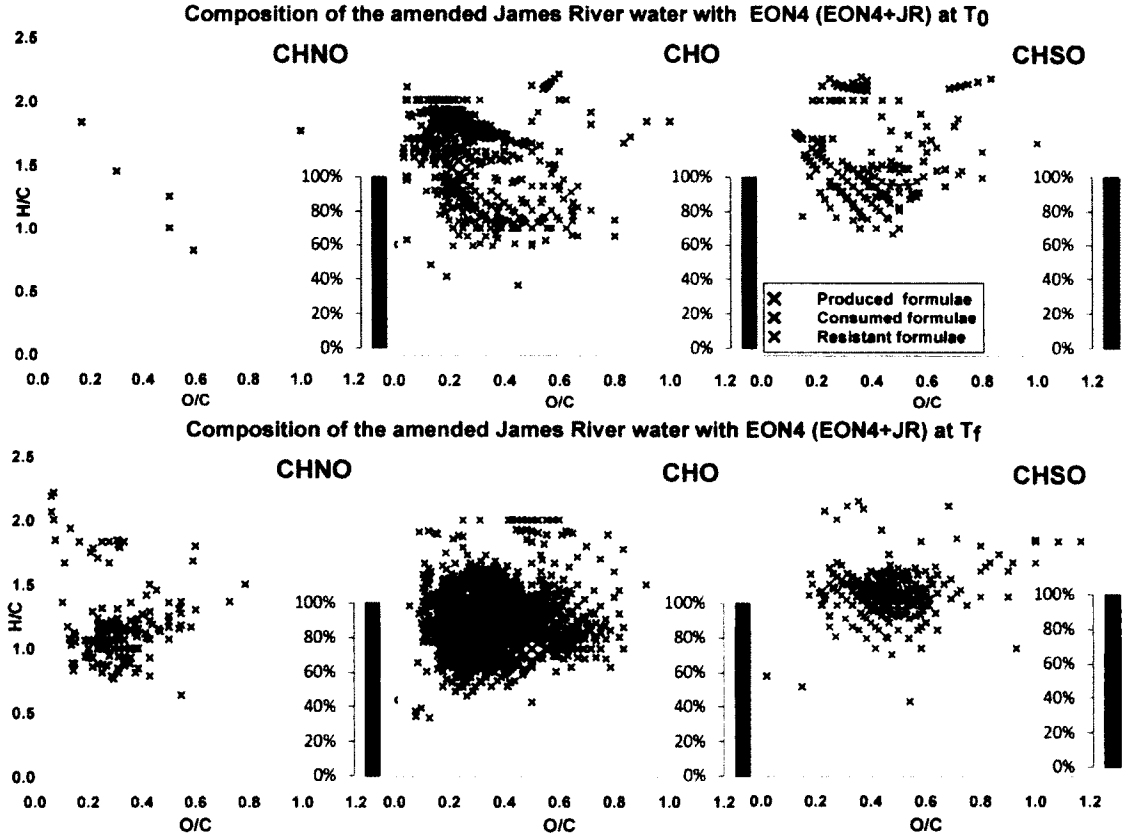

Figure 8. VK diagrams of the incubated EON4. VK diagrams showing the consumed, resistant, and produced formulae of the initial and final (CHNO, CHO, and CHSO) formulae in EON4+JR sample. Points in dark green represent EON4 peaks that disappeared upon incubation (consumed), points in red represent EON4 peaks that were unchanged (resistant), and points in blue denote new peaks that appeared during incubation (produced). Bar diagrams show the percent contribution of the consumed, resistant, and produced formulae in EON4 at time zero (T_0) and after incubation (T_f).

3.2.2.2. Chemical characterization of incubated EON4

3.2.2.2.1. Newly produced DOM

In the case of EON4, the newly produced CHNO formulae clustered mainly in region II (29%), and region III (36%), whereas the new CHO and CHSO molecules were mainly assembled in region I (35%), and region II (45%), respectively. Overall, EON4 exhibited production in all the major biochemical classes plotted in the VK diagram.

3.2.2.2.2. Refractory DOM compared to the consumed DOM

EON4 showed little resistance to degradation during incubations and a large percentage of the peaks observed in the spectrum of the incubated EON4+JR disappeared during the incubation period. Only about 0%, 30%, and 42% of CHNO, CHO, and CHSO molecules in the initial effluent, respectively, persisted through the incubation period (Figure 8, bar diagrams). These resistant molecules belonged mainly to region II (Figure 9). As in the case of EON5, these results are consistent with the belief that CRAM- and lignin-like compounds are refractory (Hertkorn et al., 2006; Opsahl and Benner, 1997). The consumed formulae were attributed mainly to region I. Approximately 33%, 82%, and 68% of the consumed CHNO, CHO, and CHSO formulae, respectively, were aliphatic (Figure 9). This preferential consumption of aliphatic molecules was more prominent in EON4 compared to EON5, where only 9%, 31%, and 54% of the consumed CHNO, CHO, and CHSO, respectively, were aliphatic. This difference in the degree of degradation and type of degradation is probably related both to differences in processes employed in the two WWTPs and the dramatic differences in influent (sewage from a collection system to EON5 versus some collection system sewage and frequently trucked septage with widely varying composition in

EON4). While the specific attributes that contribute to the differences in EON lability observed cannot be concluded here, the differences measured suggest that further evaluation of contributing factors is warranted.

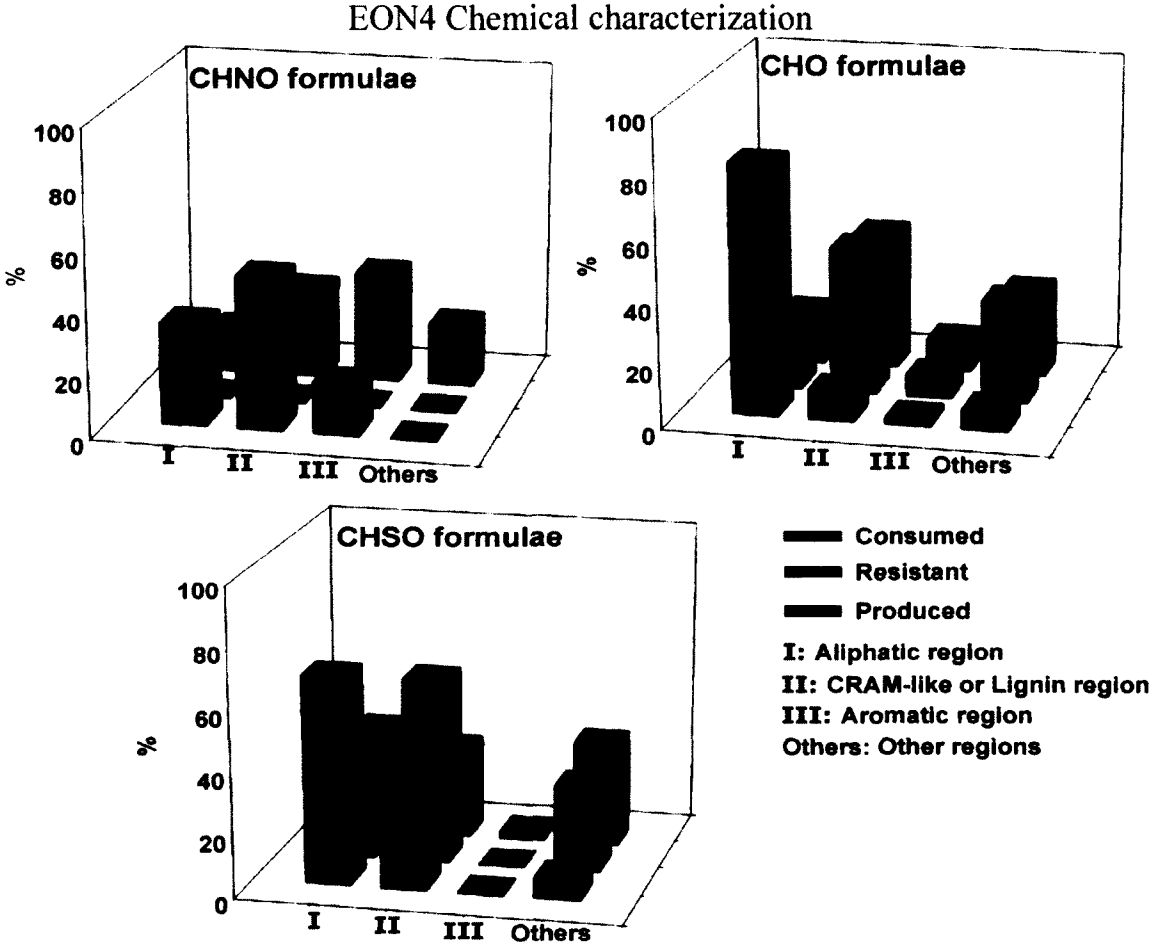

Figure 9. Chemical characterization of the EON4. EON4+JR bar diagrams showing the chemical characterization of the consumed, resistant, and produced molecules in the three major subgroups (CHNO, CHO, and CHSO) upon incubation.

4. CONCLUSIONS

EON from wastewater treatment plants that discharge into N-sensitive regions has the potential to be a significant contributor to the overall N load to a watershed. For this reason, it is important to develop methods that allow the lability of EON in natural waters to be determined. Although bioassay approaches have been used to understand the impact of effluents on microbial growth in receiving streams and estuaries (Bronk et al., 2010; Filippino et al., 2011), we demonstrate that advanced chemical analysis can demonstrate reactivity even under conditions where standard bioassays do not. Bulk chemical analyses of DON in effluents and in bioassays suggest that the net consumption of organic N in bioassays is variable (Bronk et al., 2010; Filippino et al., 2011), and that there can even be net production of DON (this study). However, the molecular-level chemical showed that many compounds are consumed and others produced during incubations with natural microbial communities and that the recalcitrant fraction of EON is low, ranging from 0-21%. Production and consumption of DON compounds within incubation bottles and natural systems masks the true bioavailability of EON in the environment. The nature of organic N varies based on the treatment processes employed and the wastewater received by those treatment plants, and this affects its reactivity in the environment. Here we examined just two treatment processes as a point of demonstration about how vulnerable bioassays are to misinterpretation in the absence of parallel chemical molecular analysis. At the same time, our advanced chemical analysis demonstrated that both the treated effluents examined here from two very different treatment processes were more reactive than was predicted from the net changes in bulk DON concentrations in the incubation bottles.

Our findings have important implications for management and suggest that it may not be appropriate to discount EON from nutrient loading estimates; rather, it should be counted towards the nutrient allocations for WWTP discharges to aquatic systems. Additional WWTP effluents should be screened to determine how labile EON is across a range of treatment plants that employ different treatment processes. Furthermore, it is not known if changes in treatment plant technologies, origin of the influent, or operation can be used to either reduce the amount of organic N contained in effluents or change its composition so that it is more recalcitrant to the environment into which it is discharged. Further studies on remediation strategies that address these questions are justified.

CHAPTER III

PHOTOCHEMICAL ALTERATIONS OF NATURAL AND ANTHROPOGENIC DISSOLVED ORGANIC NITROGEN IN THE YORK RIVER

PREFACE

The content of this chapter was submitted to the *Environmental Science & Technology* journal August 2014, and it is now *in review*.

Contributions: Rajaa Mesfioui developed experimental design with assistance from Dr. Patrick G. Hatcher. Dr. Abdulla is an expert on the two-dimensional correlation statistical analysis and provided assistance in displaying FTICR-MS results in the two dimensional correlation maps.

1. INTRODUCTION

Because they represent the interface between land and ocean, estuaries play a key role in mediating the Carbon (C), Nitrogen (N), and Phosphorus (P) biogeochemical cycles (Hedges, 1992; Howarth et al., 2011; Mackenzie et al., 2002), and in modulating the transfer of dissolved organic matter (DOM) from land to coastal ecosystems (Aufdenkampe et al., 2011; Hedges et al., 1997; Schlesinger and Melack, 1981). However, by being the downstream recipients of anthropogenic land use and urbanization, this role has been greatly impacted resulting in a shift from balanced, productive ecosystems into impaired and degraded ecosystems (Canfield et al., 2010; Dodds et al., 2008; Howarth, 2008). While land use practices and fossil fuel emissions constitute the main perturbations to the C cycle (Canadell et al., 2007; Le Quéré et al., 2009), poor management of agricultural activities and widespread urbanization represent the main perturbations to the N cycle (Galloway et al., 2004; Schlesinger and Bernhardt,

2013; Vitousek et al., 1997). Since DON is one of the main components of DOM, the above perturbations are the suspected culprits that alter DON biogeochemistry in coastal ecosystems (Altieri et al., 2009b; Lu et al., 2013; Meng et al., 2013; Williams et al., 2010).

While the lability of dissolved inorganic N (DIN, e.g., NO_x and NH_4) and its role as a pollution indicator are well established (Galloway et al., 2008; Howarth and Marino, 2006), the role of anthropogenic DON has regularly been overlooked by the scientific community (Bronk et al., 2007). The view that DON in marine environments forms a persistently stable pool of N, compared to the constantly depleted DIN pool, is responsible for the traditional belief that DON is mostly bio-refractory, cannot be taken up by phytoplankton, and hence does not contribute to eutrophication. While anthropogenic DIN export from disturbed watersheds to the oceans has been the focus of widespread international research, DON pollution has received less attention. Lately, however, Pellerin et al. (2006) compiled N data for 348 disturbed watersheds reporting that DON represents, on average, 49% of TDN concentrations in mixed watersheds and that DON concentrations are, on average, 2.5–4 times higher in surface waters from disturbed watersheds than in forested watersheds, suggesting that DON concentrations are highly influenced by N loads in human impacted catchments. Therefore, the dominant form of N in human-impacted watersheds has been overlooked as a potential source of bioavailable N and its reactivity has been neglected for almost a century.

Recently, the preconceived view that DON is bio-refractory has been challenged in the literature with emerging evidence for its bioavailability and its role in fueling primary production (Bronk et al., 2007; Mulholland and Lomas, 2008; Seitzinger et al.,

2002). While these studies have shed some light on the importance of DON in both C and N cycles, they lacked the ability to investigate its structural complexity in order to draw a conclusive picture on the dynamics of natural and anthropogenic DON from landscapes to receiving waters. Most studies of DON dynamics are limited to examining the net changes in concentrations of particular nitrogen species over time and/or quantifying the net change of DON using bulk analysis (Bronk et al., 2010; Filippino et al., 2011; Seitzinger et al., 2002). Mesfioui et al. (2012) demonstrated that true reactivity can be readily masked by examination of bulk changes in DON, mainly because degradative losses can be offset by new production in a metabolically and photochemically active system. They showed that molecular-level geochemistry capable of distinguishing between new production and degradative loss is needed to evaluate the extent of DON transformations. Such specificity is afforded by use of electrospray ionization coupled to Fourier transform ion cyclotron resonance mass spectrometry (ESI-FTICR-MS), a technique that provides the ability to obtain unique elemental formulas for components of DOM and DON. It is also of critical importance to investigate whether DON is generated *in situ* via the conversion of inorganic N or exported as DON from point and non-point sources within disturbed watersheds.

Photochemistry is considered one of the main processes that governs the fate and turnover of DOM along the land-to-river-to-ocean continuum (Opsahl and Benner, 1998) (Smith and Benner, 2005; Stubbins et al., 2010; Wiegner and Seitzinger, 2001). In contrast to the numerous studies published on DOM photochemistry (Amon and Benner, 1996; Mopper et al., 1991; Stubbins et al., 2010), little is known about the response of DON and inorganic N to photochemical transformation. This is especially true for

anthropogenic DON, considering that it is dogmatically considered to be recalcitrant and that there are limitations to methods for its characterization (Vähätalo and Zepp, 2005).

In the current study special attention is paid to assess quantitative and qualitative similarities/differences of three types of DOM and its component DON from natural and anthropogenic sources under the influence of long-term photoirradiation to better understand the ecological significance of DON in disturbed watersheds and to elucidate the impact of land-use changes on the reactivity and the transfer of DOM from sources to receiving waters of the York River System in southeastern Virginia. To the best of our knowledge, this is the first study to molecularly investigate long-term photoirradiation of anthropogenic DOM and DON while, at the same time, comparing them with natural sources of DOM and DON using ESI-FTICR-MS.

2. EXPERIMENTAL PLAN

2.1. DOM sample collection, handling, and irradiation

A total of three different types of samples were collected. The first sample was obtained from Sweet Hall Marsh (SHM) associated with the Pamunkey River, a major tributary of the York River estuary in March 2012. SHM represents a typical source of naturally derived DOM from marshes and tidal swamps that line the banks of the York River-estuary System. The other two DOM samples were collected November 2011 from anthropogenically-impacted areas of the York River System. The King William sample (KW) is a grab sample from the Pamunkey River, collected at a site impacted by agricultural runoff from the Old Town Farm located in King William County. This sample combines both natural and anthropogenic DOM. The other site is the effluent of the West Point (WP) wastewater treatment facility of the Hampton Roads Sanitation

District, a plant that is relatively small (~0.40 million gallons of effluent per day). The plant receives a variable influent containing both domestic and commercial discharges and uses primary clarifiers, trickling filters, aerobic digesters, hypochlorite disinfection and dechlorination processes. The average total nitrogen (TN) of WP effluent is around 17.1 mg-N/L (Bott, 2014).

Samples were collected using acid-cleaned and pre-conditioned polypropylene buckets and were passed through 0.2 μm filters on site, then transported to Old Dominion University on ice. Upon arrival, samples were filtered 0.1 μm to remove any residual bacteria and/or particulate matter. To better track molecular changes of extensively photodegraded DOM from these different sources, and to provide an understanding of its optical properties without going below instrument detection limits, long-term photoirradiation exposure was needed, and hence sample concentration was required. Furthermore, to prevent DOM remineralization in a short time period, and to minimize any difference in light shielding between samples, SHM, WP, and KW samples were concentrated approximately 20, 9, and 16 fold, respectively, to reach similar final DOC concentrations of about 95 ppm, using a rotary evaporator system that was maintained at 35 °C. Sub-samples of the concentrated samples were retained for nutrient and chemical analysis. After concentration, samples were subdivided into three equal volumes (330 mL) and were transferred to ~550 mL quartz round bottom flasks and exposed to irradiation for 50 days inside a solar simulator containing 12 Q-Panel ultraviolet UVA-340 bulbs (approximate integrated irradiance 25 W m^{-2}) which provides a spectral shape similar to that of natural sunlight from 295 nm to 365 nm (Minor et al., 2007). These wavelengths are responsible for nearly all photochemical reactions in the natural

environment (Mopper et al., 1991). The solar simulator provided 127% of the photobleaching that occurs under winter midday sunlight in the lower Chesapeake Bay (36.9° N latitude)(Minor et al., 2007). Knowing that integrated light-dose, and not light intensity, is entirely responsible for the generated photochemical reactions (Jankowski et al., 1999), we choose this continuous light-exposure approach to allow for reproducible irradiation conditions, which can ease the comparison between the different sources of DOM. The flasks were covered with combusted glass lids to avoid bacterial contamination. All flasks were opened and agitated twice a day to assure saturation of dissolved oxygen. Temperature was monitored during the entire photo-irradiation time and was found to be constant at 26.5-28.5 °C. Because of limitation on sample volume and solar simulator space, dark controls of the studied samples were not used. However, a dark control of terrestrial DOM subjected to the same experimental conditions showed no detectable carbon losses throughout a 60 days light-exposure (Chen et al., 2014). Aliquots of 10 mL were retrieved at the frequency of 2d from each flask and were sub-sampled for UV-visible absorbance spectroscopy, NH_4, NO_x, DOC, and TDN analyses. Sub-aliquots (5mL) of 13-selected time point were saved for ESI-FTICR-MS analyses (discussed bellow).

2.2. Bulk analysis

Dissolved organic carbon (TOC) and total dissolved nitrogen (TDN) concentrations were measured for each aliquot using the high temperature combustion (720°C) catalytic oxidation method (Shimadzu TOC/TN-5000) (Peltzer et al., 1996). Ammonia (NH_4) concentrations were analyzed using the phenol hypochlorite colorimetric method (Hansen and Koroleff, 2007). We were able to measure NO_x

concentrations using a Lachat QuikChem 8500 autoanalyzer of WP aliquots only (Parsons et al., 1984); the sub-samples from KW and SHM were exhausted by another unreliable NO_x method employed initially and later abandoned. DON concentrations were determined by subtracting the concentrations of NO_x and NH_4 from TDN concentrations (Bronk et al., 2000).

2.3. UV-visible absorption spectroscopy

UV-visible absorption spectra (190-900 nm) were measured for the irradiated samples using an Agilent 8453 diode array spectrophotometer with a 1 cm quartz cuvette. Samples were diluted 10 times before measurements. Ultrapure water (Millipore) was used as the blank. Absorbance values were corrected to account for instrument baseline drift, refractive index, and temperature variation according to Green and Blough (1994) and converted to Napierian absorbance coefficients using the following formula:

$$a = 2.303A/l$$

where a= absorbance coefficient (m^{-1}), A= absorbance, and l = path length (m). Spectral slope ratios (S_R) and specific UV absorbance (SUVA) were calculated using the approach of Helms et al. (2008) and Weishaar et al. (2003).

2.4. Mass spectral analyses

Sub-aliquots (5ml) of each selected time point at 0, 3, 5, 7, 11, 16, 18, 23, 25, 28, 33, 42, and 50 days were prepared for mass spectral analysis by passing the samples through PPL solid phase extraction cartridges (Agilent, Bond Elut PPL) following the procedure recommended by Dittmar et al. (2008). The whole cartridge was kept at low temperature (4°C) 1-2 weeks before MS analyses.

All MS analyses were performed at the College of Sciences Major

Instrumentation Cluster (COSMIC) at Old Dominion University using an Apollo II ESI ion source coupled to a Bruker Daltonics 12 Tesla Apex Qe FTICR-MS. Prior to analysis, the instrument was externally calibrated using polyethylene glycol. Right before introduction to the ESI, each sample was eluted from the PPL cartridge using 4 mL of LC-MS grade methanol and later diluted with LC-MS grade water to a uniform TOC concentration (~10 ppm). Samples were then spiked with 0.1% ammonium hydroxide (increasing the pH to 8) to increase the ionization efficiency. Sample flow rate was maintained using a syringe pump and the ESI voltages for each sample were maintained at 3.4 kV on the spray shield and 4.1 kV on the capillary under 200 °C in order to maintain a consistent ion current entering the capillary to the MS.

All samples were analyzed in negative ion mode to minimize complications due to sodium adduct formation. Electrospray voltages and mass spectrometer parameters were held constant throughout all experiments. Ions were accumulated in a hexapole for a period of 2s before transfer to the ICR cell. This accumulation time was found to be optimal; because shorter ion accumulation times resulted in fewer peaks with lower S/N, while longer times led to poor resolution. For each sample, 300 time-domain transients were acquired (at 4M Word), zero-filled once, sine-bell apodized, and then Fourier transformed in the Bruker data analysis software, resulting in an overall analysis time of approximately 30 minutes per sample.

2.5. Mass calibration and molecular formula assignments

The general mass distribution of compounds that were ionized in all samples was in the range of 200-700 m/z, which is consistent with previous DOM studies using ESI-FTICR-MS (Koch et al., 2005; Sleighter et al., 2008b). Because low m/z peaks (<200)

have very high frequencies, the excitation required to increase the ion radius to a sufficient amplitude in order to induce enough current to be detected by the detection plates is more difficult. Furthermore ions below 200 are discriminated against in the quadrupole, where ions of a broad specified m/z range are allowed to pass through before being accumulated in the hexapole, and then transferred to the ICR cell. Our samples were analyzed in broadband mode, meaning we used a wide m/z range (100-2000) however peaks were only detected and observed in the range of 200-700 m/z. The eventual loss of peaks above 700 m/z can be attributed to space charge effects within the ICR cell that can result in a decrease of high molecular weight signals (Kujawinski et al., 2002). All acquired spectra were internally calibrated with indigenous fatty acids providing a mass accuracy of 1 ppm or less throughout the mass range of interest (Sleighter et al., 2008a). Molecular formulae were assigned to peaks with a signal to noise (S/N) ratio > 3 in the mass range of 200-700 m/z by means of a Formula Calculator Program (v.1.0 © 1998 NHMFL) that was developed at the National High Magnetic Field Laboratory in Tallahassee, FL. In our study, the vast majority of formulas were unambiguously assigned below m/z 500, because we only allow up to 0.5 ppm error in assigning correct molecular formulas. When multiple assignments existed for a single m/z value, the correct formula was assigned based on elemental rules, on elemental rules, functional group relationships, and patterns and homologous series, as described in detail previously in the literature (Koch et al., 2007; Koch et al., 2005; Stubbins et al., 2010) and in appendix C in this thesis.

2.6. Statistical analysis and 2D Correlation

To visualize and highlight geochemical differences in the large data set generated

by FTICR-MS, we applied two statistical approaches, principal component analysis (PCA) and two-dimensional correlation analysis as described by Sleighter et al. (2010) and Abdulla et al. (2013b), respectively.

2.6.1. Principal component analysis (PCA)

PCA compresses a multidimensional sample space into fewer dimensions by seeking out the directions with most variability and then projecting the information onto these dimensions. The first dimension, PC1, is aligned with the direction of maximum variance. The second dimension, PC2, in the next direction contributes to most of the residual variance, and so on. The scores represent the projection of the original data onto each PC. The loadings, however, decipher the relation between original variables and PC dimensions by plotting each variable contribution to the data variability along each PC. For each sample (WP, SHM, and KW), formulas from each category (CHO or N-containing elemental formulas) of all sub-samples (i.e., day 0, day 3) were compiled in one data sheet and then condensed by removing duplicate formulas in order to make a master list that comprises formulas existing in each sub-sample spectrum, resulting in 6 individual data matrices. Relative magnitude of each corresponding peak in each sub-sample spectrum was then calculated. When a formula from the master list is not present in the sub-sample spectrum, zero is then assigned. Herein, we choose to plot our data onto a two-dimensional PCA projection (biplots) since most variances in our datasets (50%-88%), of the total variance, were explained by PC1 and PC2.

Even with its great usefulness in depicting the differences and similarities between FTICR mass spectra and simplifying the comparison between highly complicated formula lists, PCA is geometrically oriented and lacks the ability to examine

the correlation between formulas and to illustrate their responses under different external perturbations. Therefore, we are also applying 2D correlation analysis to our datasets.

2.6.2. Two-dimensional correlation spectroscopy

This technique examines the changes between individual spectral variables (i.e., number of molecular formulas) under specific perturbations (i.e., photoirradiation exposure time) and displays the results in two kinds of two-dimensional maps: the synchronous and asynchronous maps. Herein, the 2D correlations are applied to the FTICR-MS datasets in two different ways: first, by using the H/C ratio to investigate the changes in the molecular formulas based on presence or absence of formulas; second, by correlating the changes in the carbon number of individual formulas with each other. Only synchronous data and maps were utilized.

For the H/C ratio, the CHO-containing formulas in each sample were classified according to their H/C ratio in the range from 0.00 to 2.50 with increments of 0.01. The synchronous 2D correlation was conducted to examine changes in number of formulas at specific H/C ratios along the photoirradiation exposure time (n=13 samples).

To investigate the changes in carbon structure backbone of the CHO formulas, the molecular formulas were grouped based on their number of carbon atoms, ranging from 4 to 60 carbon atoms at increments of one carbon atom. Synchronous 2D correlation analysis was applied to each dataset using photoirradiation exposure time as the perturbation. In a similar manner, 2D-correlation analysis was applied on both the H/C ratio and carbon number for nitrogen-containing formulas. These 2D correlation analyses were conducted on SHM and WP samples.

3. RESULTS AND DISCUSSION

3.1. Slope ratio and DOC

Upon irradiation S_R increases while $SUVA_{254}$ and DOC concentrations decrease (Figure 10a,b and Figure 11a). The extent of photodegradation, based on the DOC concentrations, is similar for the three samples, where we observe 59%, 55%, and 53% of DOC loss in KW, SHM, and WP, respectively, after 50 days irradiation time. S_R shows the highest increase, in the first 25 days, for WP and SHM (from 1.07 to 3.5 and from 0.98 to 3.34, respectively) in comparison to KW, which exhibits shallower increase (from 0.91 to 1.98, respectively). Helms et al. (2008) suggested that photobleaching destroys chromophores associated with high MW CDOM, causing CDOM to partially shift from the high MW to the low MW fraction. Their study demonstrates that S_R relate inversely to chromophoric DOM average molecular weight. Our FTICR-MS results confirm this relationship where changes in the magnitude weighted (M_w) MW (Figure 1d) of each sample correlate significantly with S_R. Our results show a steady decrease of each sample MW in the first 25 days of irradiation time. After 25 days S_R starts decreasing in the WP case, while continues increasing in both SHM and KW cases. This shift from high to low S_R in the WP cases, which is parallel to a shift from low to high MW compounds, can be attributed to WP system shifting from photobleaching to photohumification process (Kieber et al., 1997).

Wastewater effluents represent ideal liquors for photohumification to take place. Their distinctive organic composition (~50% proteins, 40% carbohydrates, and 10% fats and oils, besides trace amounts of priority pollutants (Shon et al., 2006)) and their high DIN content can promote photoinduced DIN incorporation to produce newly formed

DOM and/or condensation of the LMW organic substrates to form HMW molecules. This hypothesis will be further investigated using both bulk analysis and ESI-FTICR-MS analysis.

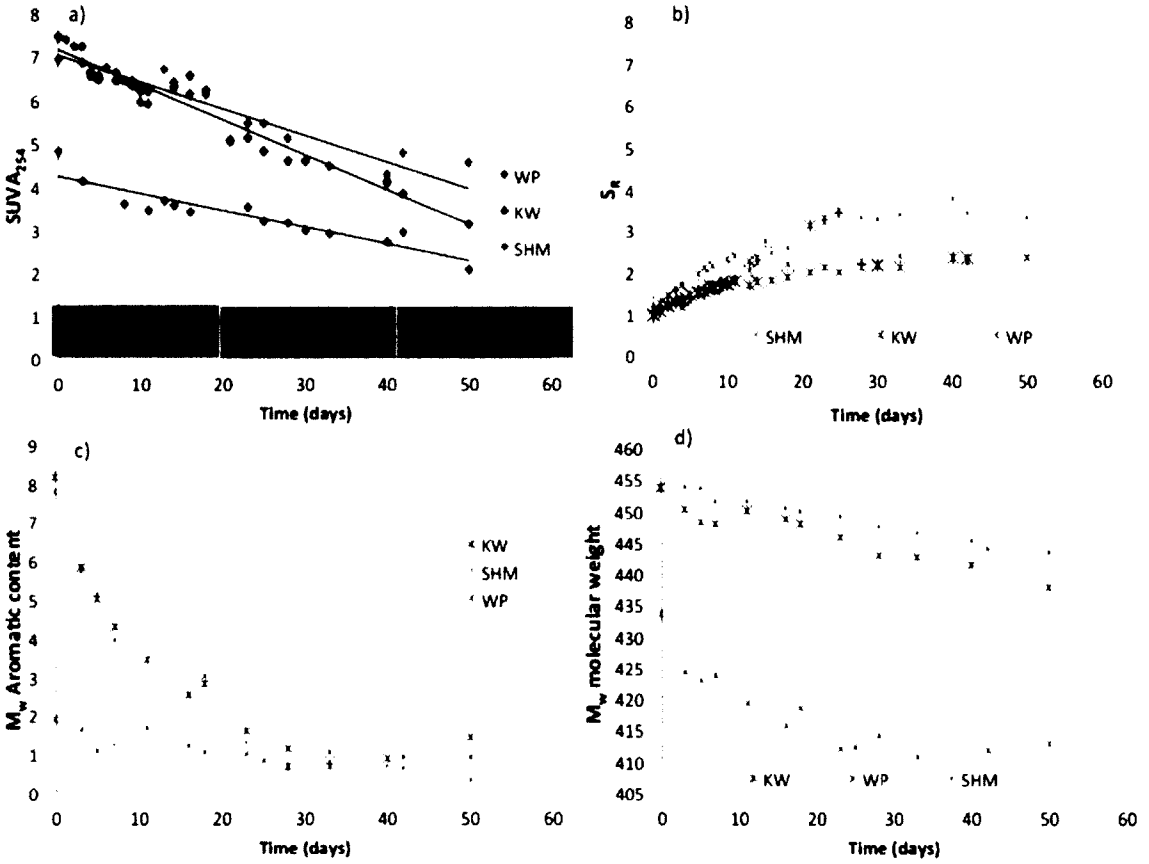

Figure 10. The trends of decreasing (a) specific UV absorbance ($SUVA_{254}$), (c) magnitude averaged aromatic content, (d) magnitude averaged molecular weight, and increasing (b) slope ratio (S_R) with increasing irradiation time.

Another heavily used DOM spectral parameter in the literature is $SUVA_{245}$, where several studies have related the decrease in this parameter to selective degradation of the aromatic and/or the highly conjugated DOM moieties (Del Vecchio and Blough, 2004). FTICR-MS data show the aromaticity losses induced by irradiation match the $SUVA_{254}$

reduction pattern in all samples (Figure 10a,c). Therefore, the elevated aromaticity and the apparent high MW compounds for SHM and KW are all indicative of terrestrial origin. On the other hand, the low apparent MW and aromaticity associate WP with "fresh" biologically produced DOM (Cory and Kaplan, 2012; Fasching and Battin, 2012). Thus, by combing these two analytical methods, we are able to substantiate our hypothesis that DOM from anthropogenic input is highly different than naturally derived DOM in term of molecular size, signature and optical properties. By using this approach we also demonstrate that DOM photo-induced alterations might depend significantly on sources and composition.

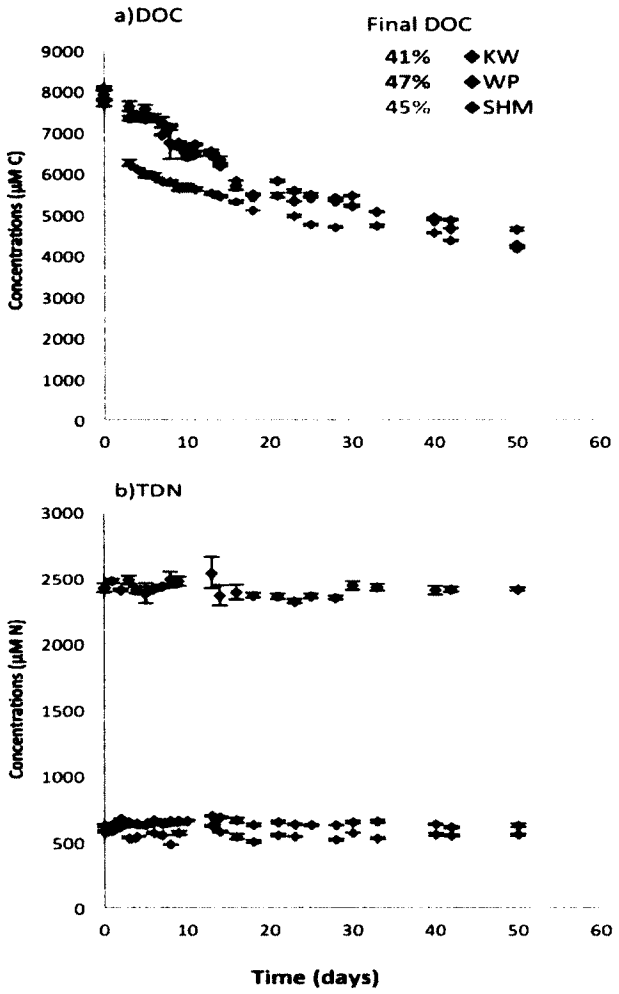

Figure 11. Total dissolved organic carbon concentrations (a) and total dissolved nitrogen (b) versus irradiation time for SHM, WP, and KW samples.

3.2. Inorganic N species and DON

Light exposure has little to no effect on the TDN concentrations, that are similar before and after light exposure (Figure 11b), in agreement with previous studies by Simsek et al. (2013). The fact that TDN remains constant is important from a mass balance perspective because it indicates that the system remains a closed system with no possible bacterial contamination throughout the experiment. While TDN remains

constant, there are significant shifts in concentrations among the different components of TDN.

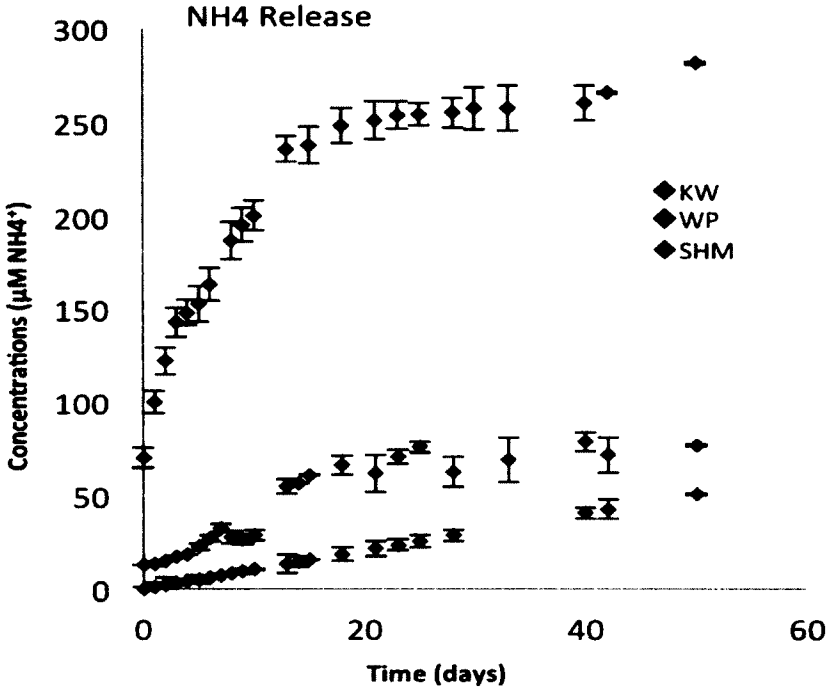

Figure 12. Ammonia release versus irradiation time for WP, SHM, and KW samples.

Photoproduction of ammonia is observed in all three samples (Figure 12), consistent with previous studies (Bronk et al., 2010; Tarr et al., 2001). However the extent of ammonia production is higher in the WP case, an expected trend considering that WP has the highest TDN concentration. We do notice a steeper production of ammonia before day 25 and a leveling of concentration afterwards. In the specific case of the WP samples, the only ones for which we have NO_x concentrations, the steady increase in ammonia is coincident with a slight production of NO_x (Figure 13). However, a sharp decrease in NO_x is observed when ammonia production stabilizes after day 25.

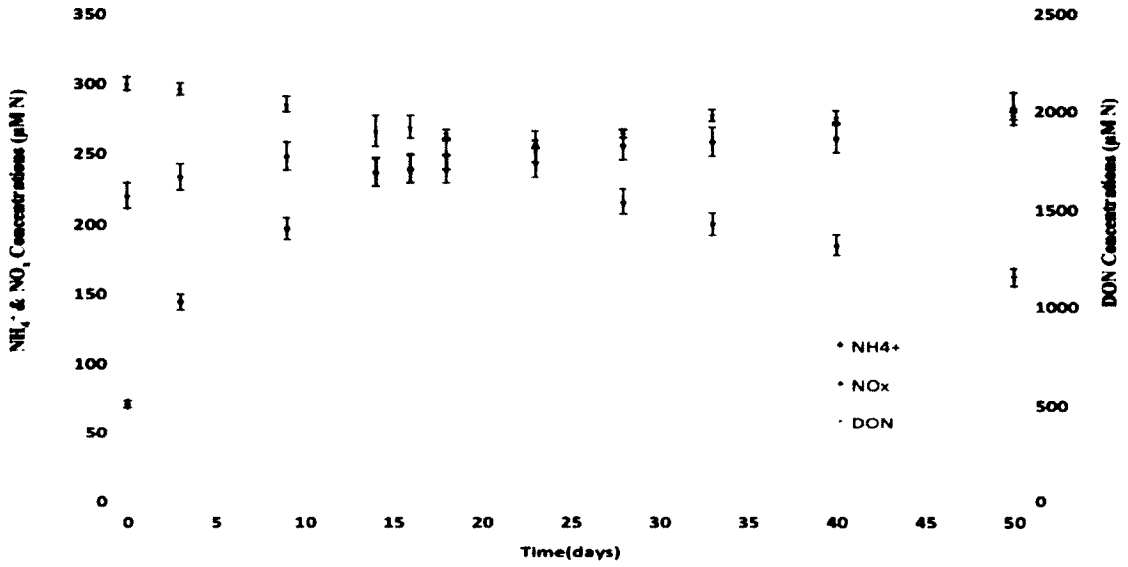

Figure 13. Ammonia, NOx, and DON concentrations versus time for WP effluent.

Upon photodegradation, DON initially declines due to significant mineralization of the organic matter in the samples. This trend is observed before day 25 and coincides with the buildup of ammonia and NO_x (Figure 13). After day 25, however, DON concentrations show a reversal and start increasing while NO_x concentrations decrease. This can be explained by the reaction of either NO_x or ammonia with DOM to produce newly formed DON. While this explanation has been suggested previously by Helms et al. (2013), it is additionally supported by state-of-the-art analytical and statistical methods discussed below. Although, bulk analyses may show a significant mineralization of DON into bioavailable DIN, under light exposure, they lack the ability to draw a clear picture of the DON molecular changes when exposed to a long-term photoirradiation. We used ESI-FTICR mass spectrometry along with PCA and the 2D

correlation statistical tools to elucidate theses changes more accurately where bulk analyses do not.

3.4. ESI-FTICR-MS analysis

All obtained ultra-high resolution mass spectra of DOM contain the routinely observed complex pattern of multiple peaks at each nominal mass over the studied range (m/z 200-700) (Kim et al., 2003; Kujawinski et al., 2004; Sleighter and Hatcher, 2008b; Stenson et al., 2003). We extracted exact formula assignments for the thousands of peaks in each sample and sub-categorized them according to their elemental make up as being those of DOC (formulas containing C, H, and O only) or DON (formulas containing N). For WP, KW, and SHM, respectively, the initial percent contribution to total peaks, based on numbers of peaks, is 55%, 74%, and 74%, for CHO formulas and 16%, 19.7%, and 22.8% for N-containing formulas. Furthermore, the percent based on peak relative magnitudes is 52%, 91%, and 90%, for CHO formulas, and 21%, 6%, and 9%, for N-containing formulas for WP, KW, and SHM, respectively. This data shows a clear difference between the wastewater effluent WP and the two other samples KW and SHM, where the magnitude-weighted percentages for WP N-containing formulas are higher than their corresponding number percentages, signifying that these formulas are for peaks present at higher magnitudes in the FTICR mass spectra. Whether this indicates that their corresponding molecules exist at higher concentrations in the original sample is impossible to assess due to the unknown ionization responses of these molecules and it is beyond the scope of our current ability to differentiate.

The assigned formulas can also be subcategorized into specific compound classes in DOM using van Krevelen (VK) plots, two-dimensional plots of O/C ratio versus H/C

ratio (Kim et al., 2003; Stubbins et al., 2010). The VK diagrams of the three initial samples including all types of formulas before irradiation are shown in Figure 14. The VK diagram shows WP comprising mainly aliphatic-like structures where 45% of the assigned formulas plot in the aliphatic region of the VK diagram (Perdue, 1984). On the other hand, KW and SHM largely comprise molecules that are lignin-like or carboxylic-rich alicyclic molecules (CRAM/lignin-like), where 60% and 58% of their formulas fall, respectively, in this region of the diagram (Hertkorn et al., 2006). Moreover, changes in carbon number, double bound equivalent (DBE), N/C, and O/C molar ratio confirm the distinctive characteristics of WP in comparison to SHM and KW (Figure 15). In fact, while SHM and KW molecular patterns demonstrate extensive photobleaching indicated by carbon backbone cleavage and loss of aromaticity (decrease in C number and DBE), WP shows a shift from photobleaching to photohumification denoted by an increase in carbon number and DBE after day 25, implying condensation of LMW molecules to form HMW molecules. Furthermore, the sharp increase in N/C molar ratio, in the WP case after day 25, substantiates the photoinduced DIN incorporation hypothesis (Figure 15c). Hence, our findings suggest that anthropogenic input will drive substantial variation in riverine DOM, and, thus, estuarine optics and photochemistry and therefore bioavailability (Fasching and Battin, 2012; Hopkinson et al., 1998; Ortega-Retuerta et al., 2007).

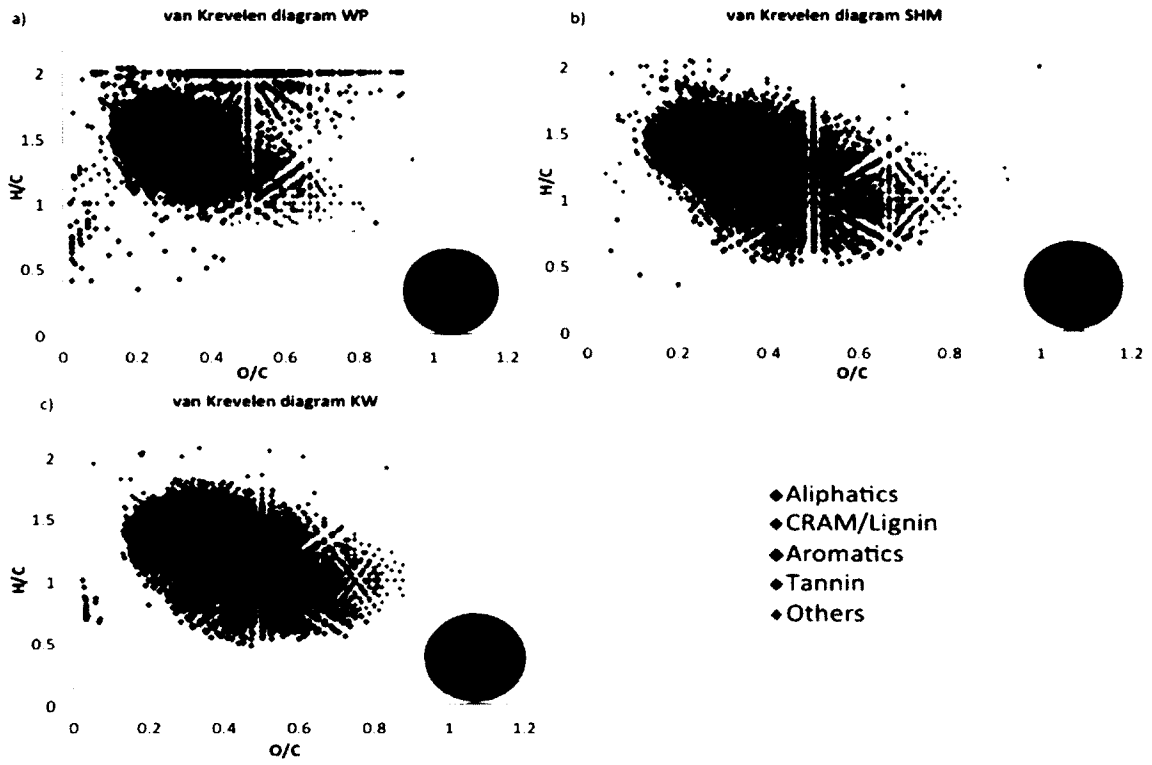

Figure 14. van Krevelen diagrams of WP, SHM, and KW, color coded to highlight the formulas aligning in the regions of the major biomolecular classes of DOM. Pie charts show the percent composition of each compound class for each sample.

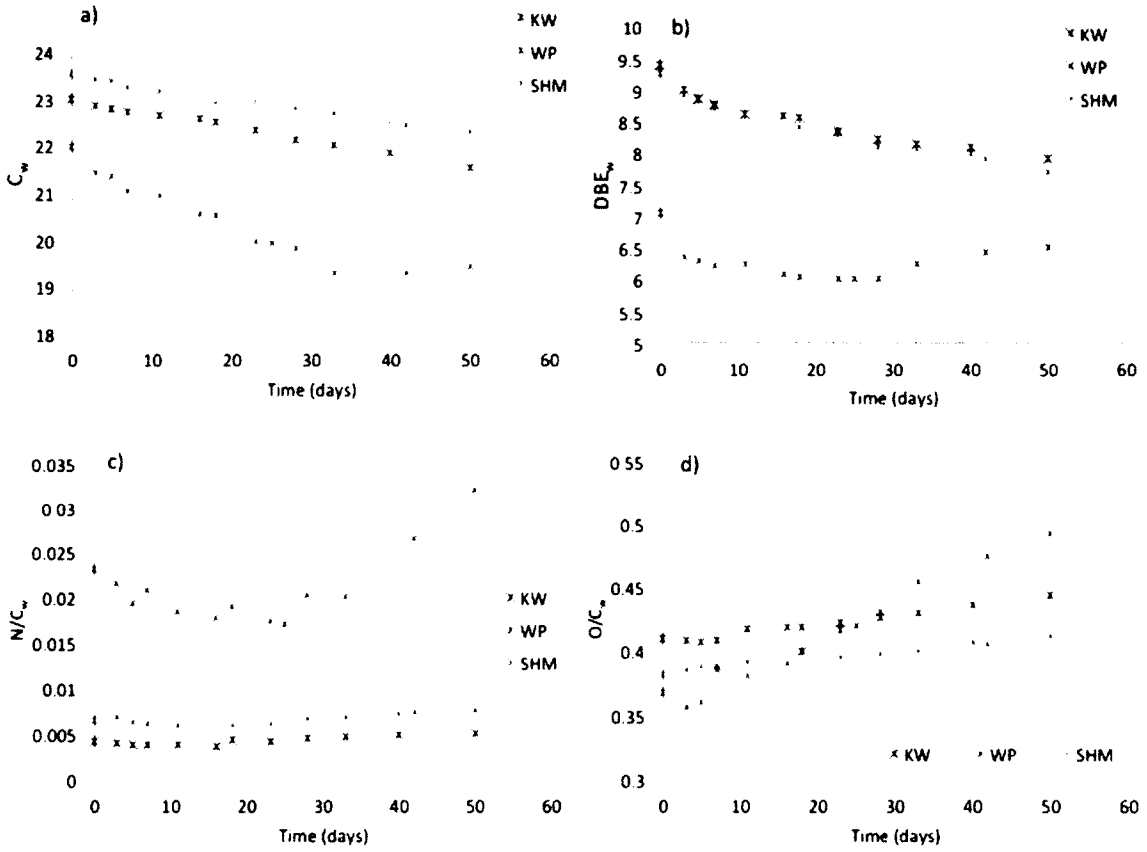

Figure 15. Magnitude-weighted (a) carbon number, (b) DBE, (c) N/C, and (d) O/C values for WP, SHM, and KW samples with irradiation time.

3.5. Statistical analysis

3.5.1. Principal component analysis

Molecular changes occurring during irradiation are recorded by measuring the disappearance and appearance of specific molecular formulas in the FTICR-MS data set for each sample. By individually applying PCA analysis to each of the 13-time series of each sample using CHO formulas or the N-containing formulas as the variables, we can identify molecules associated with the photo-labile and photo-produced pool of DOM from each source while photoirradiation progresses. The resulting PCA biplots, using CHO formulas as variables, are shown in figures 16-18. The biplots of the scores (i.e.,

Figures 16a-18a) represent the projections of the original samples onto each principal component (PC). However, the variables' loadings (i.e., Figures 16b-18b) signify the projections of all the chosen variables (i.e., the relative magnitude of the WP-CHO formulas) against each PC (i.e., PC1 and PC2), which explains the variable's contribution to samples variability along each PC. PC1 and PC2 explain ~53% and 16% of the variance for WP-CHO and 63% and 25% for SHM-CHO compounds, and 62% and 12% for KW-CHO. The high values of PC1 and PC2, for the three samples, imply a linear relationship between the two PC components, and suggest that the majority of the photoirradiated sub-samples can be included in a two dimensional space (Sleighter et al., 2010). According to the three samples' scores (Figures 16a-18a), the PCA analysis separated the irradiated subsamples along PC1, where the initial sample (0) had a very high positive PC1 score and the final sample (50) had the lowest PC1 score. It is also clear that the sub-samples can be grouped into three area clusters, area 1 (A1) denotes sub-samples at early stages of photodegradation including the untreated sample, area 2 (A2) represents sub-samples at the middle stages of the photodegradation experiment, and area 3 (A3) characterizes sub-samples at the end of the experiment. By relating the location of the scores of the samples (Figures 16a-18a) and the juxtaposed formulas from the variables' loading (Figures 16b-18b), corresponding to A1, A2, and A3 in each sample, we can extract formulas that are enriched in samples of each area cluster, and by plotting theses formulas on VK diagrams, we can extrapolate changes occurring at the molecular level as the photodegradation progresses. By plotting formulas contained in each boxed area cluster, the resulting VK diagrams (panels (c-e) in Figures 16-18) show clusters in specific regions of the diagram associated with each area. Thus, the clusters

indicate which type of formulas explains most of the variance in PCA.

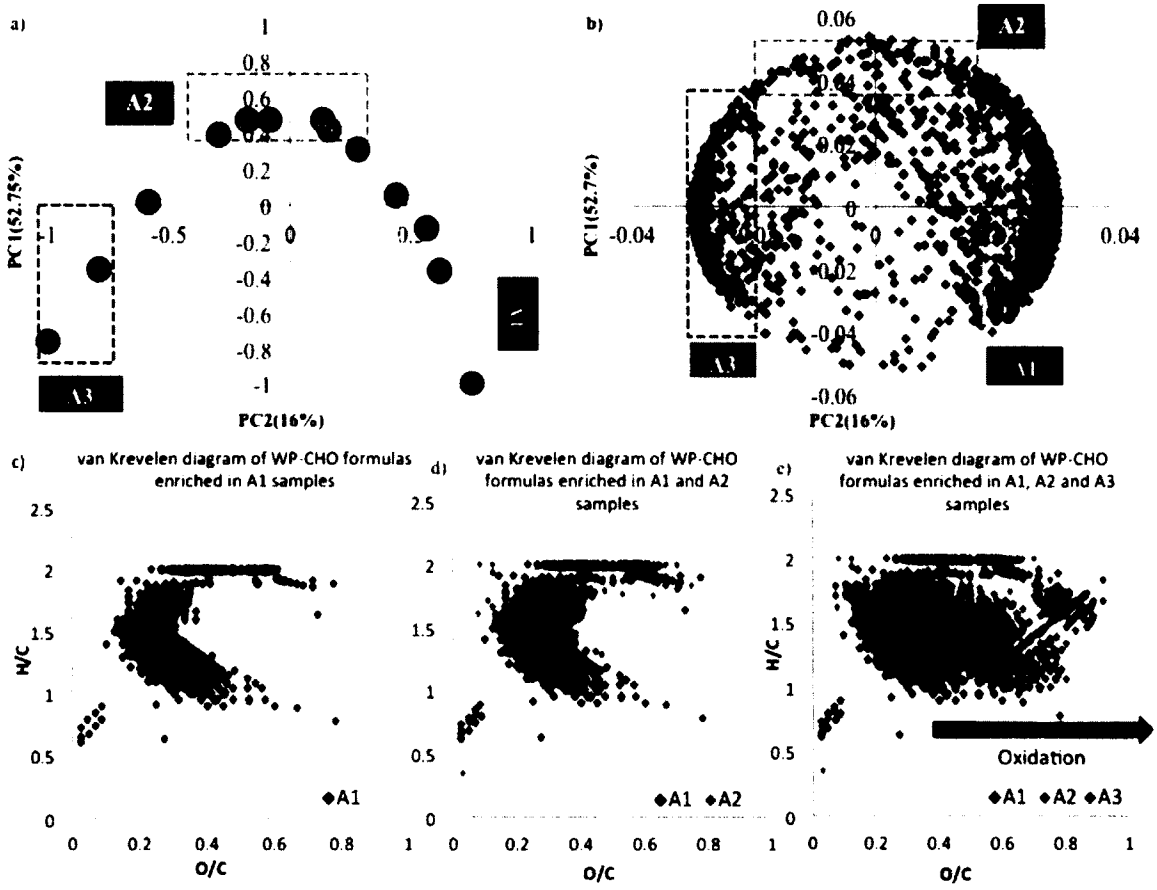

Figure 16. PCA results using the relative magnitudes of all WP-CHO formulas showing the biplot of the sample scores (a) and variable loadings (b), along with the van Krevelen diagrams of the CHO formulas included in the colored boxed areas (c-e).

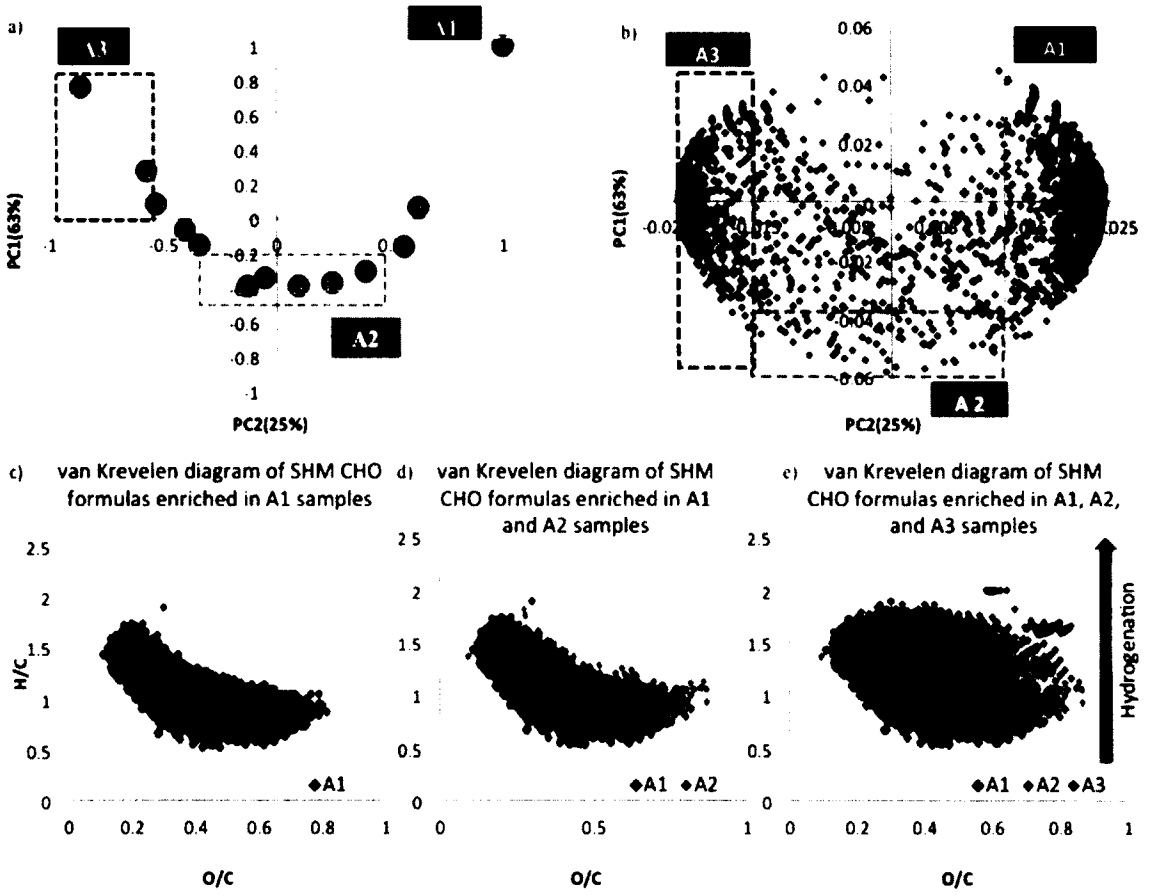

Figure 17. PCA results using the relative magnitudes of all SHM-CHO formulas showing the biplot of the sample scores (a) and variable loadings (b), along with the van Krevelen diagrams of the CHO formulas included in the colored boxed areas (c-e).

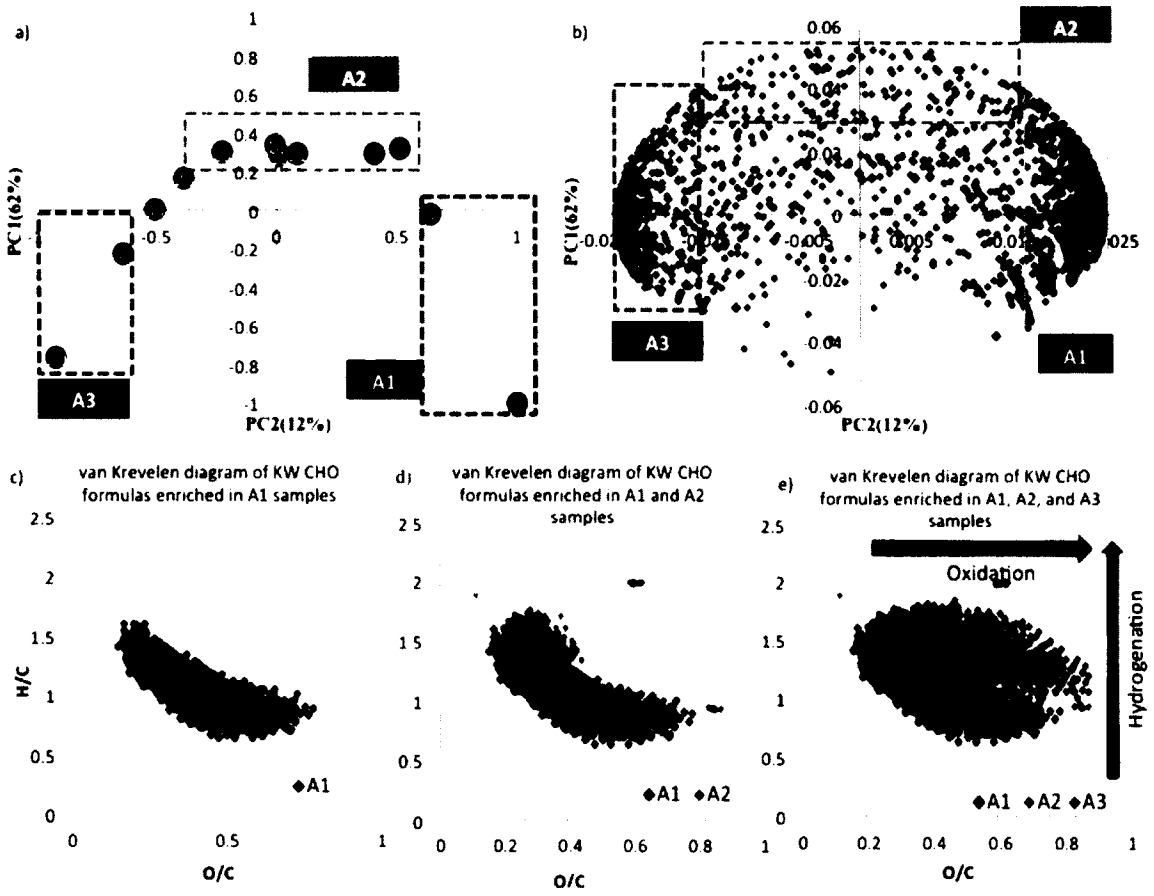

Figure 18. PCA results using the relative magnitudes of all KW-CHO formulas showing the biplot of the sample scores (a) and variable loadings (b), along with the van Krevelen diagrams of the CHO formulas included in the colored boxed areas (c-e).

A1 which we interpret as representative of the photo-labile compounds (Figures 17c-18c), comprises more aromatic- and CRAM/lignin-like structural entities identified by their low and medium H/C ratios (Helms et al., 2014; Stubbins et al., 2010) in the SHM and KW cases (Figures 18-19), but more aliphatic formulas having low O/C (0.3-0.6) and high H/C (>1.5) ratios in the WP case (Figure 16c). Extensively photoirradiated sub-samples characterized by A3 formulas, show an aliphatic signature identified by high H/C ratios (> 1.5) in the SHM sample (Figure 17e and Figure 19c), which is consistent

with recent observations from wetland-derived DOM subjected to photo-irradiation (Rossel et al., 2013). In contrast, the WP sample reacts quite differently under photo-irradiation with most of the A3 formulas trending to higher O/C (Figure 16e and Figure 19d). Such a trend indicates that photooxidation is rendering the DOM in the WP more oxygenated. The KW sample, however, shows A3 enclosing both more aliphatic and more oxygenated formulas, influenced by the presence of both anthropogenic and natural DOM. The trend towards higher O/C appears to be less pronounced in the SHM case and it probably indicates that photooxidation of natural DOM from SHM is not as extensive as in the WP and the KW cases that contain more anthropogenic DOM. We suggest that the DOM from these two samples is more prone to photooxidation because it contains molecules that are photo-labile and are more readily oxidized due to their anthropogenic nature. The SHM sample has already undergone some photooxidation prior to sampling and may be less prone to further photooxidation. What we do observe is an apparent hydrogenation trend in the SHM case, an oxidation trend in the WP case, and the combination of both trends in the KW cases (Figures 16e-18e), as the photoirradiation progresses. These two trendlines might define some important transformations of the DOM from complex structural entities to aliphatic molecules in the SHM and the KW cases or extensively oxidized molecules that could be easily digested by biota in the WP and the KW cases. Area 2 (A2), which is confined between A1 and A3 in both VK diagrams, comprises formulas that have H/C and O/C ratios intermediate between the photo-labile entities and the photo-produced entities

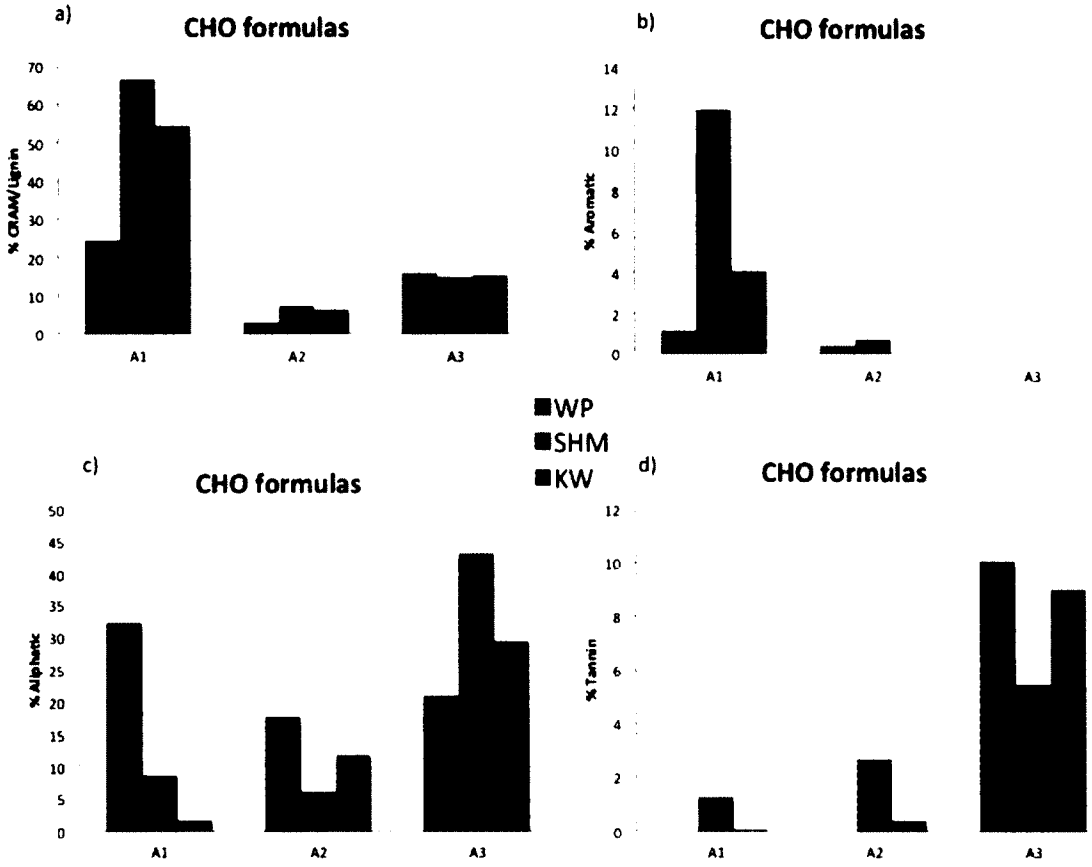

Figure 19. Bar diagrams showing the percent contribution of CRAM/lignin-like formulas (a), aromatic formulas (b), aliphatic formulas (c) and tannin formulas (d) in the 3 selected colored areas of the PCA biplots shown in Figures 16-18 for the WP, KW, and SHM.

The PCA plots of N-containing formulas, for both WP and SHM samples, show similar trends as those of the CHO formulas, where the inferred oxidation trend prevails in the WP case and the hydrogenation trend dominates the changes in the SHM sample (Figures 20e-22e). However, A2, which characterizes the transition between photodegradation and photoproduction shows a high density of formulas, for both WP and SHM, in comparison to A1 and A3 areas (panels (c-e) in Figures 20-22). The CHO formulas do not show this similar phenomenon. This is an indication that photochemistry plays a role in mediating DIN reactions and incorporating DON into the DOM (as shown

in Figure 13), modifying the DOM and producing fresh DON from both anthropogenic and natural sources even in low DIN systems like SHM. If this fresh DOM is shown to be bioavailable, then it could indicate that photochemical transformations contribute to the enhanced bioavailability of terrestrial DOM in rivers and estuaries.

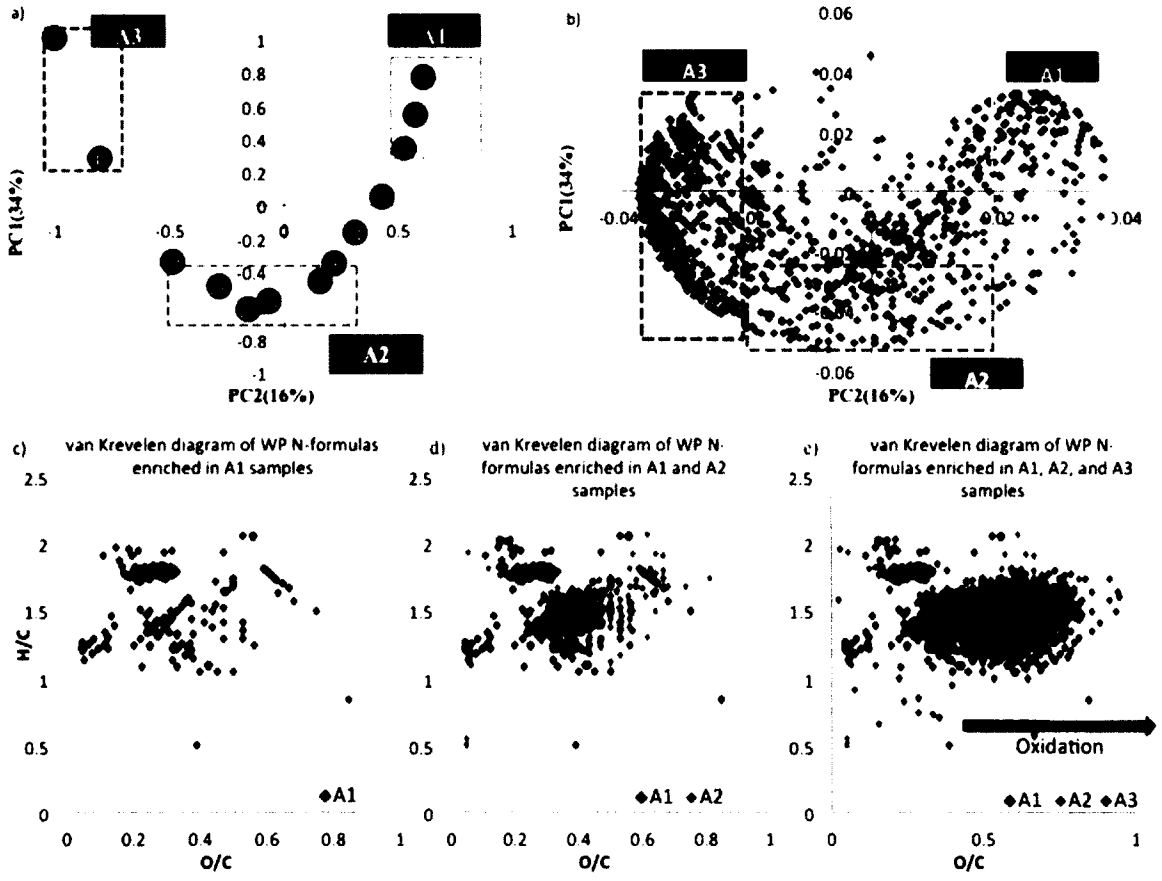

Figure 20. PCA results using the relative magnitudes of all WP N-containing formulas showing the biplot of the sample scores (a) and variable loadings (b), along with the van Krevelen diagrams of the N-containing formulas included in the colored boxed areas (c-e).

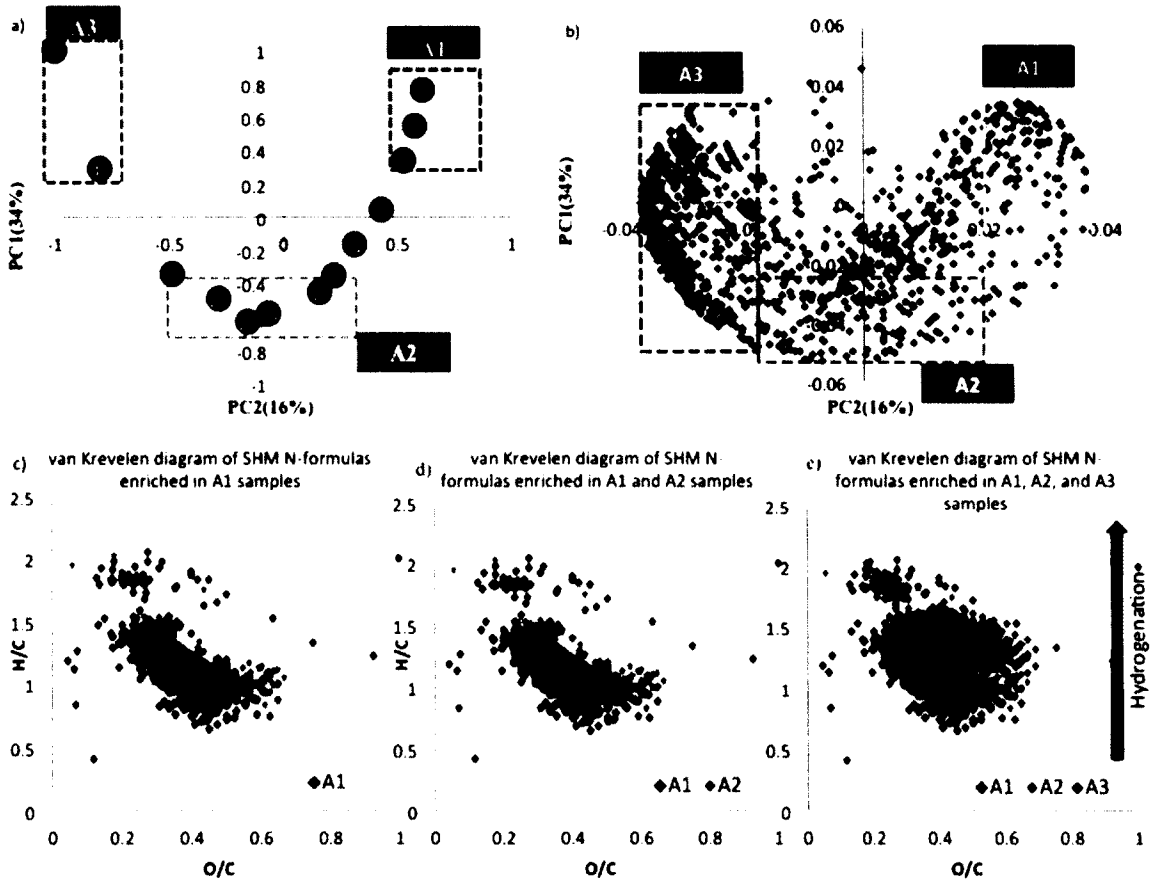

Figure 21. PCA results using the relative magnitudes of all SHM N-containing formulas showing the biplot of the sample scores (a) and variable loadings (b), along with the van Krevelen diagrams of the N-containing formulas included in the colored boxed areas (c-e).

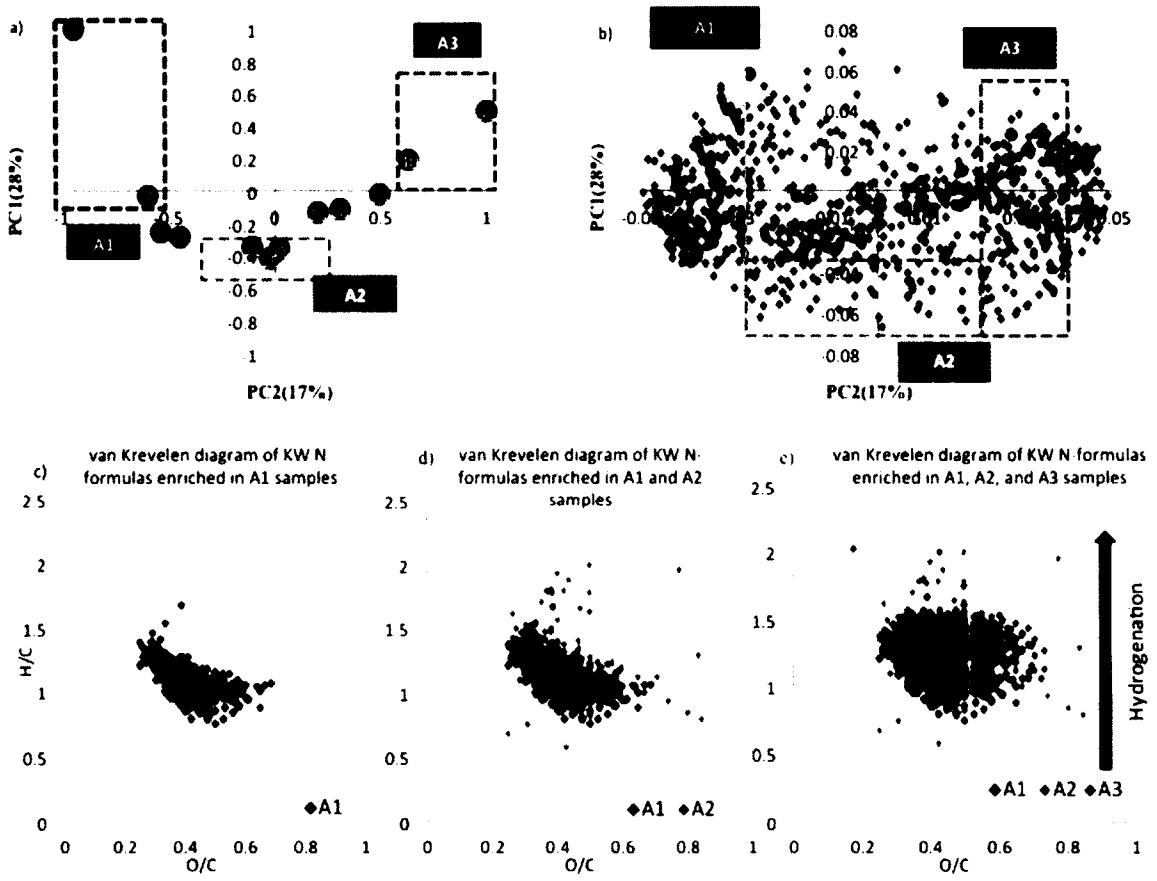

Figure 22. PCA results using the relative magnitudes of all KW N-containing formulas showing the biplot of the sample scores (a) and variable loadings (b), along with the van Krevelen diagrams of the N-containing formulas included in the colored boxed areas (c-e).

3.5.2. Two Dimensional correlation analysis

The advantage of 2D correlation analyses is that one can visualize changes, either correlated or non-correlated, in single (auto-correlation) or multiple (hetero-correlation) parameters during a process. Lack of change generates white space on the map, so the observation of a signal on a 2D map is indicative of change. Synchronous 2D auto-correlation analysis of H/C ratios of SHM-CHO formulas results in a 2D map that

highlights the major changes in the H/C ratios of formulas for SHM samples induced by increasing photoirradiation exposure time (Figure 23). The intensity along the diagonal line represents the auto-correlation at each H/C ratio with itself. In this case intensity measures the number of formulas measured and is not the intensity of the individual mass spectral peaks. The off-diagonal cross peaks represent the cross correlation intensity (number of formulas) between the different H/C ratios. Cross peaks are color-coded to indicate positive (red color) or negative correlation (green color). The intensity along the diagonal line of Figure 23a is greatest at H/C ratios of 0.50-1.25 and at H/C 1.60-1.80, indicating that most of the changes occur in these regions upon irradiation. The cross correlation (off-diagonal) signals reveal that the formulas that fall in the region of H/C 0.50-1.25 have positive correlations (red color) with other peaks in this region. Upon closer inspection of the FTICR-MS data for each sub-sample, it is clear that the number of molecular formulas in this region actually decreases with photoirradiation exposure time. On the other hand, the formulas in the H/C 0.50-1.25 region shows a negative correlation (green color) with the changes in number of formulas at H/C 1.60-1.80, which suggests that as compounds with H/C ratios of 0.5-1.25 are photodegraded, new compounds with higher H/C ratios are photoproduced. Furthermore the lack of intensity at the diagonal and off-diagonals at H/C ratios of 1.25-1.50 implies that these formulas do not display significant changes in number of formulas during photoirradition. A close look at the VK diagrams of the SHM sample verifies the presence of these formulas in all the SHM sub-samples. This indicates the formulas at H/C 1.25-1.50 belong to a photoresistant pool of compounds. We do not know whether there are diminutions in peak intensities caused by photoirradiation because the correlation is not based on peak

intensity but numbers of formulas.

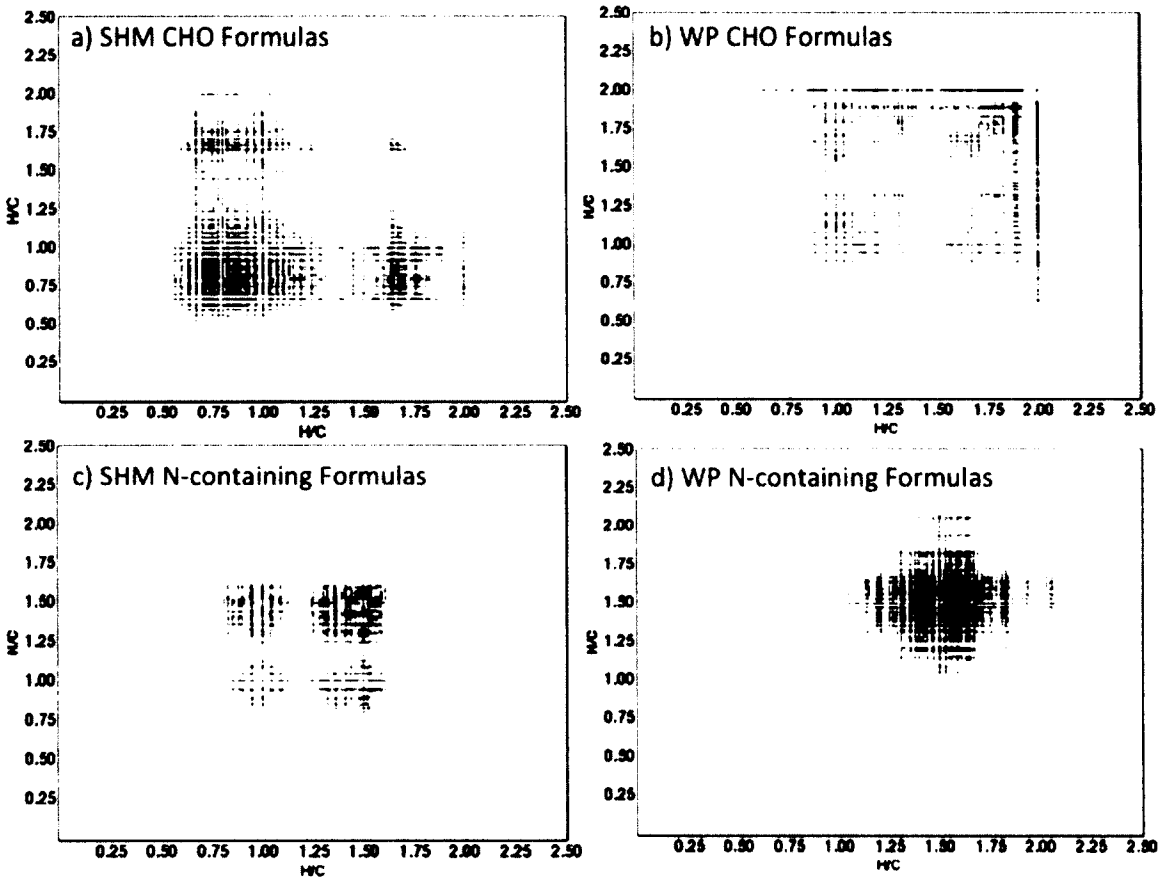

Figure 23. The H/C vs. H/C synchronous plots generated by applying 2D correlation on the a) SHM CHO formulas, b) WP CHO formulas, c) SHM N-containing formulas, and d) WP N-containing formulas. The correlation was based on the presence/absence of each individual formula as the irradiation time progresses. Red indicates a positive correlation, while green indicates a negative correlation.

In the case of WP CHO formulas (Figure 23b), the change in number of formulas at H/C 1.75-2.00 shows the highest auto-correlation, followed by H/C 0.80-1.25, then at H/C 1.50-1.75. The cross correlation signals and the FTICR-MS data sets reveal that while formulas with the highest and lowest H/C ratios are photodegraded, formulas with

H/C ratios at 1.50-1.75 are photoproduced. Similar to SHM samples, the lack of the diagonal peaks at H/C ratios 1.25-1.50 implies that these CHO formulas are likely to be the photoresistant pool of compounds in the DOM. These maps also suggest that while the photodegradation of CHO formulas is intense (the intensity of the diagonal peak is high indicating a high loss of formulas in this range), the photoproduction indicated by negative cross peaks is weak. However, when we apply the 2D correlation to the N-containing formulas (Figure 23c,d), an opposite trend is observed, where the photoproduction of N-containing formulas is intense even in the SHM case, where SHM is relatively N-poor compared to the WP effluent. The intensity along the diagonal line of figures 23c,d indicates that most of the changes in the number of SHM and WP N-containing formulas occur at H/C 1.25-1.75. In contrast to the changes noted above for CHO formulas, the FT-ICR-MS data for each subsample reveals that the number of molecular formulas in this region increases with photoirradiation time. A negative correlation is observed at H/C 0.80-1.20 and at 1.75-2.00 with the change in the number of formulas for SHM and WP, respectively. This is an indication that photochemistry is altering the molecular structure of DOM in almost a similar fashion regardless of the source. Furthermore, photochemistry plays a key role in producing new DON compounds, some of which might be bioavailable when released in rivers and estuaries. In the case of wastewater effluent DOM like WP, photochemical alteration of the released DOM is producing new compounds. If the latter are utilized as food sources for organisms, then one can argue that the released DON cannot be considered refractory N.

Another synchronous 2D correlation analysis was employed to examine the auto-correlation between the number of carbons in each formula, examining both CHO and N-

containing formulas for both SHM and WP datasets using the photoirradiation exposure time as the external perturbation parameter. The 2D correlation clearly classifies the SHM CHO formulas into three regions (Figure 24a). The first region includes the formulas that have a carbon number between 10-13. The number of such formulas increases as photoirradiation progresses. In the opposite direction, there is a decrease in the number of formulas with carbon number between 16-35. At the same time, the number of formulas that fall into the third region (carbon number between 14-16) shows no significant changes with photoirradiation, which implies a pool of photoresistant compounds.

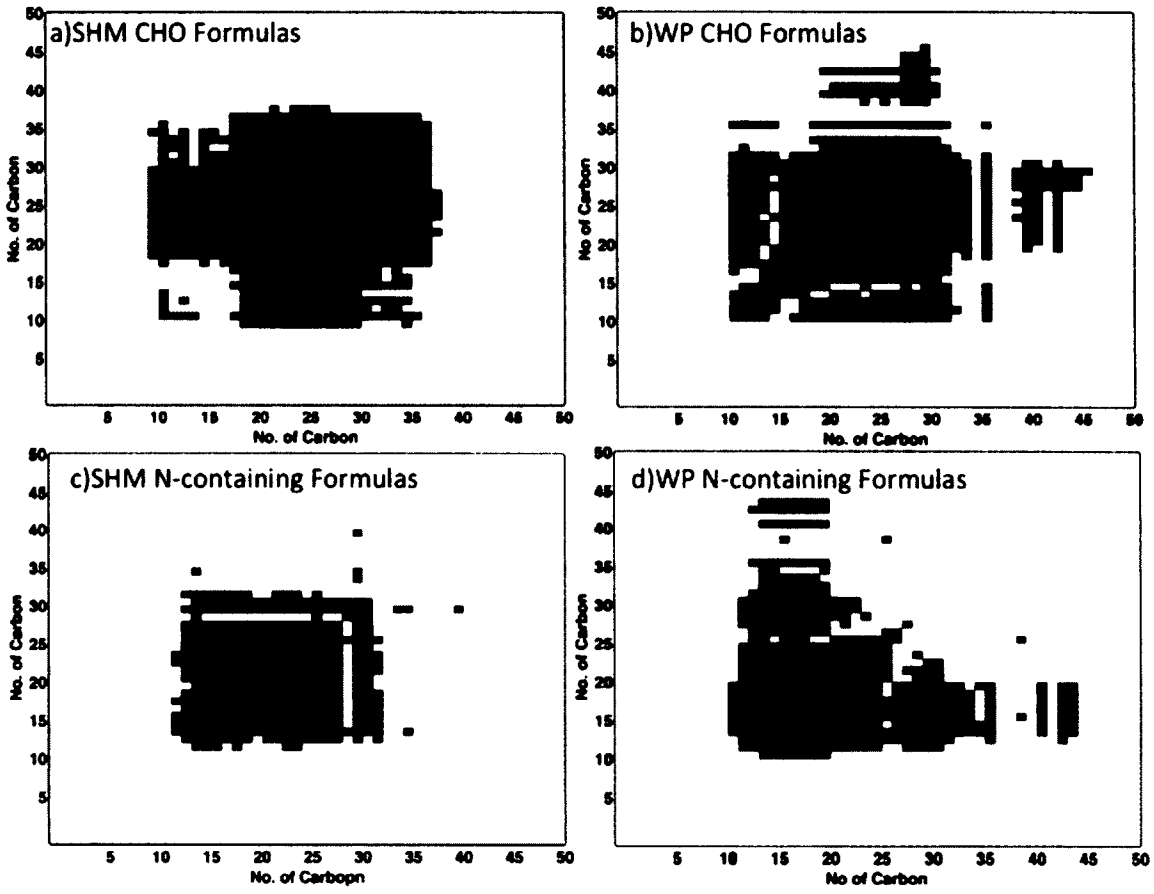

Figure 24. The carbon number vs. carbon number synchronous plots generated by applying 2D correlation on the a) SHM CHO formulas, b) WP CHO formulas, c) SHM N-containing formulas, and d) WP N-containing formulas. The correlation was based on the presence/absence of each individual formula as the irradiation time progresses. Red indicates a positive correlation, while green indicates a negative correlation.

The WP CHO formula map shows four distinct regions (Figure 24b); the first region with carbon numbers between 10-13 shows an increase in number of formulas, while the second and the third regions with carbon numbers between 17-33 and carbon number 35 exhibit a decrease in number of formulas as photoirradiation progresses. The fourth region with carbon numbers between 39-45 displays little to no change in number

of formulas. Likewise, formulas with carbon numbers between 14-16 exist in all the FT-ICR-MS data sets of WP CHO compounds but are missing in the 2D correlation maps, which imply a resistant pool. These maps suggest an aggressive photodegradation of CHO formulas with carbon number between 17-33 for both samples, which is indicated by the highly intense diagonal peaks in both maps.

In the same fashion, WP N-containing formulas with carbon number between 11-23 show an intense rate of photoproduction while the photodegradation of the higher carbon number formulas (>35) is either weak or missing (Figure 24d). In comparison, SHM N-containing formulas show a moderate photoproduction of formulas with carbon numbers between 12-28 while the photodegradation of formulas with carbon numbers between 29-31 is more intense. This difference in the photoproduction rate of new DON, between SHM and WP, is probably due to the difference in their DIN contents (Figure 11b). It is likely that photochemistry plays a significant role in producing new DON from SHM, which is a relatively N-poor sample, a fact that is hardly observed when using classical bulk analytical and statistical measurements (e.g., nutrient analysis and cluster analysis). By using state-of-the-art analytical and statistical tools, we are able to demonstrate that photochemistry is a continuum process that transforms DOM and DON from complex structural entities to aliphatic molecules in some instances and more oxygenated molecules in other instances. We speculate that these transformed molecules may be more readily digested by biota. Therefore, we are able to validate that photochemistry is one of the main processes that shapes the DON quality in aquatic systems.

CHAPTER IV

THE BIOAVAILABILITY AND REACTIVITY OF DISSOLVED ORGANIC MATTER DERIVED FROM DIFFERENT SOURCES IN THE YORK RIVER, CHESAPEAKE BAY

PREFACE

The content of this chapter is in preparation to be submitted to *Water* journal Contributions: Rajaa Mesfioui developed experimental design with assistance from Dr. Margaret Mulholland and Dr. Patrick G. Hatcher. Dr. Hussain Abdulla is an expert on the two-dimensional correlation statistical analysis and provided assistance in displaying FT-ICR-MS results in 2D correlation maps. Dr. Thais Bittar performed flow cytometric analysis. Wastewater effluent was collected with the assistance of Dr. Charles Bott of Hampton Road Sanitation District. Nitrites+Nitrates wet analysis were measured with the generous help of the Dr. Kenneth Moore of Virginia Institute of Marine Science. All samples were prepared, processed, and analyzed by Rajaa Mesfioui. The paper is written by Rajaa Mesfioui and is in preparation pending comments by the co-authors.

1. INTRODUCTION

Dissolved organic matter (DOM) can be a source of labile organic carbon (Hedges et al., 1997; Wetzel, 1992) and nitrogen (Wiegner et al., 2006) for microbial communities in coastal areas. Terrestrially derived DOM undergoes various biological and photochemical transformations in riverine ecosystems before its residual, and most refractory portion, is discharged into the oceans (Amon and Benner, 1996; Asmala et al., 2013; Bertilsson et al., 1999). Recent evidence suggests that terrestrial DOM is utilized within streams and rivers, as well as within the estuarine and coastal receiving waters

(Benner et al., 1995). Consistent with this, budgets show that the amount of carbon delivered to the oceans from rivers is only a small portion of the amount of carbon that enters rivers from terrestrial environment and watersheds (Aufdenkampe et al., 2011; Seitzinger et al., 2005a). Because of the high rates of respiration and processing of terrestrial DOM, rivers and estuaries are among the highest emitters of CO_2 per unit area (Cole et al., 2001). DOM components may be respired by bacteria or incorporated into microbial and higher organism food webs (Dagg et al., 2008; Del Giorgio and Pace, 2008; Nakagawa et al., 2007) serving as C, N, and P sources. However, the lability of DOM and its subcomponents dissolved organic carbon (DOC) and nitrogen (DON), has been shown to vary largely according to the biochemical composition (quality) and source of constituent DOM (Benner, 2003; Lu et al., 2013; Wiegner et al., 2006). The quantity and quality of DOM discharged into rivers and streams, and ultimately its fate and dynamics in aquatic systems is greatly affected by land-use (Aufdenkampe et al., 2011; Kaushal et al., 2014), and an increase in microbial activity has been observed in human impacted watersheds relative to those with less anthropogenic input (Hosen et al., 2014; Rabalais et al., 2002; Williams et al., 2010; Wilson and Xenopoulos, 2013). Understanding microbial transformation and utilization of DOC and DON in aquatic ecosystems is a crucial step in deciphering the interrelationships between dissolved organic C and N cycles, and how they vary among different DOM source materials, and ultimately in gaining a better understanding of processes contributing to eutrophication and poor water quality. Bulk analyses of the DOM pool do not afford a molecular level understanding of DOC and DON and its reactivity (Bronk et al., 2010; Filippino et al., 2011). In addition, land-use and salinity affect the chemical composition of the DOM

such that the quality of the DOM and its biological reactivity are different or altered. Mesfioui et al. (2012) showed that DOM reactivity in two wastewater effluents (one of which discharges into the nearby James River) can be masked if only bulk chemical analyses are examined, mainly because the uptake and production of DON and DOC compounds can occur at similar rates with no net change in DOM concentrations; molecular-level characterization of DOM was necessary to evaluate the extent of transformations, consumption and production of specific compounds. Molecular-level characterization of DOM can be done using electrospray ionization coupled to Fourier transform ion cyclotron resonance mass spectrometry (ESI-FTICR-MS) (Mesfioui et al., 2012; Sleighter et al., 2014). In the present study, we examined molecular-level chemical transformation of three natural and anthropogenic sources of DOM found in the York River watershed in natural York River water samples and their resident microbial communities. Bulk measurements and molecular-level characterization (using ESI-FTICR-MS) of DOC and DON were combined to identify shifts in DOC and DON associated with biological degradation. Findings from this research will enhance our understanding of the DOM biodegradation and chemical reactivity to better assess the effects of DOM on coastal ecosystems and water quality.

2. EXPERIMENTAL PLAN

2.1. DOM sample collection and handling

DOM was collected from three distinct DOM sources of the York River watershed, Virginia, USA; the Sweet Hall Marsh (SHM), Taskinas Creek (TC) and the effluent from a wastewater facility in Yorktown (YT). The SHM is a representative of the typical marshes and tidal swamps that surround the Pamunkey River, a major tributary of the

York River. TC is also a tributary of the York River and receives runoff from an oak-hickory forested site, maple-gum-ash swamps, and freshwater marshes in York River state park. The wastewater treatment facility of YT is a relatively large plant (~13 million gallons per day) located in the Hampton Roads Sanitation District. The plant receives variable domestic and commercial wastewater and uses primary clarifiers, conventional plug flow nitrifying activated sludge, deep bed denitrifying filters with methanol addition, gravity thickening for primary sludge, dissolved air flotation for waste-activated sludge thickening, anaerobic digestion, centrifuge dewatering, and hypochlorite disinfection and de-chlorination processes. The average total nitrogen (TN) of YT effluent is around 5.9 mgN/L (Bott, 2014).

Samples from TC and SHM, were collected on August 12, 2012. The sample from YT was collected downstream of the biological process but before disinfection, and was integrated over 24h period on Novermber 9, 2011. All samples were filter-sterilized on site using 0.2 μm polysulfone cartridges (pre-conditioned for 5 min with each sample) to remove cells and most colloidal material. All samples were placed into high-density polyethylene carboys, packed into coolers chilled with ice packs, and transported to Old Dominion University within 2 hours. Upon arrival to the laboratory, samples were concentrated from 40L to 1 L for TC, from 35L to 1 L for SHM, and from 30L to 1 L for YT, using a rotary evaporator system at T< 35 °C. Samples were concentrated to achieve amendments of about 10 μMN in natural water samples with less than 10% dilution of the natural water. After concentration, samples were frozen at - 20°C until bioassay initiation.

2.2. Bioassays

2.2.1. Natural water samples

Natural water was collected from the York River on May 26, 2013, from two stations, within the mesohaline section of the York River (S2= 5‰, and S3= 12.5‰). Approximately 120 L of whole water were collected from each station, and was screened with a 20μm acid cleaned nylon mesh to remove large organisms. The mesohaline section of the York River was selected because it is often subjected to an annual summertime hypoxia and anoxia directly related to salinity-based stratification of the water column in combination with high levels of autochthonous DOM and a very high abundance of metabolically active bacteria.

York River water was diluted with 0.2 μm filtered from the same site to reach *chlorophyll a* (*Chla*) concentration of 8-10 μg/L. The dilution was performed to prevent nutrient limitation of microbial community growth and prevent excessive accumulation of biomass over the 7 days experiment.

2.2.2. Treatment and control incubation

Controls contained diluted York River water medium from stations S2 or S3 (Ctrl-S2 and Ctrl-S3) without any added DOM. Concentrated DOM from YT, SHM, and TC (2.3, 5.2 and 5.2 mL, respectively) was added to 500 mL of the diluted York River water medium to achieve a TN addition of 10μM in each incubation bottle. Duplicate Ctrls and DOM-amended bioassays were incubated for 7 days at *in situ* light and temperature conditions, in a floating cage tethered to a dock in the Lafayette River near Old Dominion University.

2.2.4.Bioassay sampling

The Ctrls and each DOM-amended bioassay were sampled twice on the first day of incubation, at time zero (T_0) and after 4 hours (T_1), and once daily (at 10:00 AM) for 6 consecutive days. At each time point, samples were collected for measurements of *Chla,* TDN, DOC, nitrate and nitrite (NO_x), and ammonia (NH_4) concentrations and for qualitative analysis of DOM by ESI-FTICR-MS (described below).

2.3. Bulk analysis

2.3.1. Nutrients analysis

Bulk DOC and TDN concentrations were measured in duplicate on the filtered samples using the high temperature combustion catalytic oxidation method (Shimadzu TOC/TN-5000) (Peltzer et al., 1996). NH_4 concentrations were analyzed using the phenol hypochlorite colorimetric method (Hansen and Koroleff, 2007). NO_x concentrations were measured using the diazotization and the cadmium reduction spectrophotometric method (Parsons et al., 1984) using the SKALAR SAN plus System at the Analytical Service Center of the Virginia Institute of Marine Science (Gloucester, VA). DON concentrations were determined by subtracting the concentrations of NO_x and NH_4 from TDN concentrations (Bronk et al., 2000). All analyses were performed on 0.2 μm-filtered aliquots.

2.3.2. Chla and bacteria abundance

To measure *Chla* concentrations, cells were collected onto 25 mm Whatman GF/F filters under low (< 15psi) vacuum pressure. The filters were immediately immersed in 10 ml of 90% acetone and placed in darkness at 4°C to extract the pigments. After 24 h, the tubes were vortexed and the fluorescence of the acetone extract was measured in

duplicate on a Turner Design Model 10-AU fluorometer (Welschmeyer, 1994).

Samples collected to enumerate heterotrophic bacteria cell abundance (cell/mL) were preserved with 0.125% glutaraldehyde (final concentration) and then frozen at -80°C for flow cytometric analyses (Vaulot et al., 1989). Samples were shipped overnight to the Skidaway Institute of Oceanography for analysis. Prior to analysis, samples were thawed in ice and stained for 30 min with SYBR Green I (100x final concentration), which is a dye that binds specifically to nucleic acids and can be excited by blue light (488 nm wavelength) (Marie et al., 1997). Standard fluorescent polystyrene beads (1.0 μm diameter) were added to each sample as internal standards and was used to access run reproducibility. Flow cytometric analyses were performed on a Becton Dickinson FACSCalibur flow cytometer, equipped with a 15 mW air-cooled argon-ion laser tuned for blue excitation (488 nm). Data were collected in list mode with CellQuest Pro and post-run analyses were done with Flowing software.

2.4. ESI-FTICR-MS Analyses

DOM samples for ESI-FTICR-MS were desalted prior to analysis using solid phase extraction cartridges (Agilent, Bond Elut PPL) Dittmar et al. (2008). The cartridge (after desalting but before DOM elution) was kept at -20 °C for 1-2 weeks before analyses. All MS analyses were performed at the College of Sciences Major Instrumentation Cluster (COSMIC) at Old Dominion University using an Apollo II ESI ion source coupled to a Bruker Daltonics 12 Tesla Apex Qe FTICR-MS. Prior to analysis, the instrument was externally calibrated using polyethylene glycol. Right before introduction to the ESI, each sample was eluted from the PPL cartridge using 4 mL of LC-MS grade methanol and then diluted with LC-MS grade water to a uniform TOC

concentration (~10 mg/L C). Samples were then spiked with 0.1% ammonium hydroxide (increasing the pH to 8) to increase the ionization efficiency. Sample flow rate (2 mL/min) was maintained using a syringe pump and the ESI voltages for each sample were maintained at 3.4 kV on the spray shield and 4.1 kV on the capillary at 200 °C in order to maintain a consistent ion current entering the capillary to the MS.

All samples were analyzed in negative ionization mode to minimize complications due to sodium adduct formation. Electrospray voltages and MS parameters were held constant throughout all experiments. Ions were accumulated in a hexapole for a period of 2 s before transfer to the ICR cell. This accumulation time was found to be optimal; because shorter ion accumulation times resulted in fewer peaks with lower S/N, while longer times led to poor resolution. For each sample, 300 time-domain transients were acquired (at 4M Word), co-added, zero-filled once, sine-bell apodized, and then Fourier transformed using the Bruker data analysis software, resulting in an overall analysis time of approximately 30 minutes per sample.

2.5. Mass calibration and molecular formula assignments

The general mass distribution of compounds that were ionized in all samples was in the range of 200-700 m/z, which is consistent with previous DOM studies using ESI-FTICR-MS (Koch et al., 2005; Sleighter et al., 2008b). Because low m/z peaks (<200) have very high frequencies, the excitation required to increase the ion radius to a sufficient amplitude in order to induce enough current to be detected by the detection plates is more difficult. Furthermore ions below 200 are discriminated against in the quadrupole, where ions of a broad specified m/z range are allowed to pass through before being accumulated in the hexapole, and then transferred to the ICR cell. Our samples

were analyzed in broadband mode, meaning we used a very wide m/z range (100-2000) however peaks were only detected and observed in the range of 200-700 m/z. The eventual loss of peaks above 700 m/z can be partially attributed to space charge effects within the ICR cell that can result in a decrease of high molecular weight signal (Kujawinski et al., 2002). All acquired spectra were internally calibrated with indigenous fatty acids providing a mass accuracy of 1 ppm or less throughout the mass range of interest (Sleighter et al., 2008a). Molecular formulas were assigned to peaks with a signal to noise (S/N) ratio > 3 in the mass range of 200-700 m/z by means of a Formula Calculator Program (v.1.0 © 1998 NHMFL) that was developed at the National High Magnetic Field Laboratory in Tallahassee, FL. In our study, the vast majority of formulas were unambiguously assigned below m/z 500, because we only allow up to 0.5 ppm error in assigning correct molecular formulas. When multiple assignments existed for a single m/z value, then the correct formula was assigned based on elemental rules, functional group relationships, and patterns and homologous series, as described in detail previously in the literature (Koch et al., 2007; Koch et al., 2005).

The three main parameters used herein for the comparative analysis of the huge data set generated by FTICR-MS are the double bond equivalents (DBE), aromaticity index (AI), and the van Krevelen diagram (VK), which are obtained from the accurately assigned molecular formulas of each peak (Kendrick, 1963; Kim et al., 2003; Koch and Dittmar, 2006).

2.5.1. Double bound equivalent (DBE)

DBE is a measure of the hydrogen saturation; it provides the number of double bonds and/ or rings in an organic molecule based on C, H, and N and P elemental ratios:

$$DBE = 1 + \#C - ({}^{H}/_{2}) + ({}^{N}/_{2}) + ({}^{P}/_{2})$$

This parameter is calculated for each assigned formula and accounts for all doubly bound carbon contributions, including the double bonds of carboxyl groups.

2.5.2. Aromaticity index (AI)

Similar to DBE values, AI values are calculated for every assigned molecular formula in a sample as follows:

$$AI = \frac{1 + C - O - S - 0.5H}{C - O - S - N - P}$$

AI was first proposed by Koch and Dittmar (Koch and Dittmar, 2006) to distinguish unambiguously between aromatic (AI > 0.5) and condensed aromatic structures (AI >= 0.67) in DOM. The latter values are indicative of thermogenic sources of condensed aromatics or ''black carbon, which have also been identified using the following rules (Hockaday et al., 2006; Kim et al., 2004)

$$0.3 \leq {}^{O}/_{C} \leq 0,6 \text{ and } 0.5 \leq {}^{H}/_{C} \leq 0.8 \text{ and } {}^{DBE}/_{C} = 0.67$$

However, the amount of condensed aromatic might be overestimated when applying this rule only. On the other hand, If only half of the oxygen in DOM is considered being present in carbonyl functional groups, as it is the case in this study, then AI is calculated as follow:

$$AI_{mod} = \frac{1 + C - 0.5\,O - S - 0.5\,H}{C - 0.5\,O - S - N - P}$$

2.5.3. Van Krevelen diagram (VK)

VK plots the molar H/C ratios of each assigned molecular formula on the y-axis and its molar O/C ratios on the x-axis. VK plots cluster elemental formulas according to their functional group compositions into major biochemical compounds classes that have

characteristic H/C and O/C ratios. These clusters help elucidate changes in the chemical composition; such as changes in oxidation state, degree of methylation, and condensation reactions to form large molecules of samples. Figure 25 shows VK diagrams of the two controls and the three types of DOM samples used in this study. The different colored regions show major compound classes identified in DOM. It is well known that the location of a point on the VK diagram relates to specific compound classes in DOM, and interested readers are referred to the literature for more details (Hockaday et al., 2009; Ohno et al., 2010; Reemtsma, 2009; Sleighter and Hatcher, 2011; Van Krevelen, 1950). These compound classes include:

(1) Aliphatic structures (Perdue, 1984), which include lipids (H/C:1.5-2 and O/C: 0-0.3), proteins (H/C:1.5-2.2 and O/C: 0.3-0.67), and carbohydrate-like (H/C:1.5-2.4 and O/C: 0.67-1.2) formulas, are denoted with red color (Ohno et al., 2010).

(2) Carboxyl-rich alicyclic molecule- (CRAM) or lignin-like formulas (Hertkorn et al., 2006; Hockaday et al., 2009) are represented with green color and are defined as:

CRAM:

$$0.3 \leq {}^{DBE}/_{C} \leq 0.68, \text{and } 0.2 \leq {}^{DBE}/_{H} \leq 0.95, \text{and } 0.77 \leq {}^{DBE}/_{O} \leq 1.75$$

and lignin: $0.1 < {}^{O}/_{C} < 0.67$ and $0.7 < {}^{H}/_{C} < 1.5$

(3) Aromatic (AI_{mod}> 0.5) and condensed aromatic structures (AI_{mod} >= 0.67) are represented with black color.

(4) Tannin indicated with blue color and are defined as peaks having:

$$0.35 < {}^{O}/_{C} < 0.85 \text{ and } 0.75 < {}^{H}/_{C} < 1.4$$

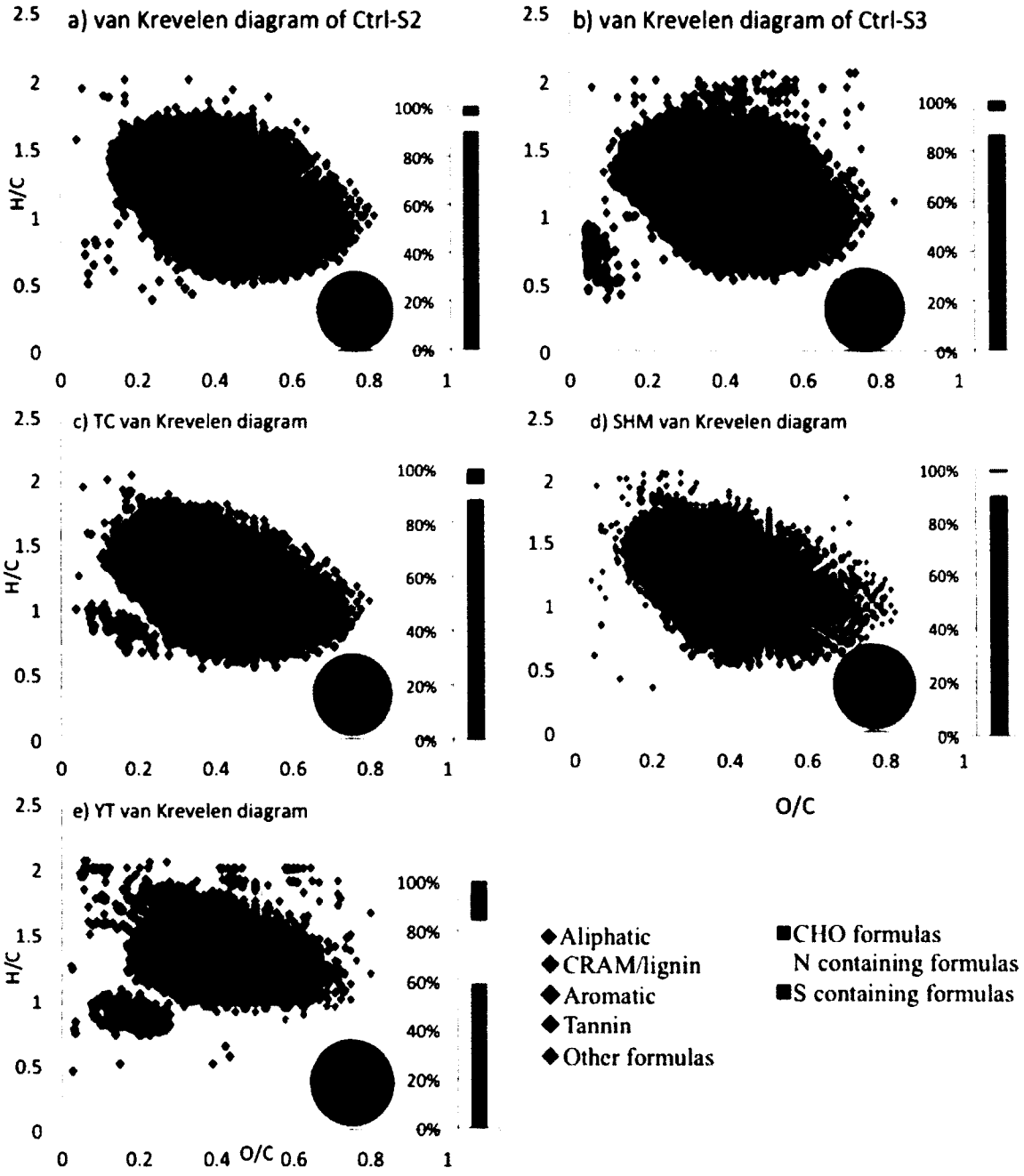

Figure 25. van Krevelen diagrams of Ctrl-S2, Ctrl-S3, TC, SHM, and YT, color coded to highlight the formulas aligning in the regions of the major biomolecular classes of DOM. Pie charts show the percent composition of each compound class for each sample, and the bar charts show the percentage of CHO, nitrogen containing and sulfur containing formulas in each sample.

2.6. Statistical analysis and two-dimensional correlation spectroscopy

To visualize and highlight geochemical differences in the large data set generated by FTICR-MS, we applied two statistical approaches, principal component analysis (PCA) and 2D correlation analysis as described in details by Sleighter et al. (2010) and Abdulla et al. (2013b), respectively.

2.6.1. Principal component analysis (PCA)

PCA was conducted on the assigned CHO formulas of the Ctrl-S2, Ctrl-S3, TC-S2, TC-S3, SHM-S2, SHM-S3, YT-S2 or YT-S3 samples at each time point, giving 8 individual data matrices. A data matrix was created for each sample time series using the relative magnitude of all CHO formulas assigned in those 9 samples. When a formula is not present in the sample, zero value is then assigned in the data matrix. Herein, we plot our data onto a two-dimensional PCA projection (biplots) since 57-72% of the total variance was explained by PC1 and PC2 for each PCA. However, the variance explained by PC1 and PC2 using CHNO formulas was very low. Therefore, we used 2D Correlation analysis to investigate any behavioral changes among CHNO formulas in all amended samples (Section *3.4*).

2.6.2. Two-dimensional correlation spectroscopy

Synchronous 2D correlations are applied to the assigned N-containing formulas by using the H/C ratio to investigate the changes in the formulas based on their presence or absence. The synchronous 2D correlation is conducted to examine changes in number of formulas at specific H/C ratios along the incubation time (n = 9 time series samples) for Ctrl-S2, Ctrl-S3, TC-S2, TC-S3, SHM-S2, SHM-S3, YT-S2, and YT-S3.

3. RESULTS AND DISCUSSION

3.1. Bioassays and bulk analyses

In all bioassays, major changes were observed in bulk analyses for both the low-salinity (S2) and high salinity (S3) bioassays, reflecting the time course of biological activity. Following bioassays preparations and deployment in to the Lafayette River, we observed a peek in *Chla* concentrations for S3 samples with the highest peek showing at day2 for the YT amendment, and at day1 for the other treatments (Figure 26a). The highest increase in *Chla* concentrations were observed in samples receiving the YT amendment, while the other S3 bioassays exhibited less pronounced increase in *Chla*. The reason for this difference might be attributed to the presence of higher NO_x and NH_4 concentrations in YT compared to the other amendments (Figure 26b,c), which have stimulated phytoplankton communities leading to increases in *Chla* concentrations. Our results confirmed this DIN-*Chla* relationship where DIN concentrations decreased in parallel with the increase in *Chla* concentrations.

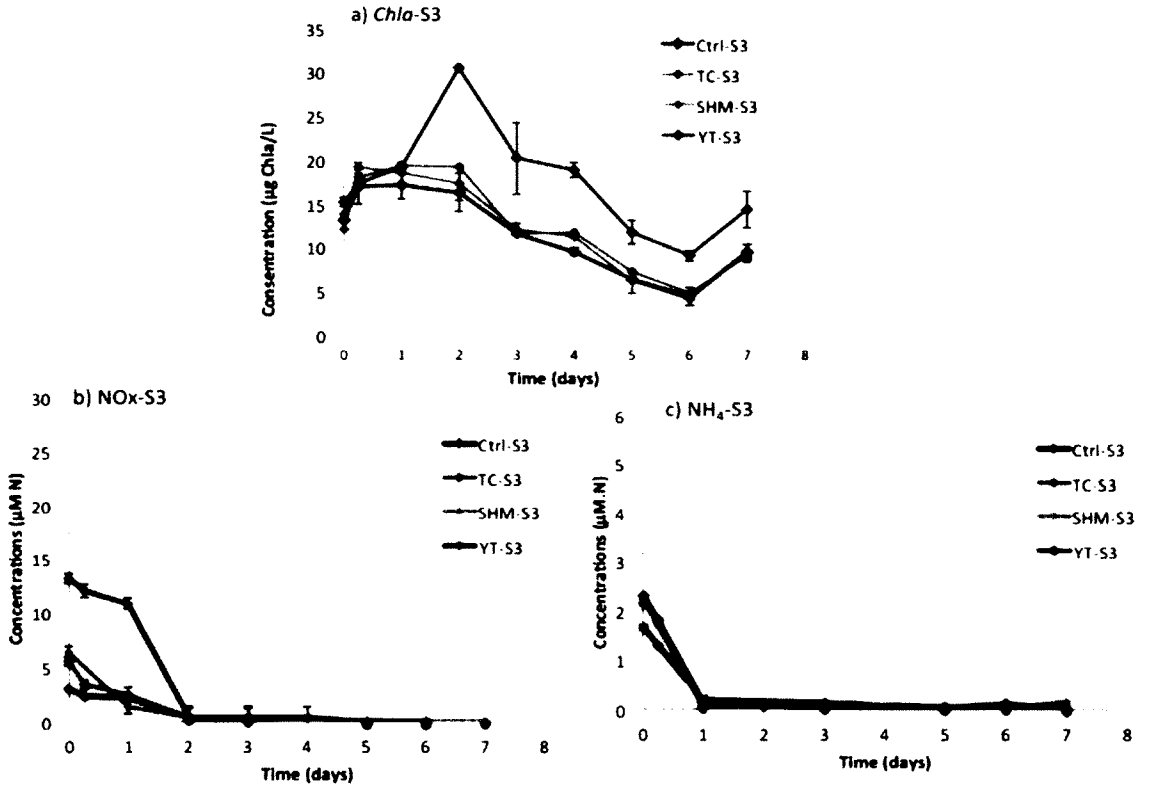

Figure 26. a) *Chla*, b) NOx, and c) NH_4^+concentrations in controls and treatment incubations with TC, SHM, and YT amendments in S3 bioassays (salinity 12.5‰) over time.

In S2 amendments we observed a lag in both phytoplankton biomass and bacterial abundance in response to experimental treatments (Figure 27a,b). This lag period might be due to a difference in physiological status of bacterial and phytoplankton communities between the two salinity regimes. We observed a sharp decrease in DIN (NO_x and NH_4) concentrations on the first day of the incubation experiment (Figure 27c,d), which continued until the entire DIN was exhausted by day 4. This trend was likely due to DIN assimilation by phytoplankton, as *Chla* concentrations increased as DIN concentrations were drawn down. After day 4 *Chla* concentrations decreased, as did bacterial

abundance. *Chla* and bacterial abundance have been shown to b tightly coupled (Ducklow et al., 2001). The secondary peek in *Chla* at day 6 was concomitant to a decrease in both DON and DOC concentrations (Figure 28a,b). DOC concentrations decreased in the first 4hrs of incubation in all samples (S2 and S3) with the exception of TC amendment (Figure 28a,c). Likewise, DON concentrations for YT amendments decreased over the first day of the bioassays experiment (Figure 28b,d). This might be due to the assimilation of these two DOM components by microbes present in the community. After day 1, DOC concentrations increased (Figure 28c) likely due to microbial productivity (Figure 27b). Similarly, DON increased in treatments incubation but not in controls. This increase in both DON and DOC was likely due to *in situ* biological activity. Overall, the biological response and nutrient drawdown were more rapid in S2 incubations than S3 amendments. The different results observed with the two salinities in regard to phytoplankton biomass changes and nutrients assimilation might be attributed to differences in microbial and phytoplankton communities in water with different salinities (from salinities of 5‰ to 12.5 ‰).

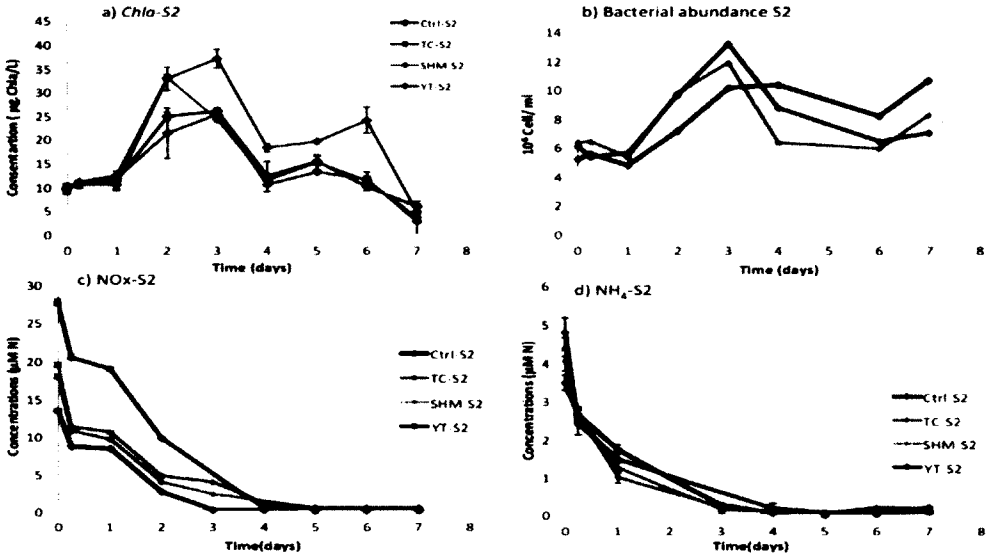

Figure 27. a) *Chla*, b) NOx, and c) $\mathbf{NH_4^+}$concentrations in controls and treatment incubations with TC, SHM, and YT amendments in S2 bioassays (salinity 5‰) over time.

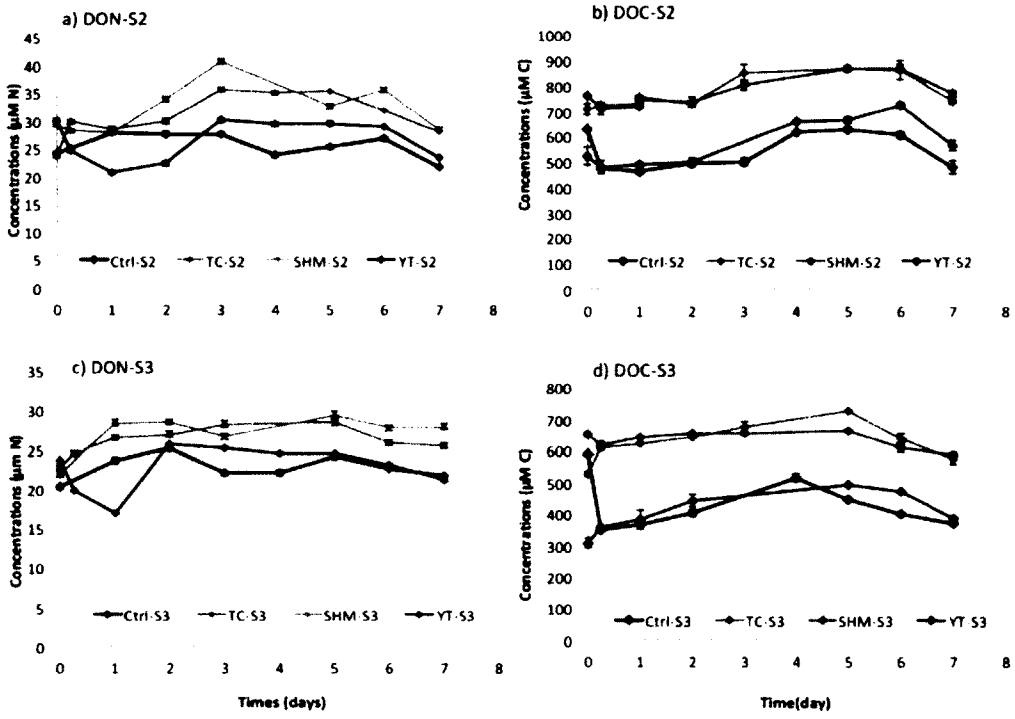

Figure 28. Total dissolved organic carbon (DOC) and dissolved organic nitrogen (DON) concentrations averaged for each time point for the control and each amended sample for S2 (a-b) and S3 (c-d) salinities.

3.2. ESI-FTICR-MS analysis

All obtained ultra-high resolution mass spectra of DOM contain the routinely observed complex pattern of multiple peaks at each nominal mass over the studied range (m/z 200-700) (Kim et al., 2003; Kujawinski et al., 2004; Sleighter and Hatcher, 2008b; Stenson et al., 2003). We extracted exact formula assignments for the thousands of peaks in each sample and sub-categorized them according to their elemental make up as being those of DOC (formulas containing C, H, and O only) or DON (formulas containing N). For Ctrl-S2, Ctrl-S3, TC, SHM and YT, respectively, the initial percent contribution to total peaks, based on numbers of peaks, is 70%, 68%, 89%, 74%, and 58%, for CHO formulas and 21%, 26%, 6%, 23%, and 30% for N-containing formulas. Furthermore, the percent based on peak relative magnitudes (Figure 25, bar diagram) is 90%, 88%, 96%, 90%, and 72%, for CHO formulas, and 7%, 10%, 1%, 9%, and 15%, for N-containing formulas for Ctrl-S2, Ctrl-S3, TC, SHM and YT, respectively. This data shows a clear difference between the anthropogenic sample and natural and riverine DOM compositions, where the percentages for N-containing formulas are highest in the anthropogenically-derived DOM (YT) and lowest in the forest-derived DOM (TC), both in number and magnitudes relative percentages, in comparison to the other samples.

The VK diagrams of both controls and the three DOM sources added to York River waters before the incubation was initiated are shown in figure 25. The VK diagram shows riverine DOM (Ctrl-S2 and Ctrl-S3) along with naturally-derived DOM (TC and SHM) largely comprise molecules that are lignin-like or CRAM-like situated in the central region of the diagram, where 74%, 70%, 53% and 58% of their formulas plot, respectively, in this region of the diagram (Figure 25a,c, green). YT, on the other hand,

comprises the highest aliphatic-like molecules content (red), where 28% of the assigned formulas plot in the aliphatic region of the VK diagram, which is remarkably different than both natural and riverine DOM. Moreover, TC and SHM encompass more aromatic formulas in comparison to all the other samples (Figure 25, black). These results agree with the general trend of terrestrial DOM in the literature (Sleighter and Hatcher, 2008b) where natural DOM generally plots in the central region of the VK diagram. Furthermore, our results show that YT comprises higher N-containing molecules, where 30% of the assigned formulas are N-containing formulas, whereas TC and SHM contain approximately 6% and 9%, respectively (Figure 25, bar diagrams). These findings confirm our hypothesis that DOM displays compositional diversity from anthropogenic and natural sources, which might affect their bioavailability potential.

3.3. Principal component analysis

To further our knowledge about the DOM turnover from these different sources, molecular changes occurring during incubation will be recorded by investigating the disappearance and appearance of specific molecular formulas in the FTICR-MS data set for each source materials. PCA analysis individually applied to each of the 8 time series of the two Ctrls and all amended samples using the CHO formulas, as the variables, enables the identification of molecules associated with the bio-labile and bio-produced pool of DOM from each source as the incubation experiment proceeds. The PCA biplots, using CHO formulas, for the incubated samples are shown in figures 29-36. The biplots of the scores (Figures 29a-36a) represent the projections of the samples onto each principal component (PC). The biplots of the loadings (Figures 29b-36b) signify the projections of all the variables (i.e., the relative magnitudes of the CHO formulas) onto

each PC, which explains the variable's contribution to the data variability along each PC. Table 2 reports the variance explained by each PC for each sample set. The high amount of variance explained by the sum of PC1 and PC2 suggests that the majority of the variability in the DOM of the incubated samples can be described in two dimensional space (Sleighter et al., 2010).

Table 2

Percentage of the total variance contributed by PC1 and PC2 for each sample.

	PC1	PC2
Ctrl-S2	63%	9%
TC-S2	36%	21%
SHM-S2	39%	25%
YT-S2	35%	22%
Ctrl-S3	30%	21%
TC-S3	29%	20%
SHM-S3	28%	20%
YT-S3	30%	21%

To fully understand why samples cluster or scatter in that space, the variables' locations in the corresponding loading biplots are further examined. It should be noted that variables (i.e., formulas) whose loadings are remote from the origin are the ones most responsible for explaining the samples' variance, dictating their scores along PC1 and PC2. In fact, variable loadings and sample scores that plot in similar areas of the biplots indicate that these specific samples have those corresponding formulas in high relative magnitude.

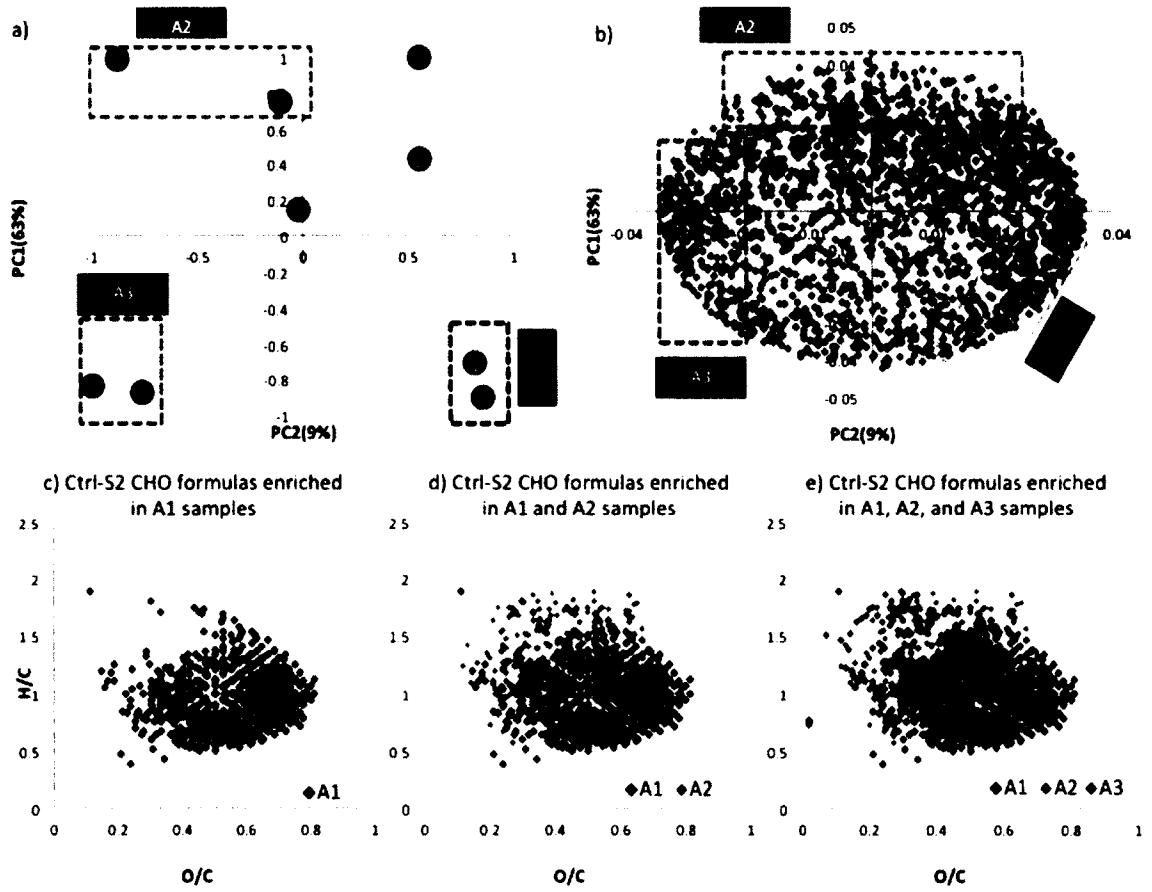

Figure 29. PCA results using the relative magnitudes of all Ctrl-S2 CHO formulas showing the biplot of the sample scores (a) and variable loadings (b), along with the van Krevelen diagrams of the CHO formulas included in the colored boxed areas (c-e).

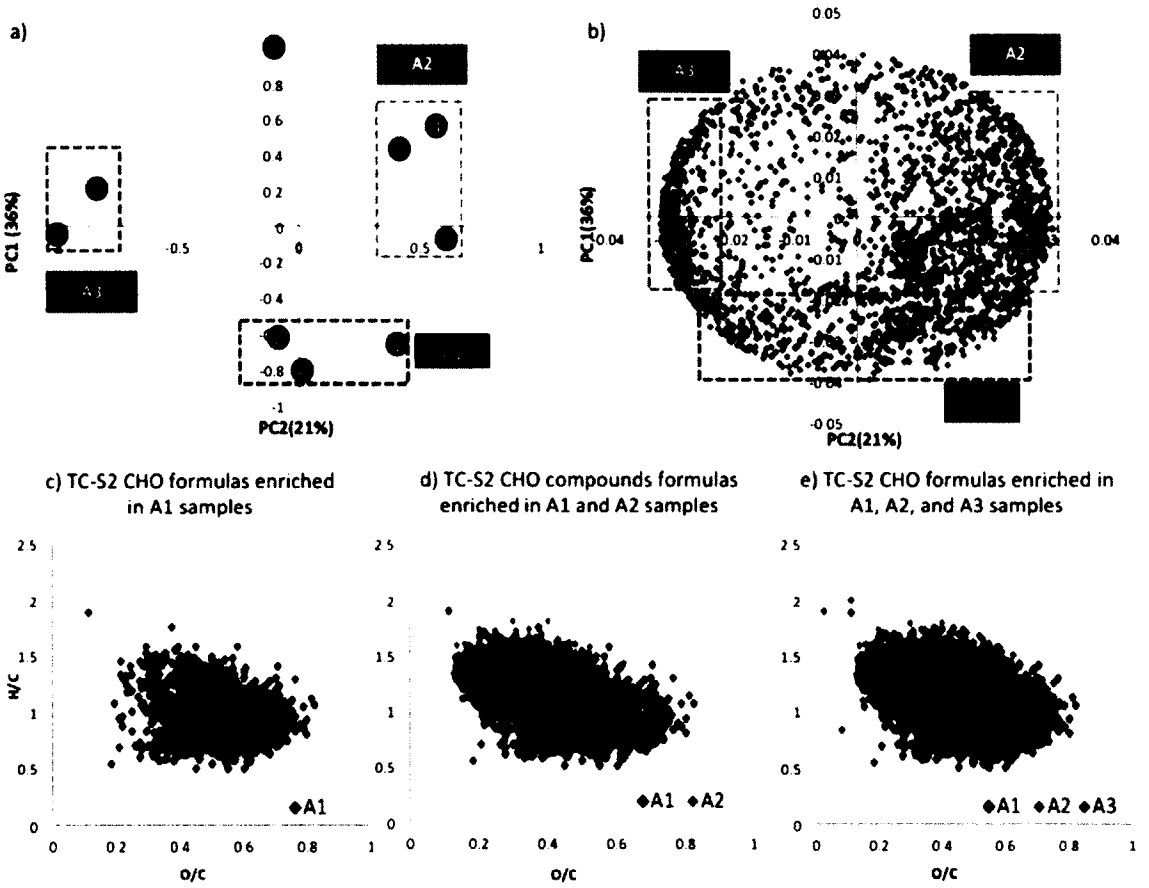

Figure 30. PCA results using the relative magnitudes of all TC-S2 CHO formulas showing the biplot of the sample scores (a) and variable loadings (b), along with the van Krevelen diagrams of the CHO formulas included in the colored boxed areas (c-e).

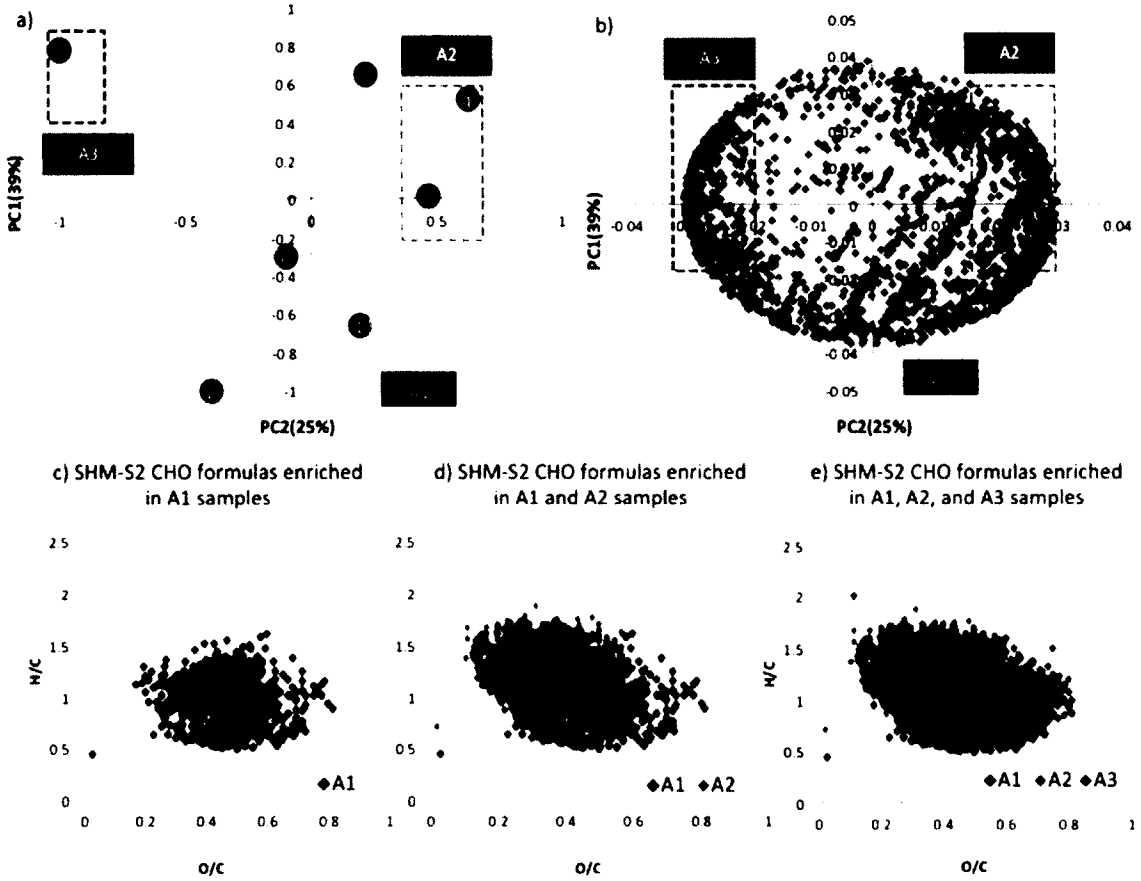

Figure 31. PCA results using the relative magnitudes of all SHM-S2 CHO formulas showing the biplot of the sample scores (a) and variable loadings (b), along with the van Krevelen diagrams of the CHO formulas included in the colored boxed areas (c-e).

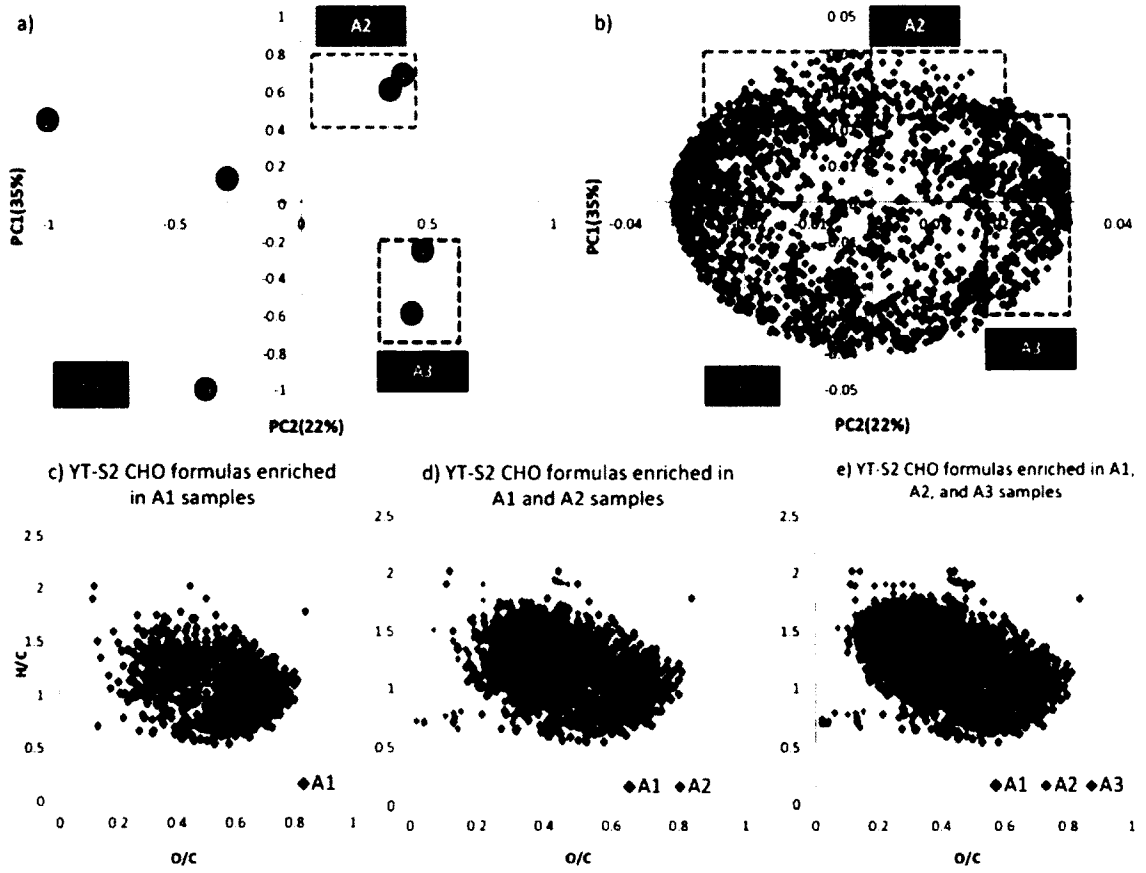

Figure 32. PCA results using the relative magnitudes of all YT-S2 CHO formulas showing the biplot of the sample scores (a) and variable loadings (b), along with the van Krevelen diagrams of the CHO formulas included in the colored boxed areas (c-e).

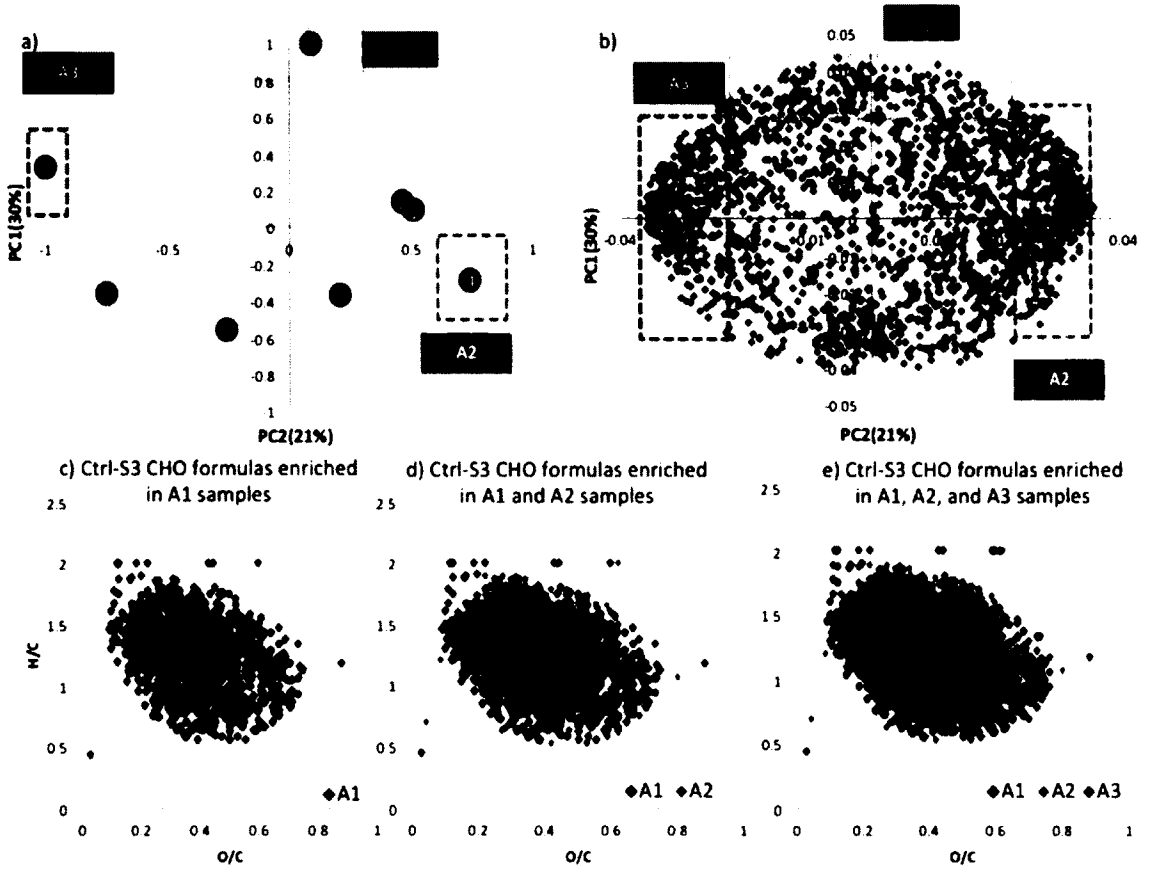

Figure 33. PCA results using the relative magnitudes of all Ctrl-S3 CHO formulas showing the biplot of the sample scores (a) and variable loadings (b), along with the van Krevelen diagrams of the CHO formulas included in the colored boxed areas (c-e).

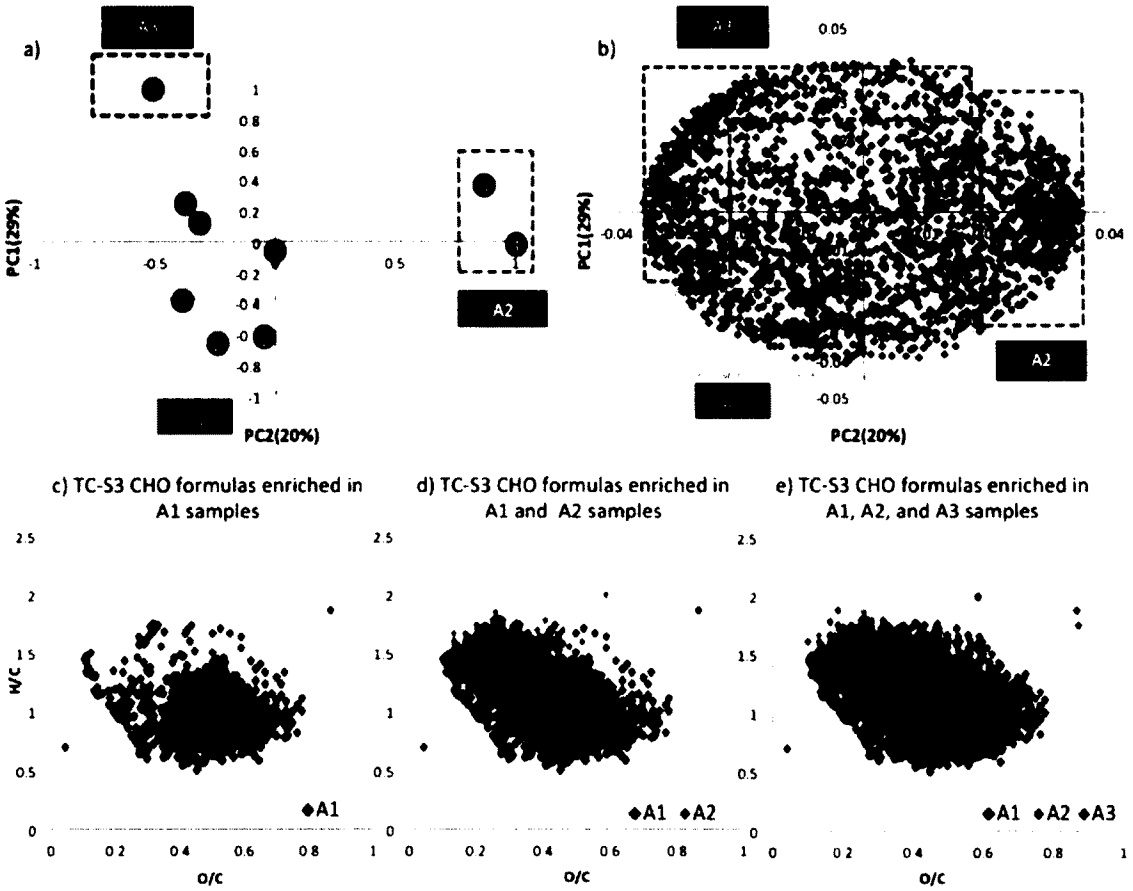

Figure 34. PCA results using the relative magnitudes of all TC-S3 CHO formulas showing the biplot of the sample scores (a) and variable loadings (b), along with the van Krevelen diagrams of the CHO formulas included in the colored boxed areas (c-e).

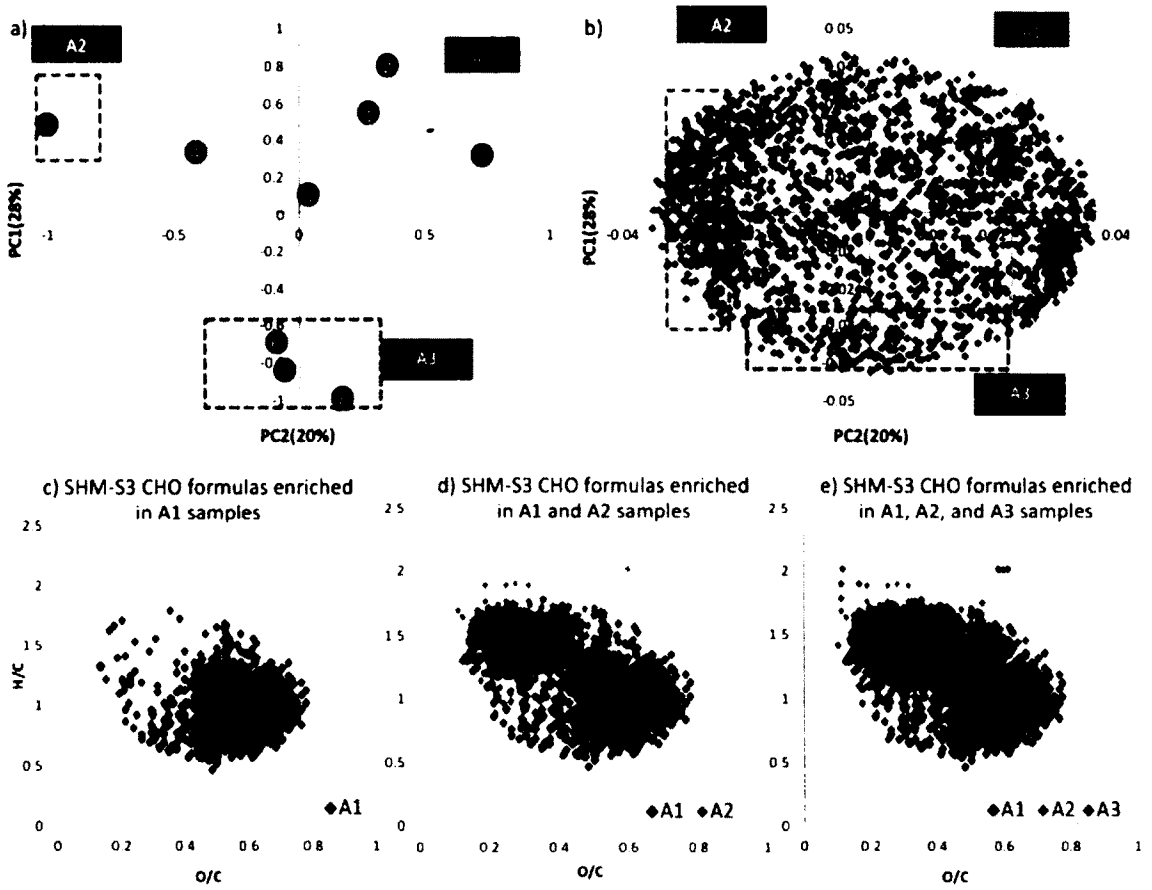

Figure 35. PCA results using the relative magnitudes of all SHM-S3 CHO formulas showing the biplot of the sample scores (a) and variable loadings (b), along with the van Krevelen diagrams of the CHO formulas included in the colored boxed areas (c-e).

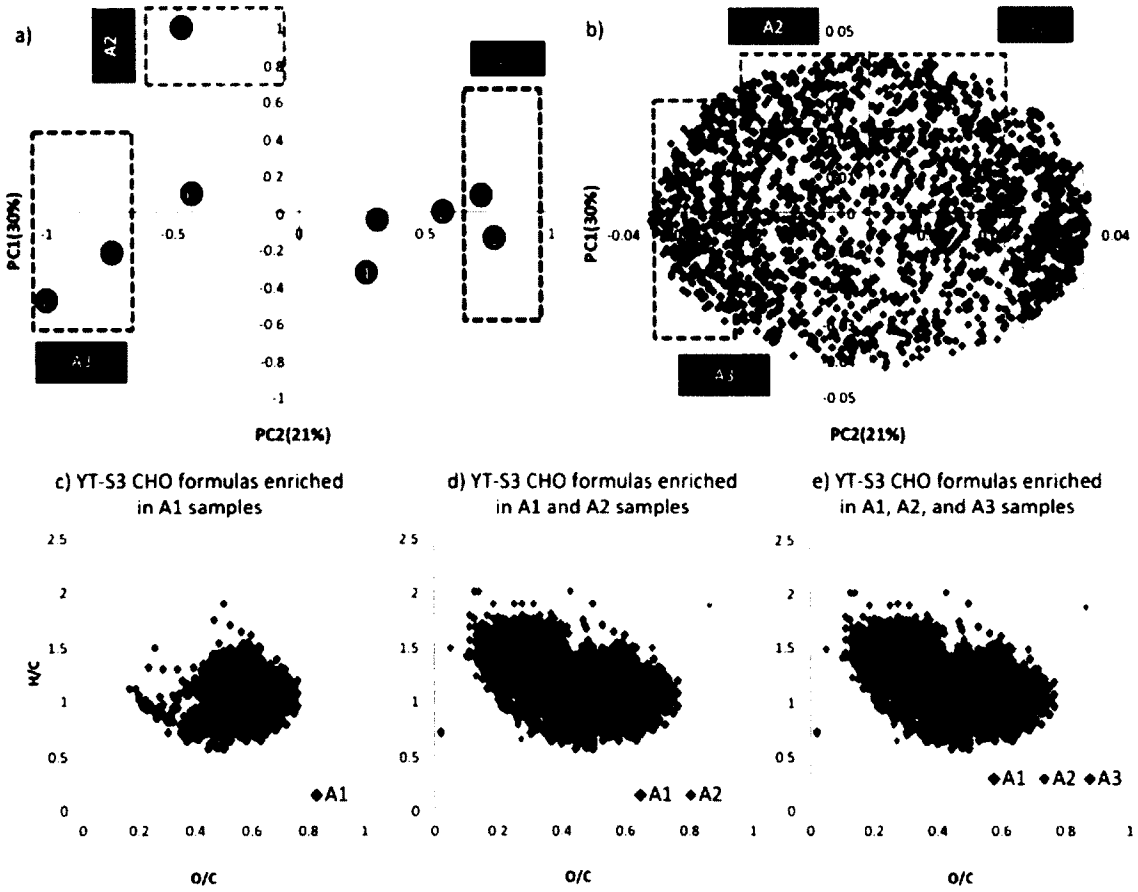

Figure 36. PCA results using the relative magnitudes of all YT-S3 CHO formulas showing the biplot of the sample scores (a) and variable loadings (b), along with the van Krevelen diagrams of the CHO formulas included in the colored boxed areas (c-e).

To better understand the changes occurring at the molecular level in the studied samples upon incubation, we assign cluster areas A1, A2, and A3 to samples at early (T_0, T_1, or T_2), middle (T_3, T_4, or T_5), and final (T_6, T_7, or T_8) stages of incubation, respectively. The juxtaposed formulas from the loading biplots, corresponding to A1, A2, and A3 in the sample score biplots highlight the changes occurring at the molecular level as the incubation progresses. By plotting formulas contained in each of these areas in VK space (panels (c-e) in Figures 29-36), we can show how clusters aligning in specific regions of the diagram are associated with each stage of the biodegradation

process. These clusters indicate which types of formulas explain most of the variance in the PCA between the incubated samples. VK diagrams for all samples showing area A1 (Figures 29c-36c), representative of the bio-labile DOM, comprising formulas enriched in aromatic molecules and lignin-like or CRAM-like structures that fall in the central region of VK space. We assign biolability to this cluster of formulas (A1) because they represent the formulas enriched in T_{0-2} samples (initial and first day of incubation). Similar to observations made by (Sleighter et al., 2014), we further define molecules enclosed in A2 having an intermediate lability. When comparing A1 to A2, the percentage of the aliphatic molecules identified by high H/C ratios (> 1.5) increases in all cases, except for Ctrl-S3, which shows a decrease in the aliphatic content at the middle stages (A2) of the incubation process (Figures 29d-36d and Figure 37a,b). In contrast, the number of aromatic formulas decreased in all samples as biodegradation proceeds (Figures 29d-36d and Figure 37c,d). One can hypothesize that biota first degrade aromatic and CRAM/lignin-like molecules to aliphatic molecules, which might render the DOM a more attractive food source for other species in the water column and/or these newly produced aliphatic molecules are of autochthonous nature that is know to be highly labile (Attermeyer et al., 2014; Sun et al., 1997). In fact, when comparing A2 and A3, we witness an increase in the aromatic and the CRAM/lignin content at the expense of the aliphatic content in all samples except for Ctrl-S3 and YT amendments (Figures 29e-36e and Figure 37), which might confirm the susceptibility of these newly formed autochthonous DOM to an *in situ* turnover. Ctrl-S3 and YT amendments sustain the increase in the aliphatic content at the final stages of incubation, while the aromatic continues to decline. This different trend might be due to either the production rate of the

newly formed DOM being high than its consumption rate, or that the presence of high DIN concentrations (in YT) might have shifted bacterial community composition and therefore the DOM turnover.

Contrary to Ctrl-S3, Ctrl-S2 behaves in a similar fashion as the natural amended samples. This can be attributed to the mixed background input to station S2 from surrounding swampy areas. YT amendments exhibited the highest aliphatic content at the final stages of the incubation experiment in both S2 and S3. The reason for this possible difference might be attributed to the anthropogenic nature of YT in comparison to the natural input from both SHM and TC. The high DIN concentrations (Figures 26-27) and N content in YT (Figure 25), along with its aliphatic signature in comparison to SHM and TC, may have triggered the different response from the microbial and phytoplankton communities in stimulating production of newly produced DOM with higher aliphatic content. The latter can be transported to higher salinities and fuel more biomass production downstream causing the unexplained algae blooms at higher salinities.

When comparing the behavior of each amended sample between S2 and S3, we noticed that the bio-produced DOM has a high density of aliphatic formulas in A3, more so for S3 in comparison to S2 (Figure 37a,b). This is also shown in panel (e) of each VK diagram (Figures 29-36) where the red dots are denser in the aliphatic region for S3 amendments than for S2 amendments. This difference might be attributed to the variation in phytoplankton and bacterial communities in relation to salinity. In fact, Schultz et al. (2003) were able to distinguish four distinct bacterial communities in the York River separated by temperature and salinity and suggest that bacterial community at

higher salinities (>12 ‰) may be more dependent upon phytoplankton as their carbon source in comparison to their low salinity counterparts. Therefore, this high production of aliphatic molecules at S3 might be a result of this dependency relationship between phytoplankton and bacteria where the former are intensively producing new autochthonous DOC to meet bacterial demand. Therefore, one can postulate that changes in salinity can affect the dynamics of both natural and anthropogenic DOM in rivers.

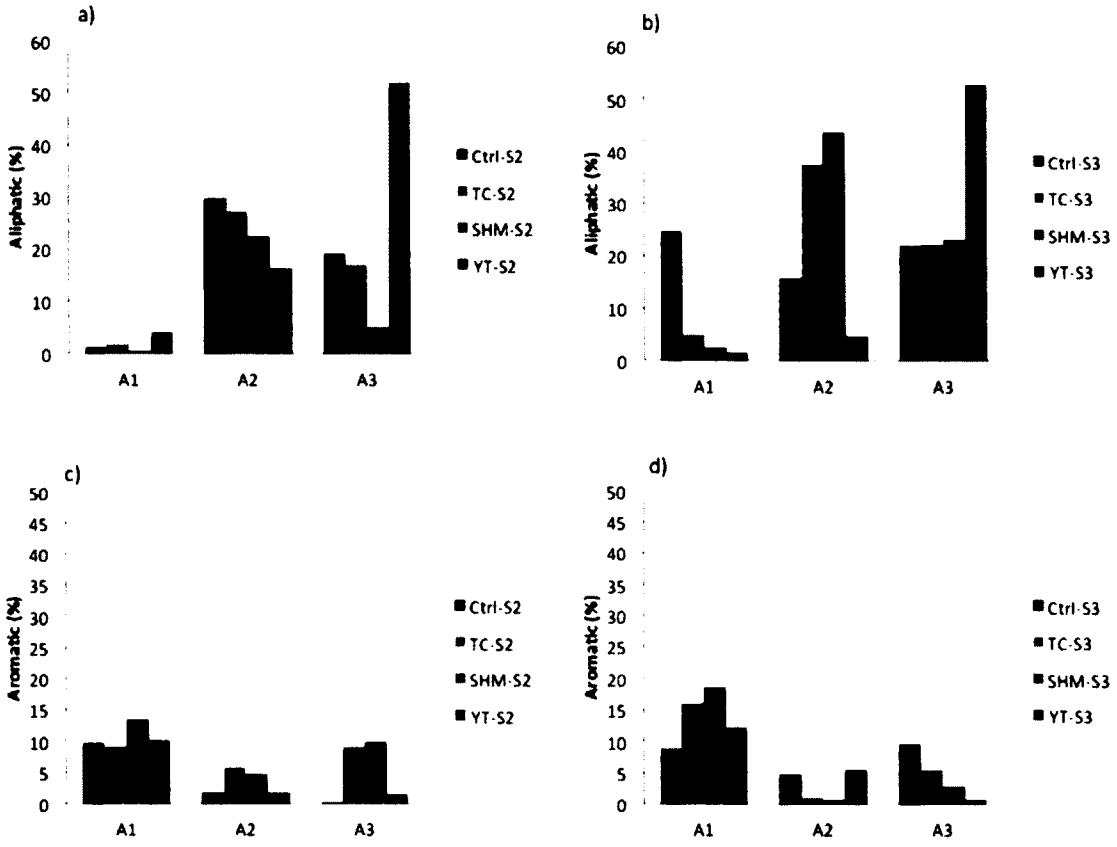

Figure 37. Bar diagrams showing the percent contribution of aliphatic formulas (a, c) and aromatic formulas (b, d) in the 3 selected colored areas of the PCA biplots shown in figures 29-36 for the controls and amended samples at both salinities (S2 and S3).

3.4. Two-dimensional correlation analysis

When examining the presence and absence of individual N-containing formulas throughout the incubation period by PCA analysis, we observe that the total number of these types of formulas decreases considerably with incubation time for all sample cases. Rather than presenting the PCA data we choose to employ 2D correlation analysis for the N-containing formulas data sets to further our understanding on what areas of the VK diagram this change is occurring most readily and how these areas correlate among themselves.

3.4.1. S2 (low salinity)

The advantage of 2D correlation analyses is that one can visualize changes, either correlated or non-correlated, using single (auto-correlation) or multiple (hetero-correlation) parameters during a process (Abdulla et al., 2013a). Lack of change generates white space on the map, so the observation of a signal on a 2D map is indicative of change.

We choose, herein, to implement the synchronous 2D auto-correlation analysis using H/C ratios of all N-containing formulas, which results in higher resolution 2D maps in comparison to the ones generated using O/C ratios (Sleighter et al., 2014). The 2D maps highlight the major changes in the number of formulas with H/C ratios induced by increasing incubation time in all incubated samples (Figure 38). The intensity along the diagonal line represents the auto-correlation at each H/C ratio among the formulas. In this case, intensity measures the number of formulas measured and is not the intensity of the individual mass spectral peaks. The off-diagonal cross peaks represent the cross correlation intensities (i.e., number of formulas) between the different H/C ratios. Cross

peaks are color-coded to indicate positive (red) or negative (green) correlations.

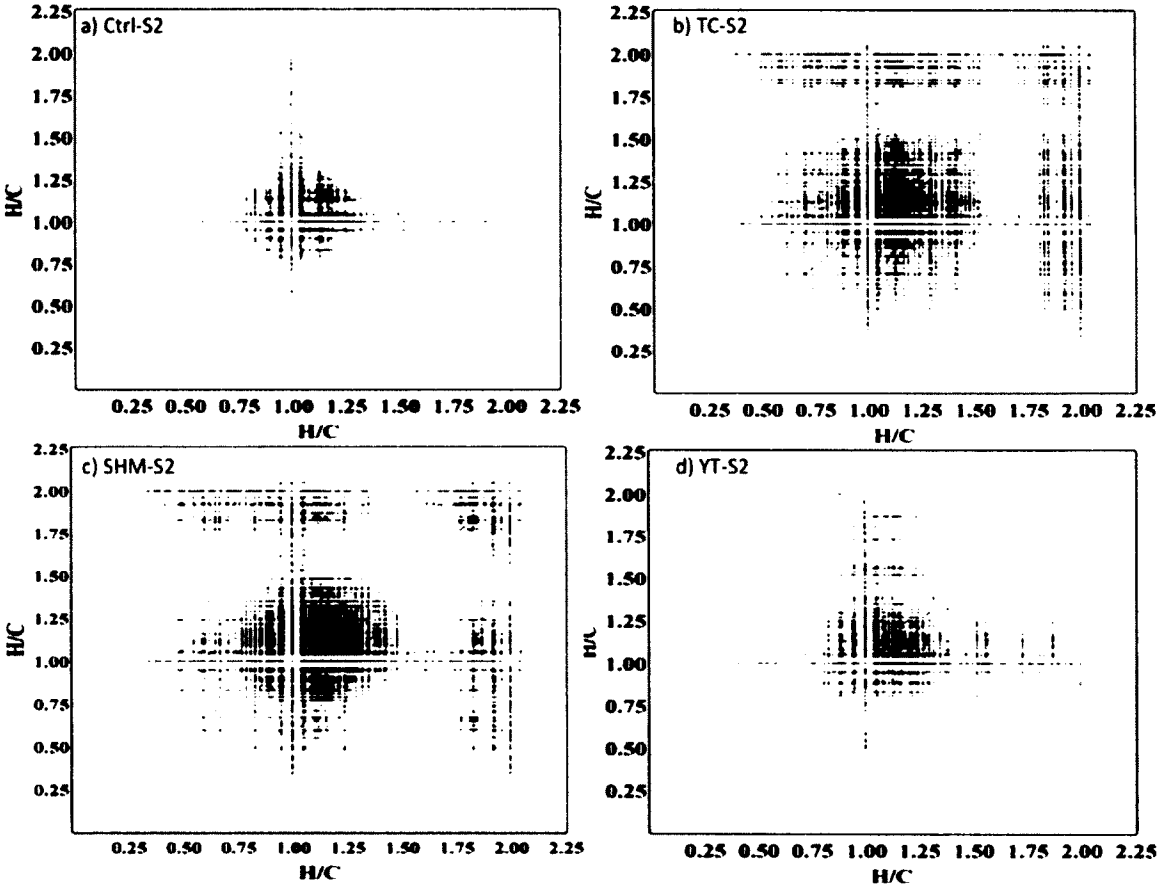

Figure 38. The H/C vs. H/C synchronous plots generated by applying 2D correlation on the N-containing formulas of a) Ctrl-S2, b) TC-S2, c) SHM-S2, and d) YT-S2. The correlation was based on the presence/absence of each individual formula as the incubation time progresses. Red indicates a positive correlation, while green indicates a negative correlation.

The intensity along the diagonal line of the Ctrl-S2 and YT-S2 samples is greatest at H/C ratios of 0.75-1.25. On the other hand, high diagonal intensity is shown at H/C ratios of 0.75-1.50 and at H/C 1.75-2.00 for TC-S2 and SHM-S2 samples, respectively, indicating that most of the changes for these samples occur in these regions upon

incubation. The cross correlation (off-diagonal) signals reveal that the formulas that fall in these regions have positive correlations (red color) with other peaks in the same general region. Upon closer inspection of the FTICR-MS data for each sample, we observe that the number of molecular formulas in these regions actually decreases with incubation time. Conversely, YT-S2 is the only sample that shows a negative correlation (green color) for the changes in the number of formulas at H/C 1.50-2.00 with the other formulas at H/C 0.75-1.25, which suggests that while the N-containing compounds with H/C ratios of 0.75-1.25, in the YT case are biodegraded, new compounds with higher H/C ratios are bio-produced. In contrast, the lack of intensity at the diagonal and off-diagonals for TC-S2 and SHM-S2 at H/C ratios of 1.50-1.75 implies that these formulas do not display significant changes in numbers during incubation. A closer look at their VK diagrams verifies the presence of these formulas in all the incubated TC and SHM samples. This indicates that formulas at H/C 1.50-1.75 in these two natural samples belong to a bio-resistant pool of compounds. In comparison, TC and SHM show a moderate to nonexistent bioproduction of N-containing formulas (specks of green color in the 2D maps). This difference in the bioproduction rate of new DON, between SHM-S2, TC-S2 and YT-S2, is likely due to their different sources, where YT-S2 may have a fresh labile anthropogenic DON pool that is easily assimilated by biota. It is also likely that the DOM source plays a significant role in producing new DON from assimilated DON and DOC by biota, a fact that is hardly observed when using classical bulk analytical measurements (e.g., nutrient analysis).

3.4.2. S3 (high salinity)

When comparing S2 incubation with S3 incubation using the 2D correlation, it is

obvious that we observe a high uptake of DON in S3 incubation in comparison to S2 incubation. First, only one color (red color) is overwhelming all 4 maps (Figure 39), suggesting similar behavior for all four samples including Ctrl-S3. Upon closer inspection of their FTICR-MS data sets, we observe that the number of molecular formulas, in the displayed regions with the high diagonal intensity in the 2D maps, is decreasing with incubation time for all 4 samples. A pattern different from the one displayed with S2, where we only witness a production of new DON in the case of YT amendments. Ctrl-S3, SHM-S3, and YT-S3 show similar rate of DON uptake in the CRAM/lignin like region displayed by the high diagonal intensity at (H/C 0.75-1.5). We also witness an uptake in TC-S3 from the same region but with less intensity. YT-S3 exhibits more DON uptake in the aliphatic region at (H/C >1.5) than TC-S3 and SHM-S3, an expected trend since YT comprises more aliphatic compounds as shown in Figure 25. The most noteworthy result is the remarkable change in the anthropogenic DON reactivity with salinity changes.

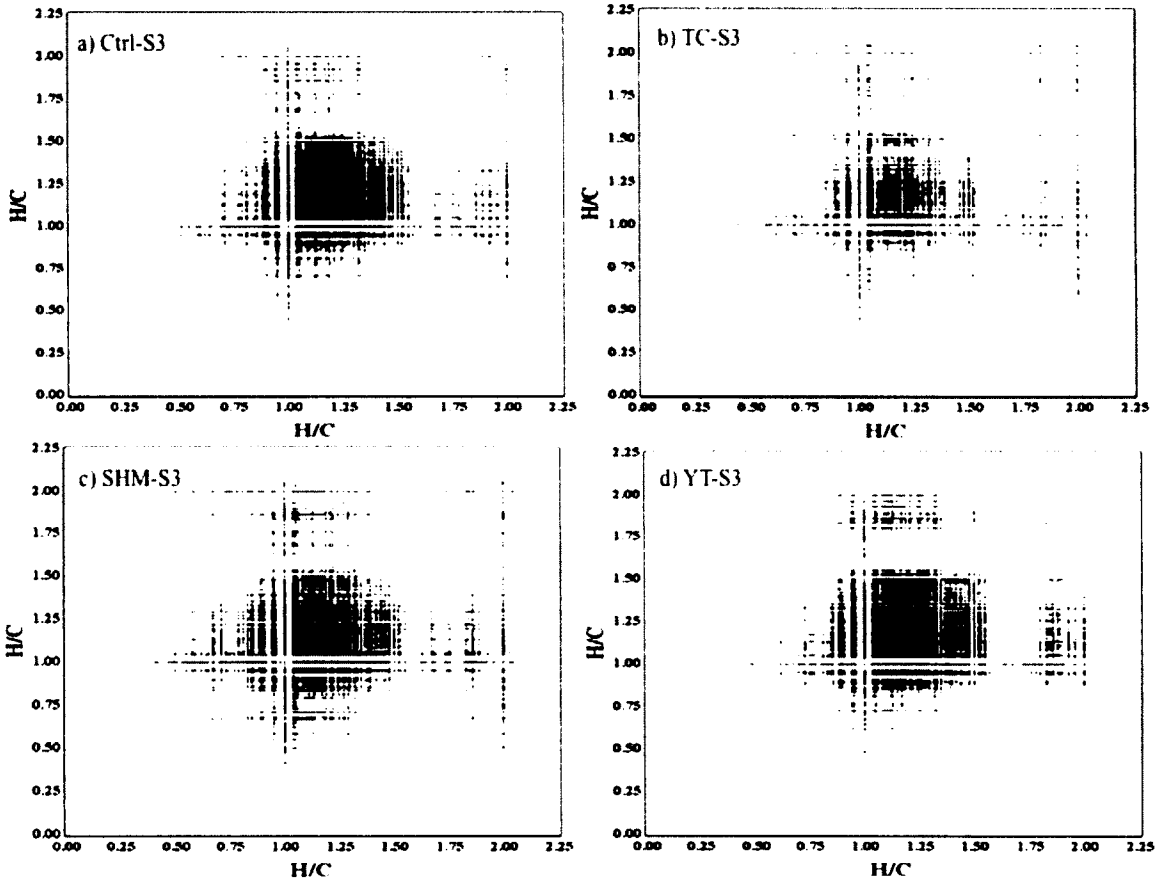

Figure 39. The H/C vs. H/C synchronous plots generated by applying 2D correlation on the N-containing formulas of a) Ctrl-S3, b) TC-S3, c) SHM-S3, and d) YT-S3. The correlation was based on the presence/absence of each individual formula as the incubation time progresses. Red indicates a positive correlation, while green indicates a negative correlation.

4. CONCLUSIONS

Our results demonstrate that DOM from the studied samples exhibits differences in the degree of biodegradation and type of bio-produced compounds, which can be related to the dramatic difference in DOM source and molecular formula signatures. We find that biomass production is higher with anthropogenic DOM amendments in comparison the naturally derived DOM, and that change in salinity enhances DOM

biodegradation, where the removal of N-containing formulas and production of new aliphatic formulas increases in high salinity incubation. Furthermore, the bio-produced DOM from the anthropogenic source exhibits a higher aliphatic signature in comparison to the one produced from natural amendments. Moreover, our findings suggest that anthropogenic DOM is highly reactive in the natural environment in comparison to the naturally derived DOM and that simple assays examining net consumption or production of bulk dissolved organic N pools are inadequate for assessing the bioavailability of DOM from these different sources. Bioavailability information is essential for coastal planning, as changes in the materials supporting food webs is decisive for sustaining estuarine ecosystems and preventing eutrophication.

CHAPTER V

CONCLUSIONS AND FUTURE DIRECTIONS

1. CONCLUSIONS

This thesis addresses two main areas of research with the unifying theme being the chemical characterization of DOM and its subcomponents DON and DOC in the James and York River systems of the Chesapeake Bay. The focus of this research is to study how DOM reactivity relates to its chemical composition, and therefore, its source material. The topics include the assessment of DOM reactivity from different source materials, in natural receiving waters, under photochemical, biological, and salinity change stressors. These studies are important for deciphering the interrelationships between C and N cycles and source material and for gaining better understanding of processes associated with downstream eutrophication.

It has been long understood that future climate change will have the highest impact on the global coastal zone, where 60% of the world population lives, a number that could reach 75% in the 2030s (Cosgrove and Cosgrove, 2012). Together with rising urbanization and land uses changes, climate change is predicted to change the physical, chemical, and biological properties of the water bodies at the fringe of the global coastal zones.

For instance, wastewater treatment plants (WWTPs) are considered an important point source for N loading in many aquatic environments. While we now know that many phytoplankton take up natural organic N (Mulholland and Lomas, 2008), there are relatively few data on the bioavailability of anthropogenic organic N. Likewise, despite its relevance to the terrestrial C budget, little is known of the nature of the organic C

decomposed and ultimately respired in aquatic systems. In particular, we do not know how this role may change in the future due to the interrelation between DOM dynamics and human impact. Furthermore, it is unclear how biological and photochemical processes would alter the dynamics of these various sources of DOM (natural and anthropogenic) in aquatic systems. Understanding the chemical composition and reactivity of both natural and anthropogenic DOM in natural receiving waters should be an important aspect of determining water quality standards. The analytical approach presented in this thesis would allow more detailed characterization of the DOM and its transformation from sources to receiving waters.

The conclusions of these research topics are discussed below.

Chapter 2 describes the use of ESI-FTICR-MS for the assessment of organic N reactivity from WWTP effluent, confirming the hypothesis that this technique could be applied to the characterization of DON from anthropogenic sources. Bioassays were performed on samples collected at the end of the biological process from two wastewater treatment plants achieving advanced N removal. The samples were concentrated, and then added to natural water samples collected from the oligohaline James River, a major tributary of the Chesapeake Bay. My results demonstrate that while the lignin-like fraction of the effluent DOM (some of which contains N) was conserved, a large portion of aliphatic and aromatic compounds containing N was removed (79-100%) during incubations, while other compounds were produced. Furthermore, the two effluents exhibited differences in the degree of degradation and type of degradation, which can be related both to the various processes employed in the two different WWTPs and the dramatic differences in the type of influent they receive. These findings suggest that this

type of anthropogenic DON is highly reactive in the natural environment and that simple assays examining net consumption or production of bulk dissolved organic N pools are inadequate for assessing its true reactivity.

I would anticipate that this information would be extremely valuable to regulatory agencies whose role is to evaluate the impact that wastewater has on DON dynamics in estuaries. Often impacts are evaluated on the basis of bulk DON measurements and I show that such measurements are not particularly effective in describing DON bioavailability. Accordingly, it is imperative that these regulatory agencies demand the use of tests that would allow for more accurate assessments than are in current use. Admittedly, implementation of ESI-FTICR-MS protocols for evaluation of DON reactivity is far from standard testing, but it behooves the agencies to seek such capabilities if there is a desire to conduct meaningful evaluations of impact.

Chapter 3 addressed the effects of photoirradiation on the turnover of DOM from both natural and anthropogenic sources at the molecular level. Analysis of long-term photoirradiated samples via Fourier-transform ion cyclotron resonance mass spectrometry (FT-ICR-MS) identified both the photolabile and the photoproduced DON from both natural and anthropogenic sources. While photoproduction of DON was prominent with natural dissolved organic matter (DOM) sources, even in low nitrogen environment, the anthropogenic source shows a shift from photobleaching to photohumification denoted by an increase in the average molecular weight (MW) and the double bound equivalent (DBE) after 25 days of a continuous exposure to UV light, implying condensation of low MW molecules (LMW) to form high MW (HMW) molecules. Furthermore, the sharp increase in N/C molar ratio, in the anthropogenic source, substantiates the photoinduced

dissolved inorganic nitrogen (DIN) incorporation hypothesis. My experimental results demonstrated that photochemistry transforms DON from complex structural entities to ammonia, aliphatic molecules, and low carbon number molecules that might enhance microbial metabolism, and eventually increases CO_2 emissions and reduces DOM concentrations in stream ecosystems. Hence, driving substantial variation in riverine DOM, and, thus, estuarine optics and photochemistry and bioavailability. Furthermore, we validate that photochemistry is one of the main processes that shapes the DON quality in aquatic systems regardless of its original source.

Chapter 4 examined the potential bioavailability of DOM and its subcomponents DOC and DON from different sources in natural receiving waters of the York River. My approach combined the use of classical bulk analysis and ultrahigh resolution mass spectrometry to detect intrinsic changes in the DOM pertinent to each source upon incubation. My results demonstrate that DOM from the studied samples exhibited differences in the degree of biodegradation and type of compounds biologically produced, which can be related to the dramatic differences of their DOM source and structural signature. I found that biomass production is higher with anthropogenic DOM amendments in comparison the naturally derived DOM, and that change in salinity enhances DOM biodegradation. Furthermore, the bio-produced DOM exhibited higher aliphatic signature in comparison to the one produced from natural amendments. Moreover, my findings suggest that anthropogenic DOM is highly reactive in the natural environment in comparison to the naturally derived DOM and that simple assays examining net consumption or production of bulk dissolved organic N pools are inadequate for assessing the bioavailability of DOM from these different sources. This

information is essential for coastal planning, as changes in the materials supporting food webs is decisive for sustaining estuarine ecosystems and preventing eutrophication.

2. FUTURE DIRECTIONS

The new scientific developments described in this thesis highlight the crucial role of DOM as a link between terrestrial and aquatic systems. My new approach with respect to molecular characterization enables a more profound understanding of the intricate interrelation between differences in DOM sources and its behavioral variability in receiving waters. However, to fully understand the exceptionally complicated dynamics of DOM and to utterly grasp how land use changes affect its role as a link between terrestrial and aquatic systems, further research is undeniably needed, in particular, research pursuing DOM molecular variation on spatial and temporal scales, along climate, nutrient, hydrologic, and land use gradients.

Storm events can account for 71-90% of the total DOM released from streams annually (Dalzell et al., 2007; Fellman et al., 2009; Raymond and Saiers, 2010). However, DOM variability due to these events are not well understood since antecedent hydrologic regimes govern the changes in DOM quality and quantity released to stream waters (Easthouse et al., 1992; Vidon et al., 2008). It is of critical importance to understand how these storm events influence the delivery of organic matter to estuaries, since variability of wet seasons and tropical cyclones frequency are expected to increase due to the global climate change (Lozano et al., 2004; Najjar et al., 2010). An understanding of the changes in DOM concentration, composition, and reactivity during storm events compared to baseflow conditions is needed in order to predict DOM biogeochemical response in aquatic systems. Furthermore, additional research is needed

to tackle the impact of watershed characteristics (topography) on the composition and reactivity of DOM. Finally, relationships between analytical approach and DOM optical parameters (i.e., S_R and SUVA) need to be investigated for a simpler assessment of DOM reactivity during different periods or seasons in different ecological systems.

REFERENCES

Abdulla, H.A.N, Minor, E.C., Dias, R.F., Hatcher, P.G., 2013a. Transformations of the chemical compositions of high molecular weight DOM along a salinity transect: Using two dimensional correlation spectroscopy and principal component analysis approaches. Geochim. Cosmochim. Acta 118, 231-246.

Abdulla, H.A.N, Sleighter, R.L., Hatcher, P.G., 2013b. Two Dimensional Correlation Analysis of Fourier Transform Ion Cyclotron Resonance Mass Spectra of Dissolved Organic Matter: A New Graphical Analysis of Trends. Anal. Chem. 85 (8), 3895-3902.

Altieri, K., Turpin, B., Seitzinger, S., 2009a. Oligomers, organosulfates, and nitrooxy organosulfates in rainwater identified by ultra-high resolution electrospray ionization FT-ICR mass spectrometry. Atmos. Chem. Phys. 9 (7), 2533-2542.

Altieri, K., Turpin, B., Seitzinger, S., 2009b. Composition of dissolved organic nitrogen in continental precipitation investigated by ultra-high resolution FT-ICR mass spectrometry. Environ. Sci. Technol. 43 (18), 6950-6955.

Amon, R.M.W., Benner, R., 1996. Photochemical and microbial consumption of dissolved organic carbon and dissolved oxygen in the Amazon River system. Geochim. Cosmochim. Acta 60 (10), 1783-1792.

Asmala, E., Autio, R., Kaartokallio, H., Pitkånen, L., Stedmon, C.A., Thomas, D.N., 2013. Bioavailability of riverine dissolved organic matter in three Baltic Sea estuaries and the effect of catchment land use. Biogeosciences 10 (11), 6969-6986.

Attermeyer, K., Hornick, T., Kayler, Z.E., Bahr, A., Zwirnmann, E., Grossart, H.P., Premke, K., 2014. Enhanced bacterial decomposition with increasing addition of autochthonous to allochthonous carbon without any effect on bacterial community composition. Biogeosciences 11 (6), 1479-1489.

Aufdenkampe, A.K., Mayorga, E., Raymond, P.E., Melack, J.M., Doney, S.C., Alin, S.R., Aalto, R., Kyungsoo, Y., 2011. Riverine coupling of biogeochemical cycles between land, oceans, and atmosphere. Front. Ecol. Environ. 9 (1), 53-60.

Benner, R., Opsahl, S., Chin-Leo, G., Richey, J.E., Forsberg, B.R., 1995. Bacterial carbon metabolism in the Amazon River system. Limnol. Oceanogr. 40 (7), 1262-1270.

Benner, R., 2003. Molecular indicators of the bioavailability of dissolved organic matter. In: Sinsabaugh R.L., Findley S. (Eds.), Aquatic ecosystem: interactivity of dissolved organic matter. Academic Press, San Diego, pp. 509-546.

Bertilsson, S. et al., Stepanauskas, R., Cuadros-Hansson, R., Graneli, W., Wikner, J., Tranvik, L., 1999. Photochemically induced changes in bioavailable carbon and nitrogen pools in a boreal watershed. Aquat. Microb. Ecol. 19 (1), 47-56.

Bott, C., 2014. Hampton Road Sanitation District, Washington, D.C. Personal Communication.

Bronk, D.A., Lomas, M.W., Glibert, P.M., Schukert, K.J., Sanderson, M.P., 2000. Total dissolved nitrogen analysis: comparisons between the persulfate, UV and high temperature oxidation methods. Mar. Chem. 69 (1), 163-178.

Bronk, D., See, J., Bradley, P., Killberg, L., 2007. DON as a source of bioavailable nitrogen for phytoplankton. Biogeosciences 4 (3), 283-296.

Bronk, D.A., Roberts, Q.N., Sanderson, M.P., Canuel, E.A., Hatcher, P.G., Mesfioui, R., Filippino, K.C., Mulholland, M.R., Love, N.G., 2010. Effluent organic nitrogen (EON): bioavailability and photochemical and salinity-mediated release. Environ. Sci. Technol. 44 (15), 5830-5835.

Burak, S., Dogan, E., Gazioglu., 2004. Impact of urbanization and tourism on coastal environment. Ocean. Coast. Manage. 47 (9-10), 515-527.

Canadell, J.G., Le Quéré, C., Raupach, M.R., Field, C. B., Buitenhuis, E.T., Ciais, P., Conway, T.J., Gillett, N.P., Houghton, R.A., Marland, G., 2007. Contributions to accelerating atmospheric CO2 growth from economic activity, carbon intensity, and efficiency of natural sinks. P. Natl. A. Sci. 104 (47), 18866-18870.

Canfield, D.E., Glazer, A.N., Falkowski, P.G., 2010. The evolution and future of Earth's nitrogen cycle. Science 330 (6001), 192-196.

Chavez, F.P., Messié, M., Pennington, J.T., 2011. Marine primary production in relation to climate variability and change. Ann. Rev. Mar. Sci. 3, 227-260.

Chen, C.T.A., Borges, A.V., 2009. Reconciling opposing views on carbon cycling in the coastal ocean: Continental shelves as sinks and near-shore ecosystems as sources of atmospheric CO2. Deep-Sea. Res. II 56 (8-10), 578-590.

Chen, H., Stubbins, A., Hatcher, P.G., 2011. A mini-electrodialysis system for desalting small volume saline samples for Fourier transform ion cyclotron resonance mass spectrometry. Limnol. Oceanogr. Methods 9, 582-592.

Chen, H., Abdulla H.A., Sanders R. L., Myneni S.C.B., Mopper K., Hatcher, P.G., 2014. Production of Black Carbon-like and Aliphatic Molecules from Terrestrial

Dissolved Organic Matter in the Presence of Sunlight and Iron. Environ. Sci.Technol. Lett. 1 (10), 399–404

Cole, J.J., Cole, J.J., Caraco, N.F., Caraco, N.F., 2001. Carbon in catchments: connecting terrestrial carbon losses with aquatic metabolism. Mar. Freshwater Res. 52 (1), 101-110.

Cory, R.M., Kaplan, L.A., 2012. Biological lability of streamwater fluorescent dissolved organic matter. Limnol. Oceanogr. 57 (5), 1347.

Cosgrove, W.J., Rijsberman, F.R., 2014. World water vision: making water everybody's business. Eearthscan, New York.

Dagg, M., Sato, R., Liu, H., Bianchi, T.S., Green, R., Powell, R., 2008. Microbial food web contributions to bottom water hypoxia in the northern Gulf of Mexico. Cont. Shelf. Res. 28 (9), 1127-1137.

Dalzell, B.J., Filley, T.R., Harbor, J.M., 2007. The role of hydrology in annual organic carbon loads and terrestrial organic matter export from a midwestern agricultural watershed. Geochim. Cosmochim. Acta 71 (6), 1448-1462.

Del Giorgio, P.A., Pace, M.L., 2008. Relative independence of dissolved organic carbon transport and processing in a large temperate river: the Hudson River as both pipe and reactor. Limnol. Oceanogr. 53 (1), 185-197.

Del Vecchio, R., Blough, N.V., 2004. On the origin of the optical properties of humic substances. Environ. Sci. Technol. 38 (14), 3885-3891.

Dignac, M.F., Ginestel, P., Bruchet, A., Audic, J.M., Derenne, S., Largeau, C., 2001. Changes in the organic composition of wastewater during biological treatment as studied by NMR and IR spectroscopies. Water. Sci. Technol. 43 (2), 51-58.

Dittmar, T., Koch, B., Hertkorn, N., Kattner, G., 2008. A simple and efficient method for the solid phase extraction of dissolved organic matter (SPE-DOM) from seawater. Limnol. Oceanogr. Methods 6, 230-235.

Dodds, W.K., Bouska, W.W., Eitzmann, J.L., Pilger, T.J., Pitts, K.L., Riley, A.J., Schloesser, J.T., Thornbrugh, D.J., 2008. Eutrophication of US freshwaters: analysis of potential economic damages. Environ. Sci. Technol. 43 (1), 12-19.

Dolman, A.J., van der Werf, G.R., van der Molen, M.K., Ganssen, G., Erisman, J.-W. and Strengers, B., 2010. A Carbon cycle science update since IPCC AR-4. AMBIO 39 (5/6), 402-412.

Ducklow, H., Carlson, C., Church, M., Kirchman, D., Smith, D., Steward, G., 2001. The seasonal development of the bacterioplankton bloom in the Ross Sea, Antarctica, 1994–1997. Deep-Sea. Res. II 48 (19-20), 4199-4221.

Easthouse, K.B., Mulder, J., Christophersen, N., Seip, H.M., 1992. Dissolved organic carbon fractions in soil and stream water during variable hydrological conditions at Birkenes, southern Norway. Water. Resour. Res. 28 (6), 1585-1596.

Fasching, C., Battin, T., 2012. Exposure of dissolved organic matter to UV-radiation increases bacterial growth efficiency in a clear-water Alpine stream and its adjacent groundwater. Aquat. Sci. 74 (1), 143-153.

Fellman, J.B., Hood, E., Edwards, R.T., D'Amore, D.V., 2009. Changes in the concentration, biodegradability, and fluorescent properties of dissolved organic matter during stormflows in coastal temperate watersheds. J. Geophys. Res-Biogeo. 114 (G1), 2005-2012.

Fellman, J.B., Hood, E., Spencer, R.G., 2010. Fluorescence spectroscopy opens new windows into dissolved organic matter dynamics in freshwater ecosystems: A review. Limnol. Oceanogr. 55 (6), 2452-2462.

Filippino, K.C., Mulholland, M.R., Bernhardt, P.W., Boneillo, G.E., Morse, R.E., Semcheski, M., Marshall, H., Love, N.G., Roberts, Q., Bronk, D.A., 2011. The bioavailability of effluent-derived organic nitrogen along an estuarine salinity gradient. Estuar. Coast. 34 (2), 269-280.

Galloway, J.N., Dentener, F.J., Capone, D.G., Boyer, E.W., Howarth, R.W., Seitzinger, S.P., Asner, G.P., Cleveland, C., Green, P., Holland, E., 2004. Nitrogen cycles: past, present, and future. Biogeochemistry 70 (2), 153-226.

Galloway, J.N., Townsend, A.R., Erisman, J.W., Bekunda, M., Cai, Z., Freney, J.R., Martinelli, L.A., Seitzinger, S.P., Sutton, M., 2008. Transformation of the nitrogen cycle: recent trends, questions, and potential solutions. Science 320 (5878), 889-892.

Green, S.A., Blough, N.V., 1994. Optical absorption and fluorescence properties of chromophoric dissolved organic matter in natural waters. Limnol. Oceanogr. 39 (8), 1903-1916.

Gruber, N., Galloway, J.N., 2008. An Earth-system perspective of the global nitrogen cycle. Nature 451 (7176), 293-296.

Han, Y., Li, X., Nan, Z., 2011. Net anthropogenic nitrogen accumulation in the Beijing metropolitan region. Environ. Sci. Pollut. R. 18, 485-496.

Hansen, K. and Koroleff, F. F., 1992. Determination of nutrients. In: Grasshoff, K., Kremling, K., Ehrhardt, M., (Eds.), Methods of Seawater Analysis. John Wiley, Hoboken, pp. 159–228.

Hedges, J.I., 1992. Global biogeochemical cycles: progress and problems. Mar. Chem. 39 (1-3), 67-93.

Hedges, J.I., Keil, R.G., Benner, R., 1997. What happens to terrestrial organic matter in the ocean? Org. Geochem. 27 (5-6), 195-212.

Helms, J. R., Stubbins, A., Ritchie, J. D., Minor, E. C., Kieber, D. J., Mopper, K., 2008. Absorption spectral slopes and slope ratios as indicators of molecular weight, source, and photobleaching of chromophoric dissolved organic matter. Limnol. Oceanogr. 53 (3), 955-969.

Helms, J.R., Mao, J., Schmidt-Rohr, K., Abdulla, H., Mopper, K., 2013. Photochemical flocculation of terrestrial dissolved organic matter and iron. Geochim. Cosmochim. Acta 121, 398-413.

Helms, J.R., Mao, J., Stubbins, A., Schmidt-Rohr, K., Spencer, R.G.M., Hernes, P.J., Mopper, K., 2014. Loss of optical and molecular indicators of terrigenous dissolved organic matter during long-term photobleaching. Aquat. Sci. 76, 353-373.

Hertkorn, N., Benner, R., Frommberger, M., Schmitt-Kopplin, P., Witt, M., Kaiser, K., Kettrup, A., Hedges, J. I., 2006. Characterization of a major refractory component of marine dissolved organic matter. Geochim. Cosmochim. Acta 70 (12), 2990-3010.

Hertkorn, N., Harir, M., Koch, B., Michalke, B., Schmitt-Kopplin, P., 2013. High-field NMR spectroscopy and FTICR mass spectrometry: powerful discovery tools for the molecular level characterization of marine dissolved organic matter. Biogeosciences 10, 1583-1624.

Hockaday, W.C., Grannas, A.M., Kim, S., Hatcher, P.G., 2006. Direct molecular evidence for the degradation and mobility of black carbon in soils from ultrahigh-resolution mass spectral analysis of dissolved organic matter from a fire-impacted forest soil. Org. Geochem. 37 (4), 501-510.

Hockaday, W.C., Purcell, J.M., Marshall, A.G., Baldock, J.A., Hatcher, P.G., 2009. Electrospray and photoionization mass spectrometry for the characterization of organic matter in natural waters: a qualitative assessment. Limnol. Oceanogr. Methods 7, 81-95.

Hopkinson, C.S., Buffam, I., Hobbie, J., Vallino, J., Perdue, M., Eversmeyer, B., Prahl, F., Cover, J., Hodson, R., Moran, M.A., Smith., E., Baross, J., Crump, B., Findlay, S., Foreman, K., 1998. Terrestrial inputs of organic matter to coastal ecosystems: An intercomparison of chemical characteristics and bioavailability. Biogeochemistry 43 (3), 211-234.

Hosen, J.D., McDonough, O.T., Febria, C.M. and Palmer, M.A., 2014. Dissolved Organic Matter Quality and Bioavailability Changes across an Urbanization Gradient in Headwater Streams. Environ. Sci. Technol. 48 (14), 7817-7824.

Howarth, R., Jensen, H., Marino, R., Postma, H., 1995. Transport to and processing of phosphorus in near-shore and oceanic waters. In: phosphorus in the global environment. Tiessen, H. (Ed.), John Wiley, New York, pp. 323–345.

Howarth, R.W. and Marino, R., 2006. Nitrogen as the limiting nutrient for eutrophication in coastal marine ecosystems: evolving views over three decades. Limnol. Oceanogr. 51 (1), 364-376.

Howarth, R.W., 2008. Coastal nitrogen pollution: a review of sources and trends globally and regionally. Harmful Algae 8 (1), 14-20.

Howarth, R., Chan, F., Conley, D.J., Garnier, J., Doney, S.C., Marino, R., Billen, G., 2011. Coupled biogeochemical cycles: eutrophication and hypoxia in temperate estuaries and coastal marine ecosystems. Front. Ecol. Environ. 9 (1), 18-26.

Inglett, P., Rivera-Monroy, V. and Wozniak, J., 2011. Biogeochemistry of Nitrogen Across the Everglades Landscape. Crit. Rev. Env. Sci. Tec. 41 (1), 187-216.

Jankowski, J.J., Kieber, D.J., Mopper, K., 1999. Nitrate and nitrite ultraviolet actinometers. Photochem. Photobiol. 70 (3), 319-328.

Kaushal, S.S., Mayer, P.M., Vidon, P.G., Smith, R.M., Pennino, M.J., Newcomer, T.A., Duan, S., Welty, C., Belt, K.T., 2014. Land use and climate variability amplify carbon, nutrient, and contaminant pulses: a review with management implications. J. Am. Water. Resour. As. 50 (3), 585-614.

Kendrick, E., 1963. A Mass Scale Based on CH2=14.0000 for High Resolution Mass Spectrometry of Organic Compounds. Anal. Chem. 35 (13), 2146-2154.

Kieber, R.J., Hydro, L.H., Seaton, P.J., 1997. Photooxidation of triglycerides and fatty acids in seawater: Implication toward the formation of marine humic substances. Limnol. Oceanogr. 42 (6), 1454-1462.

Kim, S., Kramer, R.W., Hatcher, P.G., 2003. Graphical method for analysis of ultrahigh-resolution broadband mass spectra of natural organic matter, the van Krevelen diagram. Anal. Chem. 75 (20), 5336-5344.

Kim, S., Kaplan, L.A., Benner, R., Hatcher, P.G., 2004. Hydrogen-deficient molecules in natural riverine water samples evidence for the existence of black carbon in DOM. Mar. Chem. 92 (1), 225-234.

Kim, S., Kaplan, L.A., Hatcher, P.G., 2006. Biodegradable dissolved organic matter in a temperate and a tropical stream determined from ultra-high resolution mass spectrometry. Limnol. Oceanogr. 51 (2), 1054-1063.

Koch, B.P., Witt, M., Engbrodt, R., Dittmar, T., Kattner, G., 2005. Molecular formulae of marine and terrigenous dissolved organic matter detected by electrospray ionization Fourier transform ion cyclotron resonance mass spectrometry. Geochim. Cosmochim. Acta 69 (13), 3299-3308

Koch, B.P., Dittmar, T., 2006. From mass to structure: an aromaticity index for high-resolution mass data of natural organic matter. Rapid Commun. Mass Spectrom. 20 (5), 926-932.

Koch, B.P., Dittmar, T., Witt, M., Kattner, G., 2007. Fundamentals of molecular formula assignment to ultrahigh resolution mass data of natural organic matter. Anal. Chem. 79 (4), 1758-1763.

Koprivnjak, J.F., Perdue, E.M., Pfromm, P.H., 2006. Coupling reverse osmosis with electrodialysis to isolate natural organic matter from fresh waters. Water Res. 40 (18), 3385-3392.

Kujawinski, E.B., Del Vecchio, R., Blough, N.V., Klein, G.C., Marshall, A.G., 2004. Probing molecular-level transformations of dissolved organic matter: insights on photochemical degradation and protozoan modification of DOM from electrospray ionization Fourier transform ion cyclotron resonance mass spectrometry. Mar. Chem. 92 (1), 23-37.

Koprivnjak, J.F., Pfromm, P.H., Ingall, E., Vetter, T.A., Schmitt-Kopplin, P., Hertkorn, N., Frommberger, M., Knicker, H., Perdue, E.M. 2009. Chemical and spectroscopic characterization of marine dissolved organic matter isolated using coupled reverse osmosis-electrodialysis. Geochim. Cosmochim. Acta 73 (14), 4215-4231.

Kujawinski, E.B., Hatcher, P.G., Freitas, M.A., 2002. High-resolution Fourier transform ion cyclotron resonance mass spectrometry of humic and fulvic acids: improvements and comparisons. Anal. Chem. 74 (2), 413-419.

Kujawinski, E.B., Longnecker, K., Blough, N.V., Del Vecchio, R., Finlay, L., Kitner, J.B., Giovannoni, S.J., 2009. Identification of possible source markers in marine dissolved organic matter using ultrahigh resolution mass spectrometry. Geochim. Cosmochim. Acta 73 (15), 4384-4399.

Le Quéré, C., Raupach, M.R., Canadell, J.G., Marland, G., 2009. Trends in the sources and sinks of carbon dioxide. Nat. Geosci. 2 (12), 831-836.

Lerman, A., Mackenzie, F.T., May, V.L., 2004. Coupling of the Perturbed C-N-P Cycles in Industrial Time. Aquat. Geochem. 10 (1-2), 3-32.

Lozano, I., Devoy, R., May, W., Andersen, U., 2004. Storminess and vulnerability along the Atlantic coastlines of Europe: analysis of storm records and of a greenhouse gases induced climate scenario. Mar. Geol. 210 (1), 205-225.

Lu, Y., Bauer, J.E., Canuel, E.A., Yamashita, Y., Chambers, R.M., Jaffé, R., 2013. Photochemical and microbial alteration of dissolved organic matter in temperate headwater streams associated with different land use. J. Geophys. Res-Biogeo. 118 (2), 566-580.

Mackenzie, F.T., Lerman, A., Ver, L.M.B., 1998. Role of the continental margin in the global carbon balance during the past three centuries. Geology 26 (5), 423-426.

Mackenzie, F.T., Ver, L.M., Lerman, A., 2002. Century-scale nitrogen and phosphorus controls of the carbon cycle. Chem. Geol. 190 (1), 13-32.

Marie, D., Partensky, F., Jacquet, S., Vaulot, D., 1997. Enumeration and cell cycle analysis of natural populations of marine picoplankton by flow cytometry using the nucleic acid stain SYBR Green I. Appl. Environ. Microbiol. 63 (1), 186-193.

Marshall, A.G., Hendrickson, C.L., Jackson, G.S., 1998. Fourier transform ion cyclotron resonance mass spectrometry: a primer. Mass Spectrom. Rev. 17 (1), 1-35.

Mazzoleni, L.R., Ehrmann, B.M., Shen, X., Marshall, A.G., Collett Jr, J.L., 2010. Water-soluble atmospheric organic matter in fog: exact masses and chemical formula identification by ultrahigh-resolution Fourier transform ion cyclotron resonance mass spectrometry. Environ. Sci. Technol. 44 (10), 3690-3697.

Mazzoleni, L.R., Saranjampour, P., Dalbec, M.M., Samburova, V., Hallar, A.G., Zielinska, B., Lowenthal, D.H., Kohl, S., 2012. Identification of water-soluble

organic carbon in non-urban aerosols using ultrahigh-resolution FT-ICR mass spectrometry: organic anions. Environ. Chem. 9 (3), 285-297.

McCarthy, M.D. and Bronk, D.A., 2008. Analytical methods for the study of nitrogen. In: Capone D., Bronk D., Mulholland M., Carpenter E., (Eds), Nitrogen in the Marine Environment. Elsevier, San Diego, pp. 1220-1275.

Meng, F., Huang, G., Yang, X., Li, Z., Li, J., Cao, J., Wang, Z., Sun, L., 2013. Identifying the sources and fate of anthropogenically impacted dissolved organic matter (DOM) in urbanized rivers. Water Res. 47 (14), 5027-5039.

Mesfioui, R., Love, N.G., Bronk, D.A., Mulholland, M.R., Hatcher, P.G., 2012. Reactivity and chemical characterization of effluent organic nitrogen from wastewater treatment plants determined by Fourier transform ion cyclotron resonance mass spectrometry. Water Res. 46 (3), 622-634.

Minor, E., Dalzell, B., Stubbins, A., Mopper, K., 2007. Evaluating the photoalteration of estuarine dissolved organic matter using direct temperature-resolved mass spectrometry and UV-visible spectroscopy. Aquat. Sci. 69 (4), 440-455.

Mopper, K., Zhou, X., Kieber, R.J., Kieber, D.J., Sikorski, R.J., Jones, R.D., 1991. Photochemical degradation of dissolved organic carbon and its impact on the oceanic carbon cycle. Nature 353, 60-62.

Mopper, K., Stubbins, A., Ritchie, J.D., Bialk, H.M., Hatcher, P.G., 2007. Advanced instrumental approaches for characterization of marine dissolved organic matter: extraction techniques, mass spectrometry, and nuclear magnetic resonance spectroscopy. Chem. Rev. 107 (2), 419-442.

Morel, B., Durand, P., Jaffrezic, A., Gruau, G., Molenat, J., 2009. Sources of dissolved organic carbon during stormflow in a headwater agricultural catchment. Hydrol. Process. 23 (20), 2888-2901.

Mulholland, M.R., Lomas, M.W., 2008. Nitrogen uptake and assimilation. In: Capone D., Bronk D., Mulholland M., Carpenter E., (Eds), Nitrogen in the marine environment. Academic Press, Massachusetts, pp. 303-384.

Najjar, R.G., Pyke, C.R., Adams, M.B., Breitburg, D., Hershner, C., Kemp, M., Howarth, R., Mulholland, M.R., Paolisso, M., Secor., D., Sellner, K., Wardrop., D., Wood, R., 2010. Potential climate-change impacts on the Chesapeake Bay. Estuar. Coast. Shelf Sci. 86 (1), 1-20.

Nakagawa, Y., Eguchi, M., Miyashita, S., 2007. Pacific bluefin tuna, *Thunnus orientalis*, larvae utilize energy and nutrients of microbial loop. Aquaculture 267 (1), 83-93.

Nizkorodov, S.A., Laskin, J., Laskin, A., 2011. Molecular chemistry of organic aerosols through the application of high resolution mass spectrometry. Phys. Chem. Chem. Phys. 13 (9), 3612-3629.

Ohno, T., He, Z., Sleighter, R.L., Honeycutt, C.W., Hatcher, P.G., 2010. Ultrahigh Resolution Mass Spectrometry and Indicator Species Analysis to Identify Marker Components of Soil-and Plant Biomass-Derived Organic Matter Fractions. Environ. Sci. Technol. 44 (22), 8594-8600.

Opsahl, S., Benner, R., 1997. Distribution and cycling of terrigenous dissolved organic matter in the ocean. Nature 386: 480-482.

Opsahl, S., Benner, R., 1998. Photochemical reactivity of dissolved lignin in river and ocean waters. Limnol. Oceanogr. 43 (6), 1297-1304.

Ortega-Retuerta, E., Pulido-Villena, E., Reche, I., 2007. Effects of dissolved organic matter photoproducts and mineral nutrient supply on bacterial growth in Mediterranean inland waters. Microb. Ecol. 54 (1), 161-169.

Pagilla, K.R., Urgun-Demirtas, M., Ramani, R., 2006. Low effluent nutrient technologies for wastewater treatment. Water Sci. Technol. 53 (3), 165-172.

Parkin, G., McCarty, P., 1981. Sources of soluble organic nitrogen in activated sludge effluents. Res. J. Water Pollut. C. 53 (1), 89-98.

Parsons, T.R., Maita, Y., Lalli, C.M., 1984. A manual of biological and chemical methods for seawater analysis. Pergamon Press, New York, NY.

Pehlivanoglu, E., Sedlak, D.L., 2004. Bioavailability of wastewater-derived organic nitrogen to the alga selenastrum capricornutum. Water Res. 38 (14-15), 3189-3196.

Pehlivanoglu-Mantas, E., Sedlak, D., 2006. Wastewater-Derived Dissolved Organic Nitrogen: Analytical Methods, Characterization, and Effects: a Review. Crit. Rev. Env. Sci. Tec. 36 (3), 261-285.

Pellerin, B.A., Kaushal, S.S., McDowell, W.H., 2006. Does anthropogenic nitrogen enrichment increase organic nitrogen concentrations in runoff from forested and human-dominated watersheds? Ecosystems 9 (5), 852-864.

Peltzer, E.T., Fry, B., Doering, P.H., McKenna, J.H., Norrman, B. and Zweifel, U.L., 1996. A comparison of methods for the measurement of dissolved organic carbon in natural waters. Mar. Chem. 54 (1), 85-96.

Perakis, S.S., Hedin, L.O., 2002. Nitrogen loss from unpolluted south american forests mainly via dissolved organic compounds. Nature 415, 416-419.

Perdue, E., 1984. Analytical constraints on the structural features of humic substances. Geochim. Cosmochim. Acta 48 (7), 1435-1442.

Rabalais, N.N., Turner, R.E., Wiseman Jr, W.J., 2002. Gulf of Mexico hypoxia, AKA" The dead zone". Annu. Rev. Ecol. Sys. 33, 235-263.

Raymond, P.A., Saiers, J.E., 2010. Event controlled DOC export from forested watersheds. Biogeochemistry 100 (1-3), 197-209.

Reemtsma, T., These, A., Springer, A., Linscheid, M., 2006. Fulvic acids as transition state of organic matter: Indications from high resolution mass spectrometry. Environ. Sci. Technol. 40 (19), 5839-5845.

Reemtsma, T., 2009. Determination of molecular formulas of natural organic matter molecules by ultra-high-resolution mass spectrometry: Status and needs. J. Chromatogr. A 1216 (18), 3687-3701.

Rockstrom, J., Karlberg, L., 2010. The Quadruple Squeeze: Defining the safe operating space for freshwater use to achieve a triply green revolution in the Anthropocene. AMBIO 39 (3), 257-265.

Rossel, P.E., Vähätalo, A.V., Witt, M., Dittmar, T., 2013. Molecular composition of dissolved organic matter from a wetland plant *Juncus effusus* after photochemical and microbial decomposition (1.25 yr): Common features with deep sea dissolved organic matter. Org. Geochem. 60, 62-71.

Sattayatewa, C., Pagilla, K., Pitt, P., Selock, K., Bruton, T., 2009. Organic nitrogen transformations in a 4-stage Bardenpho nitrogen removal plant and bioavailability/biodegradability of effluent DON. Water Res. 43 (18), 4507-4516.

Schlesinger, W.H., Melack, J.M., 1981. Transport of organic carbon in the world's rivers. Tellus 33 (2), 172-187.

Schlesinger, W.H., 2009. On the fate of anthropogenic nitrogen. P. Natl. A. Sci. USA 106 (1), 203-208.

Schlesinger, W.H., Bernhardt, E.S., 2013. Biogeochemistry: an analysis of global change. Academic press. Waltham, MA, USA.

Schmid, D.G., Grosche, P., Bandel, H., Jung, G., 2000. FTICR-mass spectrometry for high-resolution analysis in combinatorial chemistry. Biotechnol. Bioeng. 71 (2), 2001.

Schultz, G.E., White, E.D., Ducklow, H.W., 2003. Bacterioplankton dynamics in the York River estuary: primary influence of temperature and freshwater inputs. Aquat. Microb. Ecolo. 30 (2), 135-148.

Seitzinger, S.P., Sanders, R., Styles, R., 2002. Bioavailability of DON from natural and anthropogenic sources to estuarine plankton. Limnol. Oceanogr. 47 (2), 353-366.

Seitzinger, S., Harrison, J.A., Dumont, E., Beusen, A.H., Bouwman, A.F., 2005a. Sources and delivery of carbon, nitrogen, and phosphorus to the coastal zone: An overview of Global Nutrient Export from Watersheds (NEWS) models and their application. Global Biogeochem. Cy. 19 (4), 1-11.

Seitzinger, S.P., Hartnett, H., Lauck, R., Mazurek, M., Minegishi, T., Spyres, G., Styles, R., 2005b. Molecular-level chemical characterization and bioavailability of dissolved organic matter in stream water using electrospray-ionization mass spectrometry. Limnol. Oceanogr. 50 (1), 1-12.

Shank, G.C., Zepp, R.G., Whitehead, R.F., Moran, M.A., 2005. Variations in the spectral properties of freshwater and estuarine CDOM caused by partitioning onto river and estuarine sediments. Estuar. Coast. Shelf Sci. 65 (1), 289-301.

Shon, H., Vigneswaran, S. and Snyder, S., 2006. Effluent organic matter (EfOM) in wastewater: constituents, effects, and treatment. Critical Reviews in Environ. Sci. Technol. 36 (4), 327-374.

Simjouw, J.P., Minor, E.C., Mopper, K., 2005. Isolation and characterization of estuarine dissolved organic matter: Comparison of ultrafiltration and C18 solid-phase extraction techniques. Mar. Chem. 96 (3-4), 219-235.

Simsek, H., Wadhawan, T., Khan, E., 2013. Overlapping Photodegradable and Biodegradable Organic Nitrogen in Wastewater Effluents. Environ. Sci. Technol. 47 (13), 7163-7170.

Sleighter, R.L., Hatcher, P.G., 2007. The application of electrospray ionization coupled to ultrahigh resolution mass spectrometry for the molecular characterization of natural organic matter. J. Mass Spectrom. 42 (5), 559-574.

Sleighter, R.L., McKee, G.A., Liu, Z., Hatcher, P.G., 2008a. Naturally present fatty acids as internal calibrants for Fourier transform mass spectra of dissolved organic matter. Limnol. Oceanogr. Methods 6, 246-253.

Sleighter, R.L., Hatcher, P.G., 2008b. Molecular characterization of dissolved organic matter (DOM) along a river to ocean transect of the lower Chesapeake Bay by ultrahigh resolution electrospray ionization Fourier transform ion cyclotron resonance mass spectrometry. Mar. Chem. 110 (3-4), 140-152.

Sleighter, R.L., Liu, Z., Xue, J., Hatcher, P.G., 2010. Multivariate Statistical Approaches for the Characterization of Dissolved Organic Matter Analyzed by Ultrahigh Resolution Mass Spectrometry. Environ. Sci. Technol. 44 (19), 7576–7582.

Sleighter, R.L., Hatcher, P.G., 2011. Transform mass spectrometry for the molecular level characterization of natural organic matter: Instrument capabilities, applications, and limitations. In: Nikolic G., (Ed.), Fourier ttransforms approach to scientific principles. Tech, Vienna, pp. 295-320

Sleighter, R.L., Cory, R.M., Kaplan, L.A., Abdulla, H.A., Hatcher, P.G., 2014. A coupled geochemical and biogeochemical approach to characterize the bioreactivity of dissolved organic matter from a headwater stream. J. Geophys. Res-Biogeo. 119 (8), 1520-1537.

Smith, E.M., Benner, R., 2005. Photochemical transformations of riverine dissolved organic matter: effects on estuarine bacterial metabolism and nutrient demand. Aquat. Microb. Ecol. 40 (1), 37-50.

Stenson, A.C., Landing, W.M., Marshall, A.G., Cooper, W.T., 2002. Ionization and fragmentation of humic substances in electrospray ionization Fourier transform-ion cyclotron resonance mass spectrometry. Anal. Chem. 74 (17), 4397-4409.

Stenson, A.C., Marshall, A.G., Cooper, W.T., 2003. Exact masses and chemical formulas of individual Suwannee River fulvic acids from ultrahigh resolution electrospray ionization Fourier transform ion cyclotron resonance mass spectra. Anal. Chem. 75(6), 1275-1284.

Stubbins, A., Spencer, R.G.M., Chen, H., Hatcher, P.G., Mopper, K., Hernes, P.J., Mwamba, V.L., Mangangu, A.M., Wabakanghanzi, J.N., Six, J., 2010.

Illuminated darkness: Molecular signatures of Congo River dissolved organic matter and its photochemical alteration as revealed by ultrahigh precision mass spectrometry. Limnol. Oceanogr. 55 (4), 1467-1477.

Sun, L., Perdue, E., Meyer, J., Weis, J., 1997. Use of elemental composition to predict bioavailability of dissolved organic matter in a Georgia river. Limnol. Oceanogr. 42 (4), 714-721.

Tarr, M.A., Wang, W., Bianchi, T.S., Engelhaupt, E., 2001. Mechanisms of ammonia and amino acid photoproduction from aquatic humic and colloidal matter. Water Res. 35 (15), 3688-3696.

Urgun-Demirtas, M., Sattayatewa, C., Pagilla, K.R., 2008. Bioavailability of dissolved organic nitrogen in treated effluents. Water Environ. Res. 80(5), 397-406.

Vähätalo, A.V., Zepp, R.G., 2005. Photochemical mineralization of dissolved organic nitrogen to ammonium in the Baltic Sea. Environ. Sci. Technol. 39 (18), 6985-6992.

Van Kessel, C., Clough, T.J., Van Groenigen, J.W., 2009. Dissolved organic nitrogen: an overlooked pathway of nitrogen loss from agricultural systems? J. Environ. Qual. 38 (2), 393-401.

Van Krevelen, D., 1950. Graphical-statistical method for the study of structure and reaction processes of coal. Fuel 29 (12), 269-2.

Vaulot, D., Courties, C., Partensky, F., 1989. A simple method to preserve oceanic phytoplankton for flow cytometric analyses. Cytometry 10 (5), 629-635.

Vetter, T.A., Perdue, E.M., Ingall, E., Koprivnjak, J.F., Pfromm, P.H., 2007. Combining reverse osmosis and electrodialysis for more complete recovery of dissolved organic matter from seawater. Sep. Purif. Technol. 56 (3), 383-387.

Vidon, P., Wagner, L.E., Soyeux, E., 2008. Changes in the character of DOC in streams during storms in two Midwestern watersheds with contrasting land uses. Biogeochemistry 88 (3), 257-270.

Vitousek, P.M., Aber, J.D., Howarth, R.W., Likens, G.E., Matson, P. A., Schindler, D.W., Schlesinger, W.H., Tilman, D.G., 1997. Human alteration of the global nitrogen cycle: sources and consequences. Ecol. Appl. 7 (3), 737-750.

Weishaar, J.L., Aiken, G.R., Bergamaschi, B.A., Fram, M.S., Fujii, R., Mopper, K., 2003. Evaluation of specific ultraviolet absorbance as an indicator of the chemical composition and reactivity of dissolved organic carbon. Environ. Sci. Technol. 37 (20), 4702-4708.

Welschmeyer, N.A., 1994. Fluorometric analysis of chlorophyll a in the presence of chlorophyll b and pheopigments. Limnol. Oceanogr. 39 (8), 1985-1992.

Wetzel, R.G., 1992. Gradient-dominated ecosystems: sources and regulatory functions of dissolved organic matter in freshwater ecosystems. Hydrobiologia 229,181-198.

Wiegner, T.N., Seitzinger, S.P., 2001. Photochemical and microbial degradation of external dissolved organic matter inputs to rivers. Aquat. Microb. Ecol. 24 (1), 27-40.

Wiegner, T.N., Seitzinger, S.P., Glibert, P.M., Bronk, D.A., 2006. Bioavailability of dissolved organic nitrogen and carbon from nine rivers in the eastern United States. Aquat. Microb. Ecol. 43 (3), 277-287.

Williams, C.J., Yamashita, Y., Wilson, H.F., Jaffé, R., Xenopoulos, M.A., 2010. Unraveling the role of land use and microbial activity in shaping dissolved organic matter characteristics in stream ecosystems. Limnol. Oceanogr. 55 (3), 1159.

Wilson, H., Xenopoulos, M., 2013. Diel changes of dissolved organic matter in streams of varying watershed land use. River Res. Appl. 29 (10), 1330-1339.

Yamashita, Y., Maie, N., Briceño, H., Jaffé, R., 2010. Optical characterization of dissolved organic matter in tropical rivers of the Guayana Shield, Venezuela. J. Geophys. Res-Biogeo. 115 (G1), 2005–2012.

Zhang, C., Li, G., Lin, Q., Cao, A., Zhao, X., 2011. The dynamics of dissolved organic N in the fumigated soils. Biol. Fert. Soils 47, 833-837.

APPENDIX A

COPYRIGHT PERMISSION

Permission for Chapter II, which contains Water Research article published by Elsevier

Articles that are published in Elsevier journals do not need to seek Elsevier's permission to include them in your thesis (including being placed on your university website), as it is part of the rights that an author retains (see http://www.elsevier.com/wps/find/authorsview.authors/copyright below).

What rights do I retain as a journal author*?

As a journal author, you retain rights for large number of author uses, including use by your employing institute or company. These rights are retained and permitted without the need to obtain specific permission from Elsevier. These include:

- the right to make copies (print or electric) of the journal article for their own personal use, including for their own classroom teaching use;
- the right to make copies and distribute copies (including via e-mail) of the journal article to research colleagues, for personal use by such colleagues (but not for Commercial Purposes**, as listed below);
- the right to post a pre-print version of the journal article on Internet web sites including electronic pre-print servers, and to retain indefinitely such version on such servers or sites (see also our information on electronic preprints for a more detailed discussion on these points); the right to post a revised personal version of the text of the final journal article (to reflect changes made in the peer review process) on the author's personal or institutional web site or server, incorporating the complete citation and with a link to the Digital Object Identifier (DOI) of the article;
- the right to present the journal article at a meeting or conference and to distribute copies of such paper or article to the delegates attending the meeting;
- for the author's employer, if the journal article is a 'work for hire', made within the scope of the author's employment, the right to use all or part of the information in (any version of) the journal article for other intra-company use (e.g. training), including by posting the article on secure, internal corporate intranets;
- patent and trademark rights and rights to any process or procedure described in the journal article;
- **the right to include the journal article, in full or in part, in a thesis or dissertation**;
- the right to use the journal article or any part thereof in a printed compilation of works of the author, such as collected writings or lecture notes (subsequent to publication of the article in the journal);
- and the right to prepare other derivative works, to extend the journal article into book-length form, or to otherwise re-use portions or excerpts in other works, with full acknowledgement of its original publication in the journal.

APPENDIX B

ABBREVIATIONS AND ACRONYMS USED

A1: area 1

A2: area 2

A3: area 3

A: absorbance

a: absorbance coefficient

C: carbon

°C: Celsius

COSMIC: College of Sciences Major Instrumentation Cluster

CRAM: carboxyl-rich alicyclic molecules

Ctrl: control

Chla : chlorophyll a

2D: two-dimensional

Da: Dalton

DBE: double bond equivalents

DIN: dissolved inorganic nitrogen

DOC: dissolved organic carbon

DOM: dissolved organic matter

DON: dissolved organic nitrogen

ED: electrodialysis

EON: effluent organic nitrogen

EON4: effluent from King William county, VA wastewater plant

EON5: effluent from Reno, NV wastewater plant

ESI: electrospray ionization

ESI-FTICR-MS: electrospray ionization Fourier transform ion cyclotron resonance mass spectrometry

FTICR-MS: Fourier transform ion cyclotron resonance mass spectrometry

GF/F: 0.7 μm glass fiber filters

H: hydrogen

JR: James River

KW: King William

l :path length

LC-MS: liquid chromatography- mass spectrometry

m/z: mass to charge

μm: micron

M: molarity

mL: milliliter

MS: mass spectrometry

MW: molecular weight

M_w: magnitude weighted

N: nitrogen

NH_4^+: ammonia

NHMFL: national high magnetic field laboratory

NMR: nuclear magnetic resonance

NOM: natural organic matter

NO_2^-: nitrite

NO_3^-: nitrate

NOx: Nitrite+Nitrate

O: oxygen

P: phosphorus

PC: principal component

PCA: principal component analysis

PPL: styrene-divinyllbenzene polymer for solid phase extraction

ppm: parts per million

RO/ED: reverse osmosis/ electrodialysis

S: slope

S2: Salinity 2 (5‰)

S3: Salinity 3 (12.5‰)

SHM: Sweet Hall marsh

S/N: signal to noise

S_R: slope ratio

SUVA: specific Ultraviolet AbsorbanceT: tesla

T_0: time initial

T_f: time final

TC: Taskinas creek

TOC: total organic carbon

TOF: time of flight

TDN: total dissolved nitrogen

TN: total nitrogen

UV-Vis: Ultraviolet / Visible Spectroscopy

YR: York River

YT: York Town

WWTP: wastewater treatment plant

VK: van Krevelen

VIMS: Virginia Institute of Marine Sciences

WP: West Point

WW: whole water

XAD: Registered Trade Name for Amberlite Hydrophobic Resins

APPENDIX C

ESI-FTICR-MS PRINCIPLE AND DATA ANALYSES

1. DOM ESI-FTICR-MS analyses

The potential of FTICR-MS to play a major role in the characterization of DOM in aerosols (Mazzoleni et al., 2010; Mazzoleni et al., 2012; Nizkorodov et al., 2011), rainwater (Altieri et al., 2009a), marine (Chen et al., 2011; Hertkorn et al., 2013; Kujawinski et al., 2009), and fresh water systems (Seitzinger et al., 2005b; Sleighter and Hatcher, 2007; Stubbins et al., 2010) has recently been recognized. This technique allows the exact elemental composition of ions to be calculated offering a major breakthrough for the characterization of DOM and its subcomponents DOC and DON (Mesfioui et al., 2012; Stenson et al., 2002). Because of its ultrahigh resolving power (>200,000) and high mass accuracy (<1ppm), ESI-FTICR-MS is capable of determining the exact mass for the thousands of molecules in a single complex sample of DOM (Kim et al., 2003; Kujawinski et al., 2002). The mass accuracy is sufficiently high to allow for the assignment of a unique molecular formula to each constituent (Stenson et al., 2003). Currently, ESI-FT-ICR-MS is the most powerful analytical tool for elucidating the detailed molecular characterization of DOM, which can be accomplished by assigning unambiguously single formula to each peak in the mass spectrum.

2. FTICR-MS Cyclotron Motion

The power of FT-ICR-MS comes from the precise measurement of the ion cyclotron frequency that is independent from the ion velocity, and therefore its kinetic energy. The measured signal results from induced charge on the FTICR trap detection plates caused by the cyclotron motion of ions in a static magnetic field. After a sweep with a radio

frequency, "ion-packet" of the same mass m and charge (q or z) oscillates perpendicularly to the magnetic field (B) at a frequency dependent on their mass to charge ratio (m/z) (Figure 40). The forces on the ions are the Lorenz force ($F_L = q.v.B$) and the centrifugal force ($F_z = \frac{m.v_{xy}^2}{r}$). When $F_Z = F_L$ the characteristic cyclotron frequency v_c for each ion-packet is expressed as: $\left(v_c = \frac{q.B}{2\pi.m}\right)$, hence, the cyclotron frequency depends only upon the ion's charge q, its mass m and the magnetic field B, which is, in general, constant. The resulting signal is a free induction decay and the data is extracted by a Fourier transform to generate the mass spectrum.

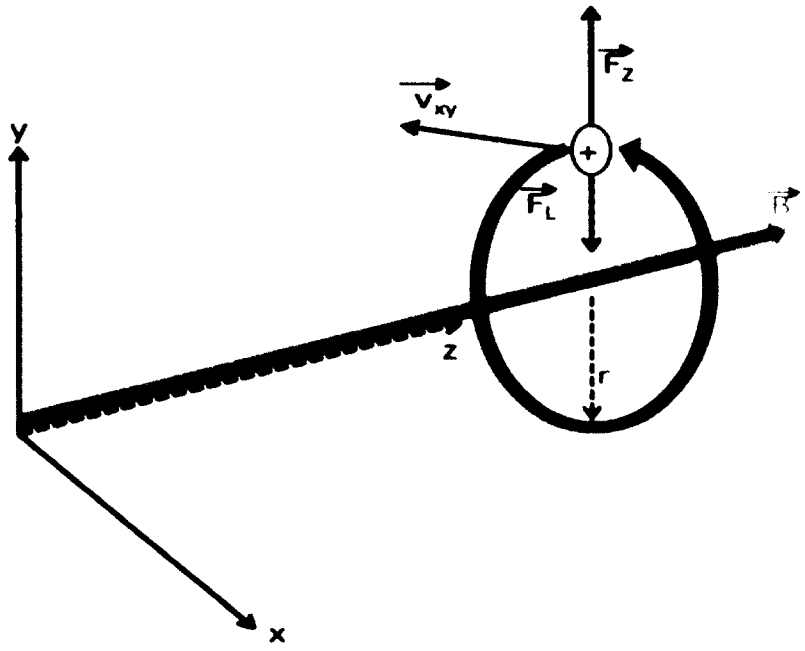

Figure 40. Cyclotron motion of ions in a magnetic field. Fz (centrifugal force), FL (Lorentz force), B (magnetic field), vxy (ion velocity), r = orbital radius. Ions (+) are separated on the basis of their cyclotron frequency, adapted from Schmid et al. (2000).

3. Mass spectrometry resolutions and mass accuracy

The performance of mass analyzers is typically quantitated in terms of resolution and mass accuracy. In fact, Fourier transform ion cyclotron resonance mass spectrometer is capable of extremely high mass resolution (R), which is the degree of separation of neighboring peaks. Mass resolutions of up to 600,000 can be achieved for low m/z values. The resolution or resolving power is defined as $R = \frac{m}{\Delta m_{50\%}}$, where m is the m/z at which the signal is observed and $\Delta m_{50\%}$ denotes the full width at half maximum (FWHM) of the measured peak, which is nowadays accepted as a general definition of mass spectrometric resolution.

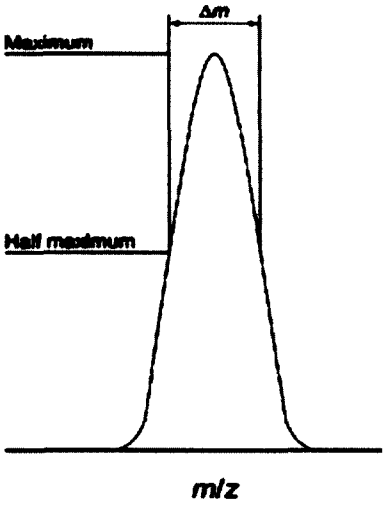

Figure 41. Method to determine full width at half maximum $\mathbf{\Delta m_{50\%}}$.

The second most important parameter to FT-ICR mass spectrometry is the mass accuracy, which is defined as the ratio of the difference between the measured m_{exp} mass and the theoretical mass m_{theo}, expressed in ppm and calculated using the following equation:

$$\text{mass accuracy} = \frac{m_{exp} - m_{theo}}{m_{theo} \cdot 10^6}$$

4. ESI-FTICR mass spectrometry data analysis

The ultrahigh resolving power of FTICR-MS (> 400,000) and mass accuracy of (< 1 ppm) provides the ability to assign unique molecular formulas to thousands of components in a single DOM sample.

The three main parameters for the comparative analysis of the huge data set generated by FT-ICR-MS are the double bond equivalents (DBE), van Krevelen diagram (VK), and the aromaticity index (AI), which are calculated from the accurately assigned molecular formulas for each peak (Kendrick, 1963; Kim et al., 2003; Koch and Dittmar, 2006).

4.1 Double bound equivalent

DBE is a measure of the H saturation; it provides the number of double bonds and/ or rings in an organic molecule based on C, H, and N and P elemental ratios:

$$DBE = 1 + \#C - ({}^{H}/_{2}) + ({}^{N}/_{2}) + ({}^{P}/_{2})$$

This parameter accounts for all doubly bound carbon contributions, including the double bonds of carboxyl groups.

4.2 Aromaticity index

Similar to O/C, H/C, and DBE values, AI values are calculated for every assigned molecular formula in a sample as follows:

$$AI = \frac{1 + C - O - S - 0.5H}{C - O - S - N - P}$$

AI was first proposed by Koch and Dittmar (Kim et al., 2006; Koch and Dittmar, 2006) to distinguish unambiguously between aromatic (AI > 0.5) and condensed aromatic

structures (AI >= 0.67) in NOM. The latter values are indicative of thermogenic sources of condensed aromatics or ''black carbon, which have also been identified using the following rules (Hockaday et al., 2006; Kim et al., 2004)

$$0.3 \leq {}^{O}/_{C} \leq 0,6 \ and \ 0.5 \leq {}^{H}/_{C} \leq 0.8 \ \ and \ {}^{DBE}/_{C} = 0.67$$

However, the amount of condensed aromatic might be overestimated when applying this rule only.

If only half of the oxygen in DOM is considered being present in carbonyl functional groups, as it is the case in our study, then AI should be calculated as follow:

$$AI_{mod} = \frac{1 + C - 0.5\,O - S - 0.5\,H}{C - 0.5\,O - S - N - P}$$

4.3 Van Krevelen diagram

van Krevelen diagram (VK) plots the molar H/C ratios of each assigned elemental formula on the y-axis and its molar O/C ratios on the x-axis. VK plots cluster elemental formulae according to their functional group compositions into major biochemical compounds classes that have characteristic H/C and O/C ratios. These clusters help elucidate changes in the chemical composition such as changes in oxidation state, degree of methylation, and condensation reactions to form large molecules of samples. Figure 42 shows van Krevelen diagram of EON5, a wastewater effluent studied in Chapter 2, the overlain black circles show major compound classes identified in DOM. It is well known that the location of a point on the VK diagram relates to specific compound classes in DOM, and interested readers are referred to the literature for more details (Hockaday et al., 2009; Ohno et al., 2010; Reemtsma, 2009; Sleighter and Hatcher, 2011; Van Krevelen, 1950). These compound classes include:

- Aliphatic structures (Perdue, 1984) defined as peaks with

$$^{DBE}/_{C} < 0.3 \; and \; 1.0 < {}^{H}/_{C} < 3.0$$

- Carboxyl-rich alicyclic molecule-like structures [CRAM (Hertkorn et al., 2006)] defined as:

$$o.3 \leq {}^{DBE}/_{C} \leq 0.68, and \; o.2 \leq {}^{DBE}/_{H} \leq 0.95, and \; o.77 \leq {}^{DBE}/_{O} \leq 1.75$$

or Lignin-like structures defined as :

$$0.1 < {}^{O}/_{C} < 0.6 \; and \; 0.6 < {}^{H}/_{C} < 1.7 \; and \; Al_{mod} < 0.6$$

- Aromatic and condensed aromatic structures defined above in section 4.2.
- Tannin defined as peaks having:

$$0.35 < {}^{O}/_{C} < 0.85 \; and \; 0.75 < {}^{H}/_{C} < 1.4$$

- Carbohydrate-like structures defined as formulas with

$$0.7 < {}^{O}/_{C} < 1 \; and \; 1.6 < {}^{H}/_{C} < 2$$

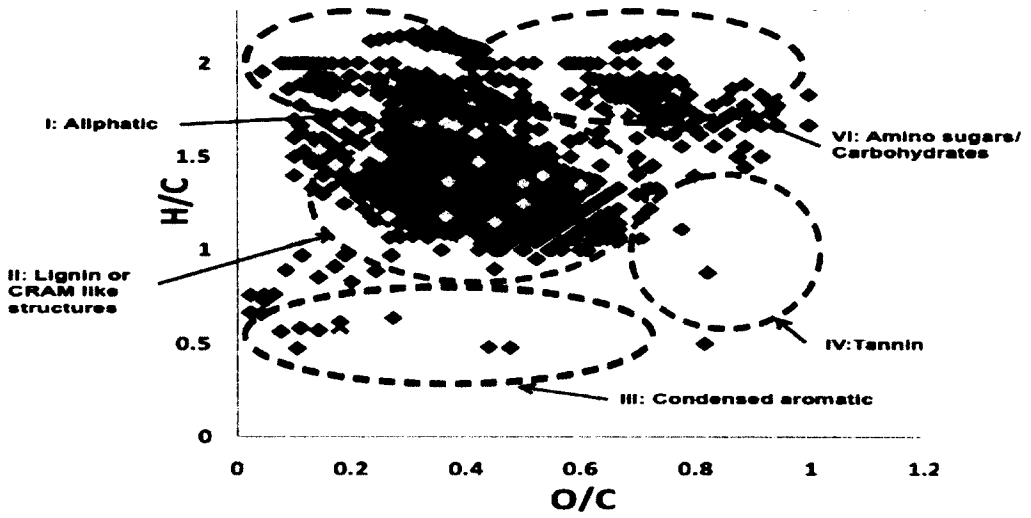

Figure 42. van Krevelen diagram of EON5 sample. The overlain black circles show major compound classes identified in DOM.

VITA

Rajaa Mesfioui

January 27, 1978 ..... Born-Beni Mellal, Morocco.

May 2001 ..... B.S. Chemistry, University of Cady Ayad
Beni Mellal, Morocco

June 2006-May 2008..... Chemistry Graduate Student, Old Dominion University
Norfolk, Virginia

May 2008 ..... M.S. Chemistry, Old Dominion University
Norfolk, Virginia

June 2008-present ..... Chemistry Graduate Student, Old Dominion University
Norfolk, Virginia

December 2014 ..... Ph.D. Chemistry, Old Dominion University
Norfolk, Virginia